Cardiff University
School Of Chemistry

Metal Ligand Complex Syntheses for Imaging Applications

Thesis submitted for the degree of Doctor of Philosophy by:

Mauro Monti

Supervisors: Prof. P. G. Edwards & Dr. I. Fallis

September 2016

DECLARATION

This work has not been submitted in substance for any other degree or award at this or any other university or place of learning, nor is being submitted concurrently in candidature for any degree or other award.

Signed……(candidate) Date.....……

STATEMENT 1

This thesis is being submitted in partial fulfilment of the requirements for the degree of PhD.

Signed……(candidate) Date..……

STATEMENT 2

This thesis is the result of my own independent work/investigation, except where otherwise stated, and the thesis has not been edited by a third party beyond what is permitted by Cardiff University's Policy on the Use of Third Party Editors by Research Degree Students. Other sources are acknowledged by explicit references. The views expressed are my own.

Signed……(candidate) Date……..……

STATEMENT 3

I hereby give consent for my thesis, if accepted, to be available online in the University's Open Access repository and for inter-library loan, and for the title and summary to be made available to outside organisations.

Signed……..…..…..(candidate) Date..……

STATEMENT 4: PREVIOUSLY APPROVED BAR ON ACCESS

I hereby give consent for my thesis, if accepted, to be available online in the University's Open Access repository and for inter-library loans after expiry of a bar on access previously approved by the Academic Standards & Quality Committee.

Signed……..……(candidate) Date..……..……

ABSTRACT

This thesis describes an investigation into the roles and effects of nitrogen-donor chelating ligands and complexes containing metal centres as tools for molecular imaging.

Chapter 1 gives a brief introduction to Positron Emission Tomography (PET) imaging, the radionuclides and metal centres currently available for therapeutic use, and a discussion and comparison between metal and organic-based contrast agents. Chapter 1 also contains an introduction to macrocycles and their role as ligands, with particular focus on azamacrocycles and their applications. Finally, a brief introduction to luminescence spectroscopy and optical imaging is made.

Chapter 2 reports the synthetic procedures used, and gives characterisation data for the compounds synthesised and discussed in subsequent chapters.

Chapter 3 investigates the role of the triazine core of the azamacrocycles, showing some compounds of biological interest and the synthesis of new ligands and complexes based on a tetraazamacrocycle (DO3A) moiety with a triazine core. One example has been successfully used to study the coordination chemistry and structure of different metal centres, while another has shown promise with a potential application in mimicking dipyridamole compounds. Moreover it has been conducted a study to determinate the empirical formula and the nature of the complexes in solution.

Chapter 4 contains an introduction to the benzothiazole group, which has relevance in the study of Alzheimer's disease as it is a biological marker for metal-dependant formation of Aβ plaques. The synthesis of new ligands derived from several macrocycles (including those reported earlier, and those containing an acyclic moiety with a benzothiazole core) are reported, including procedures to produce complexes of lanthanides and PET-active metal centres including copper, vanadium and gallium. Benzothiazole ligands and complexes have been characterised by fluorimetry, allowing discussion of the role of the ligand.

Finally, in chapter 5 results for one compound (V-DO3A-Bz-epox) are reported, showing encouraging results *in vivo* studies (in a mice model) as a novel PET contrasting compound.

ACKNOWLEDGEMENTS

First I would like to thank Professor Peter G. Edwards and Dr. Ian Fallis for giving me the opportunity and for all the advices and guidance to become a better chemist.
Dr Stephen Paisey for the PET data and for the help in the PETIC centre; Professor Paul Morgan and Dr. Timothy Hughes to provide the mice used to collect the PET data; Dr. Simon Pope for the collection of the fluorescence measurements and finally thanks must to be given to Dr. Paul Newman for the help and advices along these years.

I am very grateful also to all the professional services staff at Cardiff University; especially Dr Rob Jenkins, Robin Hicks, Simon Waller, Tom Williams, Jamie Cross, Simon James and Gaz Coleman; without their professionalism it would have been impossible to complete this work

Thanks to all the former Edwards' group in particular Brendan, Lenali and Mark for making me feel part of this group since the first day. Thanks to all the people in the Fallis' group, particularly to Seni, Andy (the two best post doc that I had), Gez and Siôn for all the times spent working together; and to all the people across the chemistry department, in particular Adam, Alex, Corey, Emily, Lara, Sam, Stokes and Yashar.

I have to mention also Marco and Tatiana for their friendship every moment during these years and Alba, Dana, Luis and Rob who became more than housemates but friends that supported me and for the time spent outside the lab.
From this point it will be a little different...

Devo ringraziare inoltre il gruppo di italiani in erasmus (Giulio, Luca, Ludovica, Max e Nicolò) è stata una breve ma intensa esperienza e mi avete fatto sentire come se fossi a casa. I miei amici sparsi per l'Europa e chi è rimasto in Italia con cui è stato come non

esserci mai lasciati ogni volta che tornavo a casa; non posso dire che grazie a Lara in particolare per gli ultimi mesi del dottorato.

Infine devo ringraziare i miei genitori e mia sorella Monica che sono sempre stati presenti anche se lontani e che mi hanno sostenuto nelle mie scelte lungo tutto il mio percorso per arrivare a questo punto.

Thank you, Grazie, Diolch.

"La carpa è diventata un drago"

G. Picariello

ABBREVIATIONS

AD	Alzheimer's disease
AP	Atmospheric pressure
APP	Amyloid precursor protein
Arg	Arginine
Asp	Aspartic acid
Aβ	β-amyloid
BBB	Blood-brain barrier
BFC	Bifunctional chelator
br	Broad
$CHCl_3$	Chloroform
CT	Computed Tomography
cyclam	1,4,8,11-tetraazatetradecane
cyclen	1,4,7,10-tetraazacyclododecane
d	doublet
DCM	Dichloromethane
DFO	deferoxamine
DMSO	Dimethyl sulfoxide
DO3A	2,2',2''-(1,4,7,10-tetraazacyclododecane-1,4,7-triyl)triacetic acid
DOTA	1,4,7,10-tetraazacyclododecane-1,4,7,10-tetraacetic acid
DTPA	Pentetic acid
EC	Electron Capture
ECM	Extracellular matrix
EI	Electron ionisation
ENT	Equilibrative nucleoside transporter
ES	Electrospray
Et_2O	Diethyl ether
Et_3N	Triethylamine
EtOH	Ethanol
FDA	Food and Drug Administration
FDG	Fluorodeoxyglucose
Gly	Glycine
HMM	hexamethylmelamine
HOPO	Octadentate hydroxypyridinonate

HR	High resolution
ITLC	Instant Thin Layer Chromatography
m	multiplet
MeOH	Methanol
MRI	Magnetic Resonance Tomography
MS	Mass spectra
NIR	Near infrared
NMR	Nuclear Magnetic Resonance
OTf	Triflate
PET	Positron Emission Tomography
PI3K	Phosphatidylinositol 3-kinase
PiB	Pittsburgh compound B
Pro	Proline
RGD	Arg-Gly-Asp
s	singlet
S_NAr	nucleophilic aromatic substitution
t	triplet
TACN	1,4,9-triazacyclononane
TETA	1,4,8,11-tetraazatetradecane-1,4,8,11-tetraacetic acid
TFA	Trifluoroacetic acid
THF	Tetrahydrofuran
ThT	Thioflavin T
UV	ultraviolet
Val	Valine
WHO	World Health organisation
ZSTK474	2-(2-Difluoromethylbenzoimidazol-1-yl)-4, 6-dimorpholino-1, 3, 5-triazine

CONTENTS

CHAPTER 1

INTRODUCTION

1.1 - Positron Emission Tomography

During the past ten years molecular imaging has become the technique of choice for the management of patients with cancer and other diseases, as well as a valuable investigative method for the study of drug action and the development of new therapeutic approaches. Positron Emission Tomography (PET) is a nuclear medicine tomography modality and at present one of the fastest growing research areas. PET imaging is currently used in three main areas: cancer diagnosis and treatment, cardiac surgery and neurology. In cardiac surgery the PET imaging finds application mainly through the use of ^{13}N-ammonia to measure myocardial perfusion, and how the heart functions through blood flow studies. In neurology PET is used for management of brain tumours, especially those causing para neoplastic symptoms, and has been shown to give earlier diagnosis and determination of dementia like Alzheimer's disease. Finally oncological PET is used for a wide variety of reasons as well as diagnosis of active and regressive tumours, the aggressiveness of tumour, the identification and spread of the cancer, and the response to therapies.

The wide possible applications of PET imaging led researchers and engineers to improve different technical aspects. The imaging regime requires a tracer that can be administered to the patients; typically the structure can be divided in two different moieties, a biomolecule that must interact with the selected targeting group and a positron emissive radionuclide (Figure 1.1). After administration, suitable time is allowed for the radiomolecule to locate the tumour mass or the β-amyloid protein in the case of Alzheimer's disease for example, then the patient is placed within a detector and an image of the scan recorded and analysed. This is a fast growing research field, many results have been obtained since the first human scan in 1974; with more specific molecules able to react better with the targeting group and leaving the patients less exposed to the radionuclide, with more and more sensitive detectors being designed, allowing patients to be scanned with a higher resolution and at a higher turnover.

Currently modern PET scanners are combining different imaging modalities to allow fusion of various imaging techniques, such as PET-CT (Computed Tomography) or PET-MRI (Magnetic Resonance Tomography), giving anatomic and metabolic information; so that areas of abnormality on the PET imaging can be more perfectly correlated with anatomy with the second technique.[1]

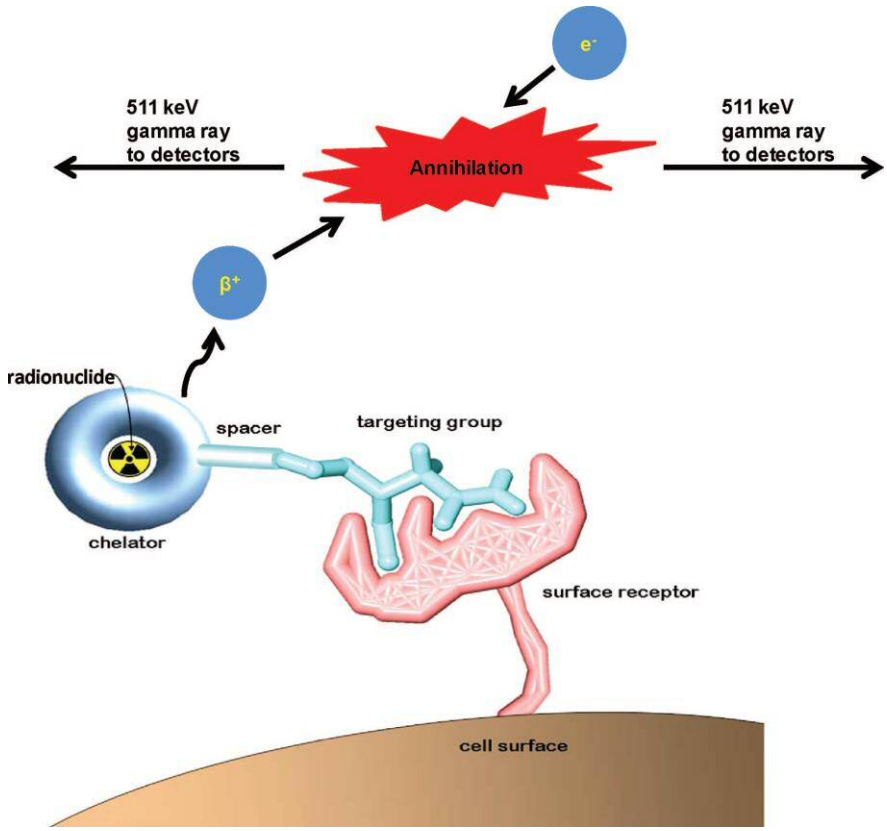

Figure 1.1: structure of a chelate radionuclide with linker[2]

1.1.1 - Physical foundation of PET

The essential concept underpinning positron emission tomography is the capacity of a positron to annihilate an electron with the resultant emission of two photons in opposite directions. The positron is a subatomic particle with the same mass of an electron but opposite charge, which was postulated for the first time by Dirac in 1928 and observed experimentally by Anderson in 1932.[3] When a positron interacts with an electron, it generates two photons that are emitted simultaneously in opposite directions. Positron emission is the result of radioactive decay, where an unstable nucleus loses energy

energy by emitting a β+ particle and an anti-neutrino, which is required to conserve the lepton number of the nuclear reaction.

The radioactive process that results in positron emission is known as nuclear transmutation, which is the conversion of one element into another through radioactive decay, in this case the production of a positron and anti-neutrino (ν*) as product of the decay of a proton into a neutron, following the general equation:

where Y is the stable neutral daughter nucleus with an atomic number one less than the generator element, and to keep the neutrality an electron is also emitted; X is the proton rich atom that undergoes radiative decay when a proton converts to a neutron with the emission of a positron. The ejected positron can have an energy up to a given maximum which is typically much higher than thermal energy and is slowed by collision with neighbouring atoms until its energy matches that of electrons in the surrounding atoms, the collision can create a positronium, a new particle combining a positron and electron with an half life of around 10^{-7} s. The probability of positronium faormation is higher in gases and metals and much lower in human tissue where direct annihilation is more favourable.

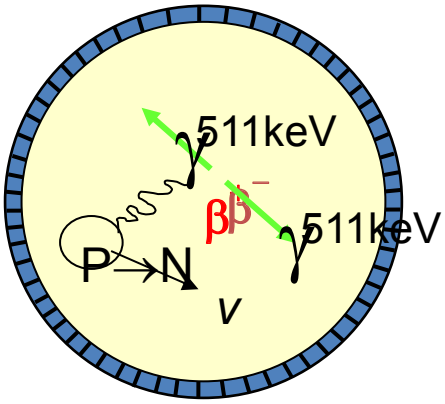

Figure 1.2: emission and annihilation of a positron

Consequently, after the positron is emitted, it travels a short distance before it is annihilated by combination with an electron in a near neighbouring atom (Figure 1.2).

The annihilation process generates two photons of the same energy 511 keV, which can be calculated using Einstein's energy-mass equation:

The two photons are emitted in almost exactly opposite directions and are detected by the PET detector (scintillation counters). Importantly, the energies of the photons are much different from the energies of photons arising from natural background or other non-PET isotopes limiting improvinf signal-to-noise ratios.[3-4]

1.1.2 - Radionuclides in PET

The first radionuclides used in PET were isotopes such as ^{18}F, ^{15}O, ^{13}N and ^{11}C that were incorporated into small molecules with biology activity.[5] One of the best molecules for investigating biological processes, specifically glucose metabolism, is ^{18}F-Fluorodeoxyglucose (^{18}F-FDG), which is used to image lung, heart, brain and tumours in oncology (Figure 1.3).

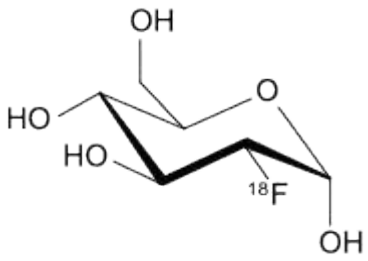

Figure 1.3: ^{18}F-FDG

Unfortunately, drawbacks such as short half-life (^{15}O = 2.03min, ^{11}C = 20min, ^{18}F = 109.8 min) and rapid clearance do not often permit a full investigation of all biological processes. These problems have driven the research towards another kind of

radionuclides, the metals. Radiometals like Zr, Y, In, Ga and Cu are able to emit positrons and, most importantly, possess a longer half-life (see table 1).[6]

Isotope	$t_{1/2}$ (h)	Decay Mode	**E β^+** (keV)	Production Method
^{60}Cu	0.4	β^+ (93%) EC (7%)	3920, 3000 2000	cyclotron, ^{61}Ni(p,n) ^{60}Cu
^{61}Cu	3.3	β^+ (62%) EC (38%)	1220, 1150 940, 560	cyclotron, ^{61}Ni(p,n) ^{61}Cu
^{62}Cu	0.16	β^+ (98%) EC (2%)	2910	^{62}Zn/ ^{60}Cu generator
^{64}Cu	12.7	β^+ (19%) EC (41%) β^- (40%)	656	cyclotron, ^{61}Ni(p,n) ^{64}Cu
^{66}Ga	9.5	β^+ (60%) EC (10%)	4150, 935	cyclotron, ^{63}Cu(α,nγ)^{66}Ga
^{68}Ga	1.1	β^+ (90%) EC (10%)	1880	^{68}Ge/^{68}Ga generator
^{86}Y	14.7	β^+ (33%) EC (66%)	1221	cyclotron, ^{86}Sr(p,n) ^{86}Y
^{89}Zr	78.5	β^+ (23%) EC (77%)	897	cyclotron, ^{86}Y(p,n) ^{89}Zr

Table 1: properties of selected PET imaging isotopes, EC = Electron Capture, some low abundance positrons have been omitted for clarity[2, 7]

The half-life of the radiometals is an important factor to consider. For practical applications, the half-life must be long enough to allow for the synthesis of the probe molecule and for its diffusion into the body, but it should also be as short as possible in order to limit the patient exposure to the radiation. Consequently, since different clinical applications might have different timescales for the distribution and localisation of the probe molecule at the site of interest (e.g. antibodies tend to have a much longer

biological half-life than small molecules), it is an advantage to have the ability to design probes of varying half lives. This in turn requires the use of different isotopes of different elements and thus the chemical approaches to the synthesis of these probes may vary widely and will require skills in inorganic, organic and biologically related chemistry.

In order to access a range of half lives, it is necessary to utilise metal isotopes. Since it is difficult to incorporate radiometals in the structure of small biological molecules, a common way to overcome this problem is to chelate the metal using a polydentate ligand and a linker which is able to interact with a biological molecule.[2] Of the various potential applications of PET, the incorporation of PET isotopes into antibodies is of current interest and has currently only been done with generic metal-binding ligand systems that are not optimised for metal binding (thus have limitations arising from loss of the radiometal during biological distribution *in vivo* and consequent loss of imaging specificity).[8]

Radiolabeled monoclonal antibodies (mAbs) have shown a considerable potential for diagnosis and treatment of cancer. Molecules like ^{64}Cu-DOTA-T/N-trastuzumab or ^{89}Zr-DFO-T/N-transuzumab[9] are able to specifically bind to target cells and attack or reveal the presence of a cancer. One of the biggest problems is the stability of the imaginging agent in the body. If the complex is not sufficiently stable, the metal can be released by the chelator and accumulate in the body and/or in non target organs. For example, ^{89}Zr is a bone seeking radiometal and if released can build up in the bones at the joints.

The significant advantage of radioactive metals is the longer half-life compared to the organic molecules. Unfortunately, they cannot be normally be directly incorporated into small molecules with relevant biological activity. Bifunctional chelators (BFC) are an attractive method to circumvent this problem, by providing a core to facilitate site-specific delivery to a biological target and another core to bind the "hot" metal. Normally a macrocycle is defined as cyclic polydentate ligand with 8 or more ring members and at least three donor atoms.[10] Macrocyclic chemistry is a vast field and there are different kind of compounds that can be included in this class like porphyrin rings, catenanes, crown ethers, cyclophanes, or cryptands to name a few (Figure 1.4).

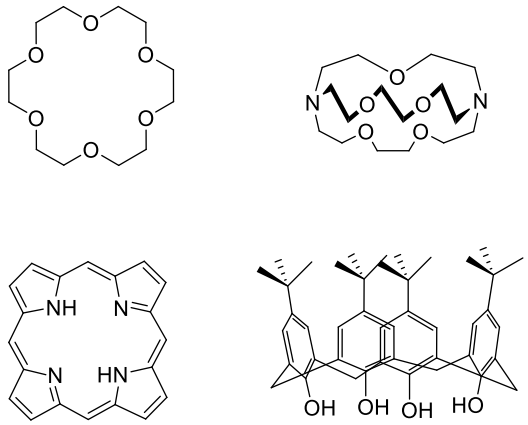

Figure 1.4: examples of macrocycles

Having a huge number of compounds included in this category make also possible varied uses such as liquid crystals[11] or surfactants[12]; but even for biological applications as anti-HIV / AIDS[13] treatments, biological tracers[14], protein labelling[15], antitumour agents[16] and imaging agents.[17] The main characteristics of these compounds are the cavity size, the dimension of the ring, the number and type of possible donor positions, steric effects present on the ring, and substitute groups able to change the number of donor atoms ligand are features that can change or influence the coordination of the metal.[18]

1.2.1 - Azamacrocycles

Azamacrocycles are a particular group in the macrocyclic ligand field, with all the compounds presenting nitrogens as donor atoms. The ability to bind a suitable metal for imaging is also improved by the easy capacity to functionalise the amine moieties on the ring. There is wide range of azamacrocycles in literature[19], but actually the research is more focused on the 1,4,7-triazacyclononane (TACN), 1,4,7,10-tetraazacyclododecane (cyclen) and 1,4,8,11-tetraazatetradecane (cyclam) (Figure 1.5).

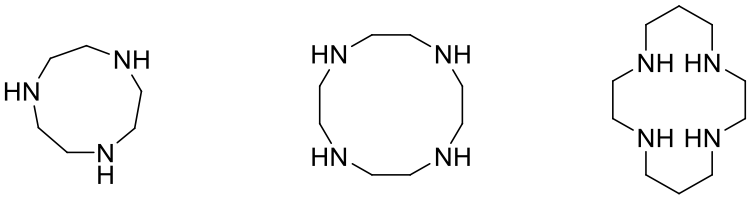

Figure 1.5: TACN (left), cyclen (centre) and cyclam (right) structures

The macrocycles have found applications in many biological areas, like radioactive diagnosis, cancer treatment or magnetic resonance imaging (MRI) contrast agent.[19] As MRI agents the main results have been obtained using a gadolinium(III) metal bound to a functionalised ring with carboxylate arms called 1,4,7,10-tetraazacyclododecane-1,4,7,10-tetraacetic acid (DOTA)[20] or 1,4,8,11-tetraazatetradecane-1,4,8,11-tetraacetic acid (TETA)[21] depending on which ring is used (Figure 1.6).

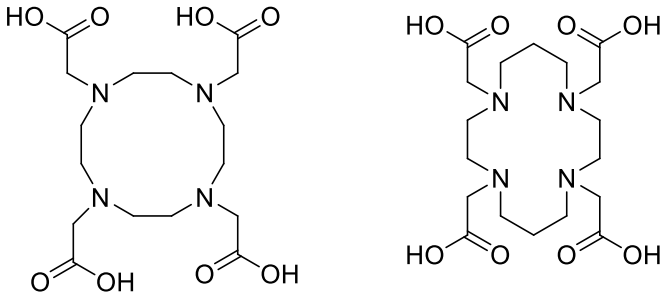

Figure 1.6: DOTA (left) and TETA (right) structures

1.2.2 - Chelate effect

The chelate effect can be described as the higher stability constant of a chelated complex than a non-chelated analogue. It can be demonstrated by comparing the reaction of a chelating ligand and a metal ion with the corresponding reaction involving unidentate ligands, an example being:

through the equation

It is possible to see that the Gibbs free energy is related to the equilibrium constant K, a larger equilibrium constant means a more stable complex; furthermore ΔG° depends on both enthalpy and entropy. While the enthalpy values are comparable due to the bond formation similar for both of the complexes, it is simple to see how the main difference is considering the entropy. The first equation involves three species being converted in three new species, not resulting in a particularly large entropy change. However the second equation is different, there are initially two different species that are converted into three new species, representing an increase in disorder in the system. This means that the entropy term of the third equation (- TΔS°) makes a larger negative contribution to ΔG°, resulting in a larger equilibrium constant.[22]

An additional factor to consider is the tethering effect, if the chelate and the monodentate ligand are in competition to coordinate the metal both have the same chance to bind the metal the first time. After that the chelate ligand is more likely to coordinate the metal

centre with a second pendant, because the second donor is closer than an unlinked donor not coordinated.[18] This is essentially a kinetic effect.

As examples of chelate ligands that have found large application in the imaging chemistry there are 3,4,3-LI-1,2-HOPO (HOPO)[23] and deferoxamine (DFO) (Figure 1.7). In particular DFO has been one of the most commonly employed chelating agents since 1970s, originally isolated from the fungus *Streptomyces pilosus*. The main use in nature and in medicine is in chelation therapy to treat iron overload. DFO is a hexadentate ligand, provided by the three bidentate hydroxamate moieties it can provide a good Fe complexation even *in vivo*, coordinating the metal centre in a distorted octahedral geometry.[24] Moreover considering these features made DFO a possible available ligand to be used with ^{68}Ga. Fe(III) and Ga(III) have similar Van der Waals radii, 62 pm for Ga^{+3} and 65 for Fe^{+3}, and according to the high charge density of the positive ion (+3) and small size, both prefer hard donors as ligands. Both Fe(III) and Ga(III) are 6 coordinate favouring octahedral geometry.[25] Considering these features it has been possible develop and test new ligands, bearing ^{68}Ga and ^{89}Zr as imaging metal, and linking the complex to an antibody to localise the desired compound.[5, 8-9, 23a, b, 26]

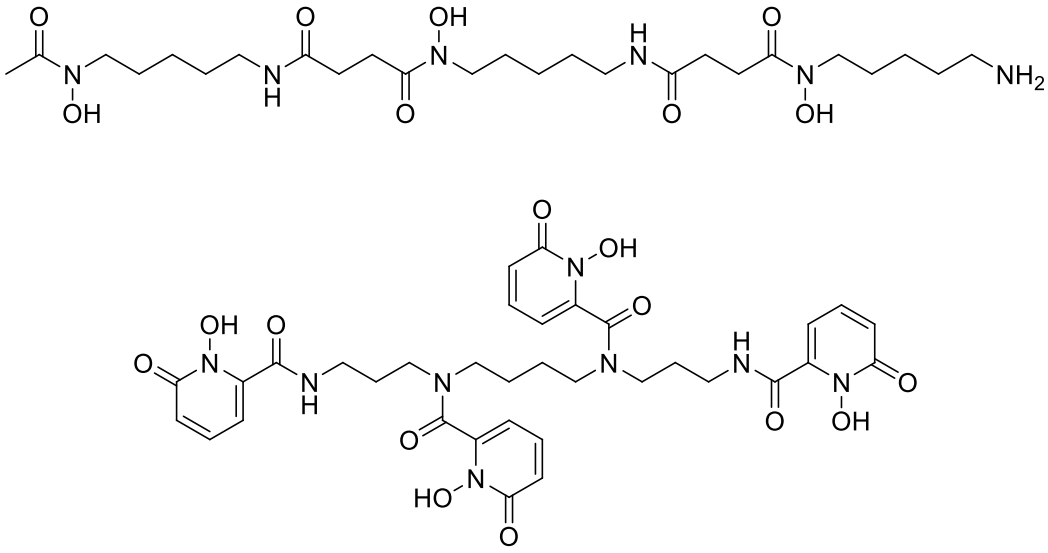

Figure 1.7: DFO (top) and HOPO (bottom) structures

1.2.3 - Macrocyclic effect

The macrocyclic effect may be regarded as an extension of the chelate effect. Macrocyclic ligand complexes tend to high stabilities and can display considerable kinetic inertness. Enthalpic and the entropic parameters are the two factors that must be evaluated considering the stability of a compound. The entropy is the cause of the increased stability for the chelate compound compared to unidentate analogues. The increase of disorder cannot be a factor analysing the equilibrium constants between a multidentate ligand and a macrocycle, since both reactions tend to have positive (favourable) entropy terms. Furthermore considering the macrocycle ligand there is a lower rotation freedom than a linear multidentate ligand, implying slower complex formation kinetics in comparison to chelate ligands. Thus the macrocyclic effect is largely enthalpic in origin. For example, if the macrocyclic ligand has the right cavity size for the metal that is going to coordinate, the metal-donor bonds will be significantly stronger that those that are strained.[22]

1.3 - LUMINESCENCE

When molecules are exposed to electromagnetic radiation there is an interaction between the electric field of the incident radiation and the electrons of the molecule. If the energy of the photon is the same as the energy difference between two electronic states of the molecule, there is a high probability that the compound will absorb a photon and pass from the ground state to an excited state of higher energy. This is the absorption process. The molecule, in returning to the ground state, loses energy that can be emitted as a photon. This process is known as luminescence. Radiation emitted or transmitted by a sample can be used to extract information on the electronic structure of the compound itself. The most common techniques to observe this phenomenon are the ones that use the wavelengths of electromagnetic radiation between 100 and 1000 nm. This spectrum includes the near UV, the visible that covers between 400 and 700 nm, and the near infrared. The photon energy range is around from 1 to 10 eV (28-280 kcal mol^{-1}).

1.3.1 - Fluorescence and Phosphorescence

When electrons move from a higher and excited level of energy to one lower, the energy released can be emitted as electromagnetic radiation. This phenomenon is called luminescence. The features about wavelengths and intensity of the emitted radiation are controlled by some rules at the base of the molecular excitation, in fact not all the transition between the energy states are allowed. The selection rules are complex and deduced from quantum mechanics. A full discussion of these rules is beyond the scope of this thesis, but the general law states that transitions are allowed when the difference between the spin quantum numbers of the two states is zero ($\Delta S = 0$, spin conservation). Generally the rule envisions the spin multiplicity, $2S+1$, that represents the number of possible orientations of spin angular momentum along the z direction. In this case the spin configurations can be classified as singlet ($2S+1 = 1$, $S = 0$), doublet ($2S+1 = 2$, $S = 1/2$), triplet ($2S+1 = 3$, $S = 1$), and so on.

Most organic molecules after the absorption of a quantum of light undergo a transition from the singlet ground state to an excited singlet state in a time scale of 10^{-15} s with the resulting excited singlet state characterised by a spin quantum number with S = 0. An electron promoted to an excited state can have the spin aligned or not aligned to the one left in the ground state (Figure 1.8). So, every promotion can, theoretically, create two different states, a singlet and a triplet; the triplet that has a lower energy level but it is not accessible due to the selection rules.

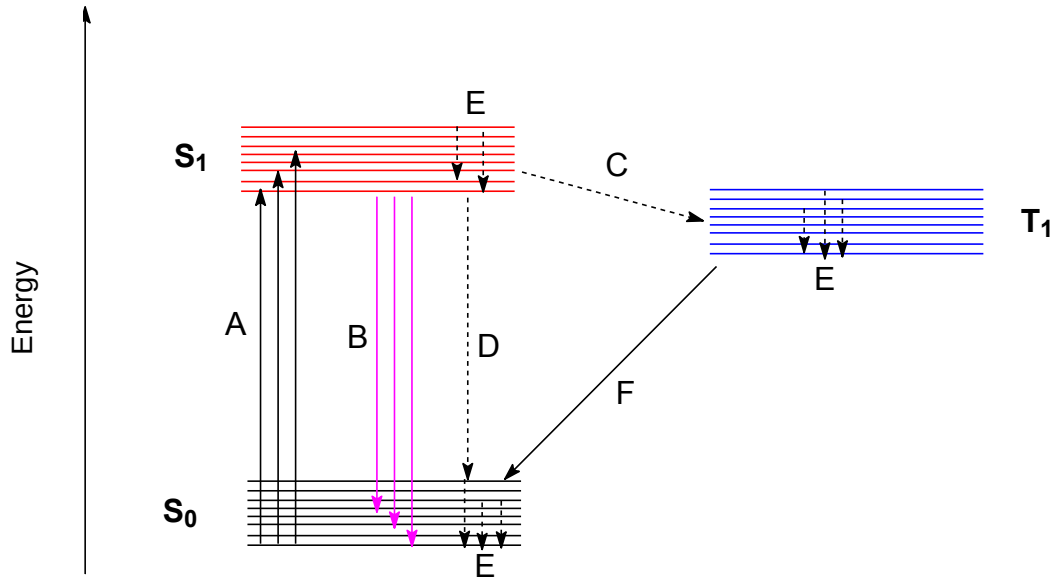

Figure 1.8: simplified Jablonski's diagram that describes the transition from the ground state (S_0) to one excited (S_1, singlet, T_1, triplet) and from this one to the ground state. The arrows represent radiative transaction, those dotted non radiative vibrational relaxation. A: absorption; B: fluorescence; C: intersystem crossing; D: internal conversion; E: vibrational relaxation; F: phosphorescence

Every excitation/relaxation process can be explained in the scheme above. When the photon is absorbed the allowed transition is between the ground singlet state, S_0, and the excited singlet state, S_1 ($\Delta S = 0$). The Franck-Condon principle rules that these transitions can be represented by the vertical lines in the figure 1.9, due to the fact that, during the electronic transition, the nuclear framework does not react, as the vibrational transitions occur much slower.

Immediately after the excitation, and before any kind of photochemical reaction or emission of radiation starts, there is a sequence of events. First of all there is an "internal

conversion": it does not matter which vibrational level of the excited singlet state has been reached, there is always a quick return to the lowest vibrational level accessible of the excited singlet state, without any emission of radiation, the excess of energy is released as heat (non radiative recombination), in a time scale on the order of 10^{-12} s and all the molecules reach the ground vibrational level of the electronic excited state (Kasha's rule). The average time scale in an excited electronic state is relatively longer: 10^{-9} s and all the molecules can relax vibrationally before the decay of the excited state. Therefore it is from this state that the molecules decay to the ground electronic state; this relaxation results in the emission being of lower energy than the excitation, and the difference between the two energies levels is referred to as the Stokes shift.

The behaviour of the molecules until this point is indistinct; the first different depends from the surrounding molecules; if these are able to absorb the remaining energy in excess of the excited molecule, this can complete its relaxation *via* non radiative recombination, otherwise fluorescence and phosphorescence processes can be detected. In order to have a fluorescence process, the molecule must reach, via non-radiative way, the lowest vibrational level of the excited electronic state, then the excess of energy is emitted as radiation in a time scale of 10^{-9} - 10^{-8} s. The transition is towards the lower energetic level and the fluorescence spectrum is referred to the vibrational structure characteristic of the lowest electronic state; this means that the relaxation process can lead to any vibrational level of the ground state. For this reason the observed emission (and absorption) spectra are broad and affected by changes in temperature.
The relaxation process can also follow a second mechanism: if the molecule has a accessible triplet state in the excited electronic state, with energy slightly lower than the singlet excited state. There is also the possibility that the potential energy curves of the two states can cross each other as reported in figure 1.10.

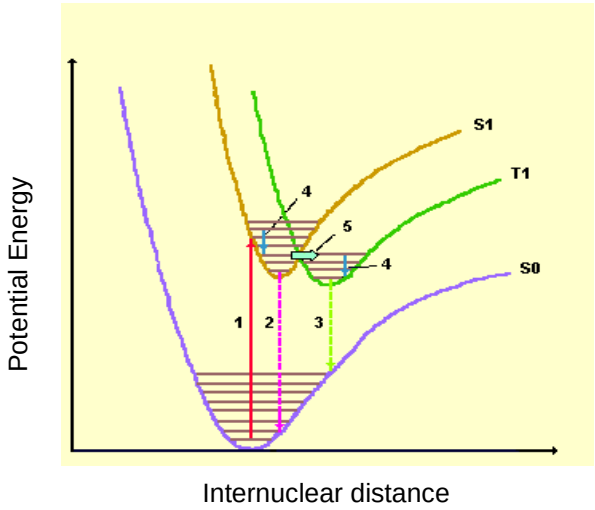

Figure 1.9: Potential energy levels for a diatomic molecule. 1, excitation; 2, fluorescence; 3, phosphorescence; 4, internal conversion of vibrational states S_1 and T_1; 5, intersystem crossing

Therefore there is the possibility of conversion from singlet to triplet called intersystem crossing; process that involves the spin-orbit interaction. Simplifying, it regards the interaction between the spin magnetic moment and the electron magnetic moment, the rotation of the electron around the nucleus; and the interaction is particularly relevant considering atoms with a high atomic number like S, Br, I, and so on.

The magnetic interaction can happen also with the spin magnetic dipole of unpaired electrons of the compounds, for example in presence of transition metals with unpaired electrons in the d orbitals (paramagnetic complexes). Once the interaction has taken place, the molecule gives energy to the environment in a non-radiative way until to reach the vibrational ground of the triplet excited electronic state. This state is lower than the singlet excited state and the molecule cannot relax because the transition to the ground state is not allowed, being a passage from a triplet state to a singlet ($\Delta S \neq 0$), but the spin/orbit interaction, that was responsible also for the intersystem crossing breaks the selection rule and allows a relaxation, even if particularly slow. The light emitted from this transition is the classical phosphorescence. Since the transition from triplet to singlet is forbidden, the average time scale of the triplet state is quite long, from 10^{-3} to 10^{3} seconds, therefore the phosphorescence can be observed also after the exciting radiation has been turned off.

1.3.2 - Lifetimes

One of most important differences between the fluorescence and phosphorescence is the length of the emissive lifetime. The lifetime ( ) is defined as the average time that molecules spend in the excited state before relaxing to the ground state. From the excited state for a compound there are different paths to relax to the ground state. A molecule can be subject to a chemical process given a different product ( ), can release in a non-radiative way the energy absorbed (k_{nr}) as mentioned and finally can relax in the radiative process, with the release of the energy from the excited state as light (k_r). The lifetime of the excited state can be expressed as the rates of the three relaxation processes mentioned before as the equation:

The equation can be rewritten considering the luminescence properties of a metal complex compound and expressed in terms of the rates of luminescence ( ), intersystem crossing, ISC ( ) and internal conversion, IC ( ).

1.3.3 - Quantum yield

Another important parameter in fluorescence is quantum yield (Φ), which is defined as the number of emitted photons in relation to the number of photons absorbed.

The efficiency of the radiative process can be expressed by the quantum yield, considering the radiative emission process and also the rate of non radiative decay k_{nr}; to have an efficient quantum yield, close to unity, the luminescence must be much greater than the non-radiative emission process and the term can be arranged in the following equation.

1.3.4 - Lanthanides as luminescence probes

The desirable features for a luminescent probe are fundamentally a large stokes shift between the emission and absorption spectra and a long luminescence lifetime. Considering the metals, these features can be found in the *d*-block and *f*-block (lanthanide) series. Lanthanides have a wide scope of emission profiles in the UV, visible or NIR regions, as well as a larger Stokes shifts than *d*-block metals and significantly longer luminescence lifetimes. However, *f* - *f* transitions associated with this series are forbidden due to the Laporte rule, and thus these transitions have low molar absorptivities. To resolve this disadvantage, the metal can be coordinated to a chelate molecule that possesses a light harvesting 'antenna group' (Figure 1.10).

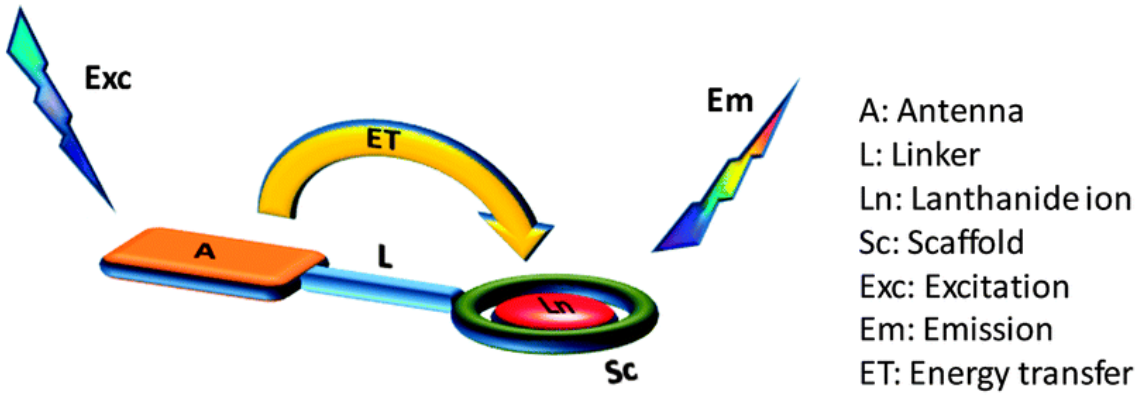

Figure 1.10: representation of an antenna system[27]

The antenna is often an organic compound that can easily absorb energy (as the electronic transitions are fully allowed) and transfer it to the 4*f* excited state of the metal, often a triplet excited state. As example of cell imaging is that reported by Wong;[28]; the group synthesised europium and terbium complexes coordinated to a DO3A macrocycle and tested *in vitro* on human cervical carcinoma cell (HeLa) to investigate the time-uptake and localization profile, showing that the compounds can enter in the cancer cells effectively and that the uptake depends from the concentration of the solutions used (Figure 1.11).

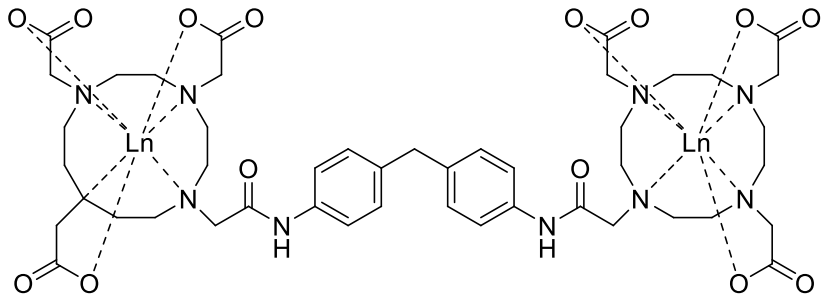

Figure 1.11: one of the compound synthesised and tested on human cervical carcinoma cells[28]

Another application for the lanthanide associate to a macrocycle has been developed by Hermann,[29] binding an europium metal centre to a DO3A ring. The compound has revealed a high sensitivity to the concentration of different anion; for instance, the replacement of the two molecules of water coordinated to the europium with picolinate acid increases the intensity of the luminescence probes, this due to the fact that the picolinate anion works better as antenna for the complex and the substitution of the water molecules removed the quenching factor provided by the vibrational O-H bonds.

The replacement of molecules of water can be obtained by substitution with another anion or changing the coordination geometry of the compound. Raymond's group investigated the geometry of 1,2-HOPO derivates coordinating an europium metal centre[30] (Figure 1.7). The luminescence properties are influenced by the length of the central bridge of the ligand, a short bridge constraint the structure in a geometry that allowed water in the inner coordination sphere, while increasing the length of the central bridge allows to the ligand a better protection of the metal centre, removing the luminescence quenching factor provided by the O-H bonds.

1.3.5 - Optical Imaging

The luminescence properties described have found application in the optical imaging, in particular in fluorescence microscopy.[4] The advantages of this technique are multifold, with high resolution at cellular level, high sensitivity and low cost; unfortunately there are also some problems with this technique as background emission (autofluorescence), photobleaching that is photochemical loss of imaging agent, low penetration in the tissues and the risk of damage to the tissues using an excitation lambda near the ultraviolet, make it unsuitable for *in vivo* excitation. Thus optical imaging is a perfect technique to understand biological pathways especially at a cellular level or to quantify and localize the uptake of a molecule in a cell.

Benzothiazoles are a perfect example of organic compounds with luminescence properties that can be used with the confocal microscopy. As previously mentioned benzothiazoles are utilised to stain β-amyloids but have found applications as antitumor agents.[31] Steven's group synthesised different 2-(4-aminophenyl)benzothiazoles derivates and investigated them as novel class of antitumor agents. The compounds have been tested *in vivo* and *in vitro* on various cell lines, resulting ineffective on prostate, colon, ovarian, melanoma and bladder cell lines, but some compounds have been discovered with an high cytotoxic activity against mammary carcinoma. The mechanism of action has not been fully understood and explained but it has been possible to investigate the uptake of two compounds into two cell lines through the confocal microscopy at different concentrations and after 24h, 72h and 7 days exposure (Figure 1.12).

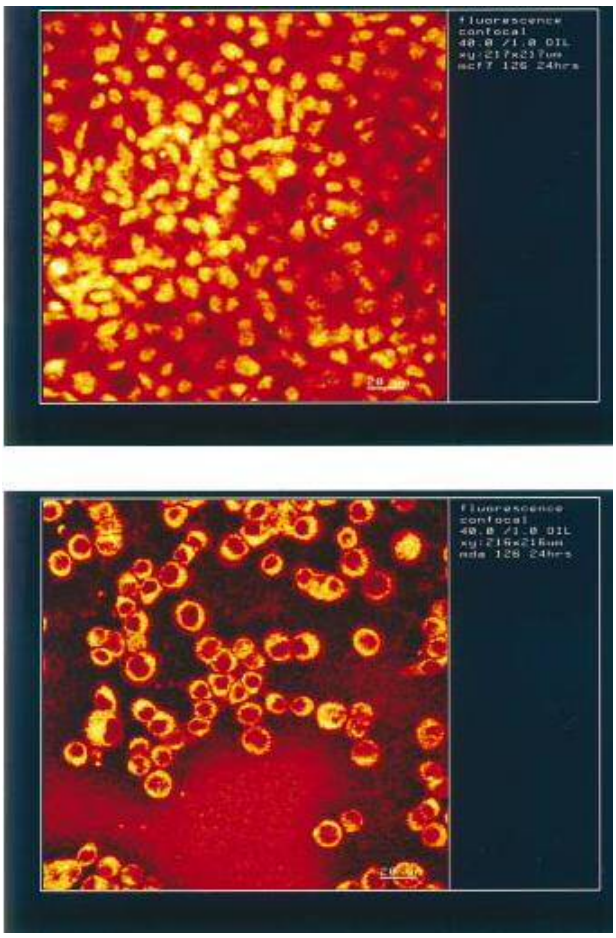

Figure 1.12: Confocal microscopy photographs of one compound tested on tumor breast cell lines after 24h exposure to 30 μM solution.[31]

As previously reported benzothiazoles can be even used to stain β-amyloid and the topic will be treated more deeply in the chapter 4. Storr's group synthesised a new class of ligands including a benzothiazole core combined with 1,2,3-triazole moiety.[32] The study investigates and characterises the photophysical properties of the compounds and tests them *ex vivo* on mouse brain sections with the presence of β-amyloids. The benzothiazole derivate shows a high-energy absorption peak at 313 nm and λ_{em} = 391 nm, then the emission and excitation spectra has been recorded in absence and presence of β-amyloids plaque, using a 50 μM solution, showing a reduced fluorescence emission intensity around the 20%, a behaviour opposite to the classic ThT, which shows and increase in the emission intensity. Finally the molecule has been tested with and anti-Aβ antibody to see if able to bind the plaques present in the mouse brain sections (Figure 1.13)

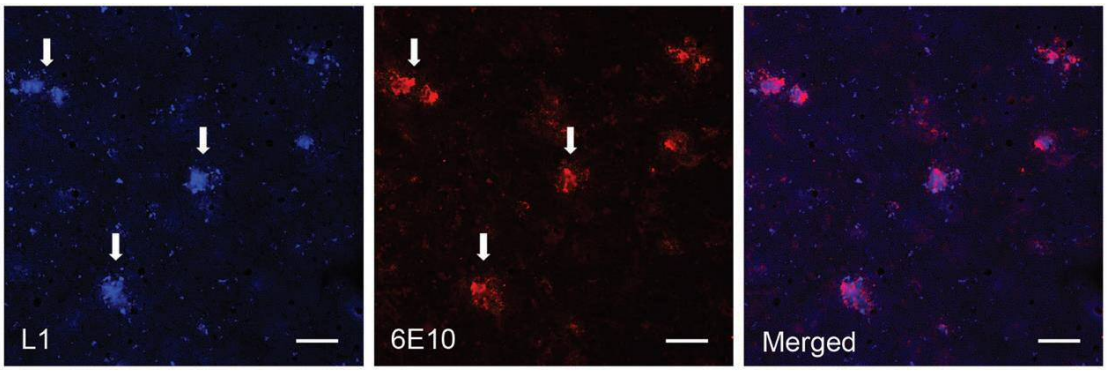

Figure 1.13: Fluorescence microscopy images of β-amyloids aggregate stained with the ligand tested (left), the anti-Aβ antibody (centre) and the two images merged (right).[32]

As the image shows the ligand is able to bind and stain Aβ plaques with the emission recorded equal to ~ 470 nm, leaving the possibility of further development in this new class of ligands.

As mentioned not only the organic molecules are used with the confocal microscopy, Long's group[33] synthesised new compounds based on rhodamine, an organic molecule widely used to determine the lower mitochondrial potential in the tumour cells, bearing a DO3A macrocycle to coordinate the lanthanide metals. The study investigated the luminescence properties of four complexes of Gd and Tb and even the *in vitro* and *in vivo* studies through the confocal microscopy of human embryonic kidney cells (HEK293) and primary mouse islet cells. The rhodamine moiety of the compound, using excitation light at 560 nm, yielding an emission band centred at 580 nm, with a small but expected Stokes shift. The Tb(III) complexes were investigated under excitation at λ_{ex} = 310 nm, showing a stronger intensity and a longer lived emissive state (λ_{em} = 490, 545, 585 and 620 nm), proving an efficient ligand for terbium(III) energy transfer. Unfortunately, due to the optical cut-off of many commercial confocal microscopy set-ups, it is generally impossible to use the λ_{ex} of the Tb complex *in vitro* or *in vivo*; so taking advantages of the possibility to use of a dual modal technique (MRI/fluorescent) one of the gadolinium complexes has been tested, showing the accumulation properties of the compounds in the mitochondria of HEK cells.

[1] D. Brasse and A. Nonat, *Dalton Transactions* 2015, *44*, 4845-4858.

[2] T. J. Wadas, E. H. Wong, G. R. Weisman and C. J. Anderson, *Chem. Rev.* 2010, *110*, 2856-2902.

[3] D. W. T. Dale L Bailey, Peter E Valk and Michael N Maisey, *Positron Emission Tomography: Basic Sciences*, Springer Ed., 2005.

[4]E. W. Price, C. Orvig, *The Chemistry of Molecular Imaging*, editors: W. Wing-Tak. N. Long, Wiley, 2014.

[5] S. L. Rice, C. A. Roney, P. Daumar and J. S. Lewis, *Semin Nucl Med* 2011, *41*, 265-282.

[6] C. J. Anderson and M. J. Welch, *Chem. Rev.* 1999, *99*, 2219-2234.

[7] a) F. Kraeber-Bodéré, C. Rousseau, C. Bodet-Milin, C. Mathieu, F. Guérard, E. Frampas, T. Carlier, N. Chouin, F. Haddad, J.-F. Chatal, A. Faivre-Chauvet, M. Chérel and J. Barbet, *International Journal of Molecular Sciences* 2015, *16*; b) T. K. Nayak and M. W. Brechbiel, *Bioconjug Chem* 2009, *20*, 825-841; c) K. Serdons, A. Verbruggen and G. M. Bormans, *Methods* 2009, *48*, 104-111.

[8] Y. Zhang, H. Hong and W. Cai, *Current Radiopharmaceutical* 2011, *4*, 131-139.

[9] a) B. M. Zeglis, P. Mohindra, G. I. Weissmann, V. Divilov, S. A. Hilderbrand, R. Weissleder and J. S. Lewis, *Bioconjug Chem* 2011, *22*, 2048-2059; b) J. P. Holland, E. Caldas-Lopes, V.

Divilov, V. A. Longo, T. Taldone, D. Zatorska, G. Chiosis and J. S. Lewis, *PLoS One* 2010, *5*, e8859.

[10] E. C. Constable, *Coordination chemistry of Macrocyclic Compounds*, Oxford University Press, 1999.

[11] G. H. Walf, R. Benda, F. J. Litterst, U. Stebani, S. Schmidt and G. Lattermann, *Chemistry – A European Journal* 1998, *4*, 93-99.

[12] I. A. Fallis, P. C. Griffiths, D. E. Hibbs, M. B. Hursthouse and A. L. Winnington, *Chemical Communications* 1998, 665-666.

[13] Y. Inouye, T. Kanamori, T. Yoshida, T. Koike, M. Shionoya, H. Fujioka and E. Kimura, *Biological & Pharmaceutical Bulletin* 1996, *19*, 456-458.

[14] S. J. DeNardo, G. L. DeNardo, A. Yuan, C. M. Richman, R. T. O'Donnell, P. N. Lara, D. L. Kukis, A. Natarajan, K. R. Lamborn, F. Jacobs and C. L. H. Siantar, *Clinical Cancer Research* 2003, *9*, 3938s.

[15] A. Lewin, J. P. Hill, R. Boetzel, T. Georgiou, R. James, C. Kleanthous and G. R. Moore, *Inorganica Chimica Acta* 2002, *331*, 123-130.

[16] K.-P. Eisenwiener, M. I. M. Prata, I. Buschmann, H.-W. Zhang, A. C. Santos, S. Wenger, J. C. Reubi and H. R. Mäcke, *Bioconjugate Chemistry* 2002, *13*, 530-541.

[17] a) K. Tanaka and K. Fukase, *Org Biomol Chem* 2008, *6*, 815-828; b) B. M. Zeglis and J. S. Lewis, *Dalton Trans* 2011, *40*, 6168-6195; c) E. W. Price and C. Orvig, *Chemical Society Reviews* 2014, *43*, 260-290.

[18] L. F. Lindoy, *The chemistry of macrocyclic ligand complexes*, Cambridge University Press, 1989.

[19] a) E. L. Que, E. J. New and C. J. Chang, *Chemical Science* 2012, *3*, 1829-1834; b) S. J. Ratnakar and V. Alexander, *European Journal of Inorganic Chemistry* 2005, *2005*, 3918-3927; c) M. Woods, G. E. Kiefer, S. Bott, A. Castillo-Muzquiz, C. Eshelbrenner, L. Michaudet, K. McMillan,

S. D. K. Mudigunda, D. Ogrin, G. Tircsó, S. Zhang, P. Zhao and A. D. Sherry, *Journal of the American Chemical Society* 2004, *126*, 9248-9256.

[20] T. J. Wadas, E. H. Wong, G. R. Weisman and C. J. Anderson, *Current Pharmaceutical Design* 2007, *13*, 3-16.

[21] a) C. A. Boswell, X. Sun, W. Niu, G. R. Weisman, E. H. Wong, A. L. Rheingold and C. J. Anderson, *Journal of Medicinal Chemistry* 2004, *47*, 1465-1474; b) E. A. Lewis, R. W. Boyle and S. J. Archibald, *Chemical Communications* 2004, 2212-2213.

[22] C. A. McAulife, *Comprehensive Coordination Chemistry Vol 2*, Pergamon, London, 1987.

[23] a) M. A. Deri, S. Ponnala, P. Kozlowski, B. P. Burton-Pye, H. T. Cicek, C. Hu, J. S. Lewis and L. C. Francesconi, *Bioconjugate Chemistry* 2015, *26*, 2579-2591; b) M. A. Deri, S. Ponnala, B. M. Zeglis, G. Pohl, J. J. Dannenberg, J. S. Lewis and L. C. Francesconi, *J Med Chem* 2014, *57*, 4849-4860; c) H. Bibi, V. Vinokur, D. Waisman, Y. Elenberg, A. Landesberg, A. Faingersh, M. Yadid, V. Brod, J. Pesin, E. Berenshtein, R. Eliashar and M. Chevion, *Redox Biology* 2014, *2*, 814-819.

[24] P. V. Bernhardt, *Dalton Transactions* 2007, 3214-3220.

[25] R. Frank and J. R. Patrick, *Current Topics in Medicinal Chemistry* 2010, *10*, 1633-1668.

[26] a) M. A. Deri, B. M. Zeglis, L. C. Francesconi and J. S. Lewis, *Nucl Med Biol* 2012; b) G. Fischer, U. Seibold, R. Schirrmacher, B. Wängler and C. Wängler, *Molecules* 2013, *18*; c) J. P. Holland, V. Divilov, N. H. Bander, P. M. Smith-Jones, S. M. Larson and J. S. Lewis, *J Nucl Med* 2010, *51*, 1293-1300; d) J. P. Holland, Y. Sheh and J. S. Lewis, *Nucl Med Biol* 2009, *36*, 729-739; e) I. Verel, G. W. M. Visser, R. Boellaard, M. Stigter-van Walsum, G. B. Snow and G. A. M. S. van Dongen, *The Journal of Nuclear Medicine* 2003, *44*, 1271-1281; f) D. J. Vugts and G. A. M. S. van Dongen, *Drug Discovery Today: Technologies* 2011, *8*, e53-e61; g) T. Yoshida, T. Ozaki, T. Ohnuki and J. Francis Arokiasamy in *Interactions of trivalent and tetravalent heavy*

metal-siderophore complexes with Pseudomonas fluorescens, *Vol. 92* 2004, p. 749; h) E. Boros, J. P. Holland, N. Kenton, N. Rotile and P. Caravan, *ChemPlusChem* 2016, *81*, 274-281.

[27] M. P. Coogan and V. Fernandez-Moreira, *Chemical Communications* 2014, *50*, 384-399.

[28] Y. O. Fung, W. Wu, C.-T. Yeung, H.-K. Kong, K. K.-C. Wong, W.-S. Lo, G.-L. Law, K.-L. Wong, C.-K. Lau, C.-S. Lee and W.-T. Wong, *Inorganic Chemistry* 2011, *50*, 5517-5525.

[29] J. Vaněk, P. Lubal, P. Hermann and P. Anzenbacher, *Journal of Fluorescence* 2013, *23*, 57-69.

[30] A. D'Aléo, E. G. Moore, J. Xu, L. J. Daumann and K. N. Raymond, *Inorganic Chemistry* 2015, *54*, 6807-6820.

[31] M.-S. Chua, D.-F. Shi, S. Wrigley, T. D. Bradshaw, I. Hutchinson, P. N. Shaw, D. A. Barrett, L. A. Stanley and M. F. G. Stevens, *Journal of Medicinal Chemistry* 1999, *42*, 381-392.

[32] C. Dyrager, R. P. Vieira, S. Nystrom, K. P. R. Nilsson and T. Storr, *New Journal of Chemistry* 2017, *41*, 1566-1573.

[33] C. Rivas, G. J. Stasiuk, J. Gallo, F. Minuzzi, G. A. Rutter and N. J. Long, *Inorganic Chemistry* 2013, *52*, 14284-14293.

CHAPTER 2

EXPERIMENTAL

Techniques and instruments: All synthetic procedures and manipulations were performed under dry nitrogen using standard Schlenk line techniques.

Solvents were freshly distilled under N_2 before use over standard drying agents.

All non-synthesised chemicals were obtained commercially from Sigma-Aldrich, Alfa Aesar, Fluorochem, CheMatech and Apollo and used as received.

The NMR spectra were recorded on a Bruker DPX-500 instrument at 500 MHz (^{1}H), and 125 MHz (^{13}C), Bruker DPX-400 instrument at 400 MHz (^{1}H) and 100 MHz (^{13}C).

Chemical shifts were determined relative to 85% H_3PO_4 (δ_P = 0 ppm) or tetramethylsilane ($\delta_{H/C}$ = 0 ppm) and are given in ppm.

Infrared spectra were recorded either as KBr disks on a Jasco FT/IR-660 Plus spectrometer or on a Shimadzu IRAffinity-1S spectrometer equipped with an ATR attachment.

Mass spectra of all the samples have been measured by direct injection into a Waters Low Resolution ZQ Mass Spectrometer at Cardiff University.

UV-Vis measurements were performed on a Perkin Elmer Lambda 20 UV/Vis spectrometer or a Shimadzu UV-1800 spectrometer.

All photophysical data was obtained on a JobinYvon-Horiba Fluorolog-3 spectrometer fitted with a JY TBX picosecond photodetection module and a Hamamatsu R5509-73 detector.

Absorbance measurements were performed on a BMG Labtech FLUOstar Omega plate reader. Samples were examined within a 4titude 4ti-0234 UV96 well plate. Data analysed by Omega Control Software and MARS data analysis software.

X-Ray Crystallography: Data were collected by Crystallography National Service at University of Southampton.

PET experiments were performed by Dr. Stephen Paisey, PETIC centre Cardiff, with mice provided by Professor Paul Morgan and Dr. Timothy Hughes's research group, School of Medicine, Cardiff University.

2.2.1 - Triazine core ligands and complexes

4-(4,6-dichloro-1,3,5-triazin-2-yl)morpholine ($TzMorphCl_2$)

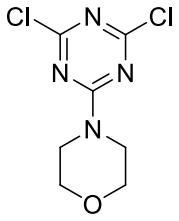

The compound was prepared based on a modified literature method.[1] Cyanuric chloride (25.0g, 135.6mmol) was dissolved in acetone (150mL) and added to ice water (150mL) to form a slurry, and cooled to 0°C. Morpholine (11.81g, 135.6mmol) was dissolved in acetone (120mL), and added dropwise to the stirred solution. $NaHCO_3$ (11.39g, 135.6mmol) was added portion-wise so as to keep the pH neutral. The solution was warmed to room temperature and stirred for 18 hours. The white solid was collected by filtration and recrystallised from hot EtOH yielding the title product as a colourless solid (27.4g, 116.6mmol, 86%). ^{1}H NMR (500 MHz, $CDCl_3$, ppm) δH: 3.85 - 3.82 (m, 4H), 3.72 – 3.69 (m, 4H); ^{13}C NMR (125 MHz, $CDCl_3$, ppm) δC: 170.4, 164.1, 66.4, 44.5.

4,4'-(6-chloro-1,3,5-triazine-2,4-diyl)dimorpholine ($TzMorph_2Cl$)

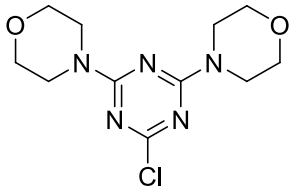

The compound was prepared based on a modified literature method.[1] $TzMorphCl_2$ (27.4g, 116.6mmol) was dissolved in acetone (100mL) and added to ice water (150mL) to form a slurry. Morpholine (10.15g, 116.6mmol) was dissolved in acetone (100mL) and added dropwise to the solution. $NaHCO_3$ (9.79g, 116.6mmol) was added portion-wise so as to keep the pH neutral. The solution was stirred for 18 hours at room temperature, the solid collected by filtration and recrystallised from hot EtOH, yielding the title product as

colourless crystals (23.0g, 80.5mmol, 69 %). ^{1}H NMR (500 MHz, $CDCl_3$, ppm) δH: 3.81 – 3.69 (m, 4H), 3.68 – 3.64 (m, 4H); ^{13}C NMR (125 MHz, $CDCl_3$, ppm) δC: 169.7, 164.5, 66.6, 43.9.

1,4,7-tris(*tert*-butoxycarbonylmethyl)-1,4,7,10-tetraazacyclododecane (DO3A)

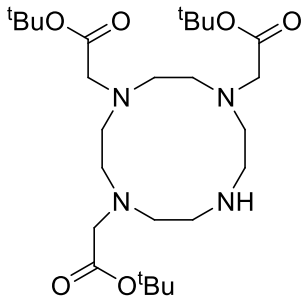

The compound was prepared by literature methodology.[2] To a suspension of cyclen (1.00g, 5,8mmol) and sodium acetate (1.57g, 19.2mmol) in dimethylacetamide (20mL) at -20°C was added a solution of *tert*-butyl bromoacetate (3.73g, 19.2mmol) in dimethylacetamide (5mL) dropwise over a period of 30 min. The temperature was maintained at -20°C during the addition, after which the reaction mixture was allowed to come to room temperature. The mixture was left under stirring overnight. The reaction mixture was poured into water to give a clear solution. Solid potassium bicarbonate was added until the product precipitated as white solid. The precipitate was collected by filtration and dissolved in chloroform. The solution was washed with water, dried with $MgSO_4$, filtered and concentrated *in vacuo* (3.17g, 5.3mmol, 92%). ^{1}H NMR (400 MHz, $CDCl_3$, ppm) δH: 1.44 (s, 9H), 1.45 (s, 18H), 2.86 (m, 4H), 2.91 – 2.92 (m, 8H), 3.08 (m, 4H), 3.28 (s, 2H), 3.37 (s, 4H); ^{13}C NMR (125 MHz, $CDCl_3$, ppm) δC: 28.1, 28.2, 47.6, 48.7, 49.0, 51.1, 51.3, 58.4, 81.4, 82.0, 169.8, 170.5.

Tri-tert-butyl **2,2',2"**-(10-(4,6-dimorpholino-1,3,5-triazin-2-yl)-1,4,7,10-tetraazacyclododecane- 1,4,7-triyl)triacetate (TzMorph$_2$DO3A)

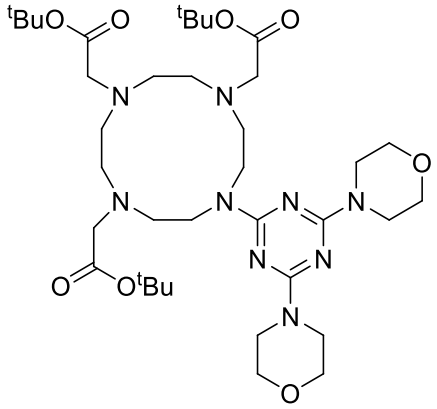

TzMorph$_2$Cl (1.52g, 5,3mmol), DO3A (3.17g, 5.3mmol) and $NaHCO_3$ (0.895g, 10.6mmol) were refluxed in acetonitrile (30mL) under an atmosphere of nitrogen for three days. The mixture was cooled down to room temperature and the solvent was removed *in vacuo*, and the solid dissolved in chloroform, washed with water, brine and then dried over $MgSO_4$. The solvent was removed *in vacuo*, yielding a colourless oil (2.19g, 2.87mmol, 54%). ^{1}H NMR (400 MHz, $CDCl_3$, ppm) δH: 1.43 (s, 9H), 1.45 – 1.46 (m, 18H), 2.81 – 2.73 (m, 12H), 3.07 – 3.04 (t, 4H, J = 6.0Hz), 3.33 – 3.20 (m, 6H), 3.72 – 3.69 (m, 16H).

2,2',2"-(10-(4,6-dimorpholino-1,3,5-triazin-2-yl)-1,4,7,10-tetraazacyclododecane-1,4,7-triyl)triacetic acid (TzMorph$_2$DO3A)

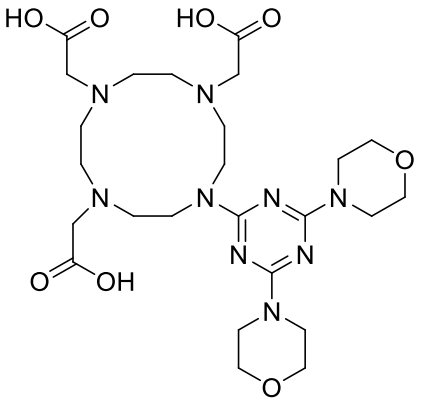

TzMorph$_2$DO3A (1.64g, 2.15mmol) was dissolved in dichloromethane (10mL) and trifluoroacetic acid (9.79g, 85.87mmol) was added. The solution was stirred at room temperature for 48 hours, obtaining a yellow solution. The solvent were removed *in vacuo*, and the residue solid was dissolved in methanol (~10mL), this was repeated at

least three times, yielding an off pale brown oil. The oil was treated with Et_2O, yielding a white solid (1.12g, 1.88mmol, 87%). ^1H NMR (400 MHz, MeOD, ppm) δH: 2.68 – 3.37 (br m, 16H), 3.44 – 3.54 (br m, 6H), 3.56 – 3.68 (m, 16H); IR (νmax, cm^{-1}) 2858 (s), 1728 (s), 1683 (s), 1550 (s), 1532 (s), 1487 (s), 1441 (s), 1362 (s), 1311 (s), 1288 (s), 1258 (s), 1204 (s), 1181 (s), 1155 (s), 1132 (s), 1114 (s), 1087 (s), 1070 (s), 1009 (s), 981 (s), 1019 (s), 912 (s), 880 (s), 861 (s), 830 (s), 808 (w).

2.2.2 - Metal complexes with $TzMorph_2DO3A$ (Et_3N method)

All the complexes have been synthesised following the same procedure. $TzMorph_2DO3A$ (0.300g, 0.50mmol) were dissolved in MeOH (~3mL). The metal salt was dissolved in MeOH (~2mL) and added to the ligand solution. The pH of the solution corrected to basic pH adding Et_3N until there was the formation of a precipitate. The solid was separated by centrifuge.

Ni(II)-$TzMorph_2DO3A$

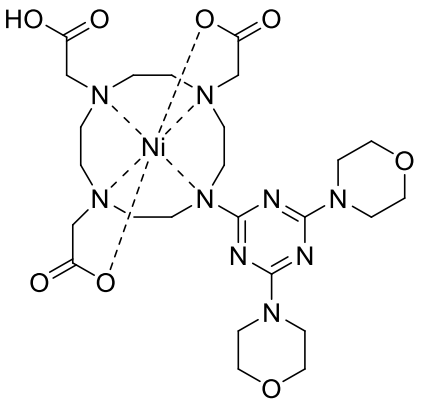

$NiCl_2*6H_2O$ (0.120g, 0.50mmol) was dissolved in MeOH, obtaining a purple solution. MS (HR ES^-) calc. for $C_{25}H_{39}N_9O_8Ni$ (M - H^+) 651.2275 found 651.4038.

Y(III)-TzMorph$_2$DO3A

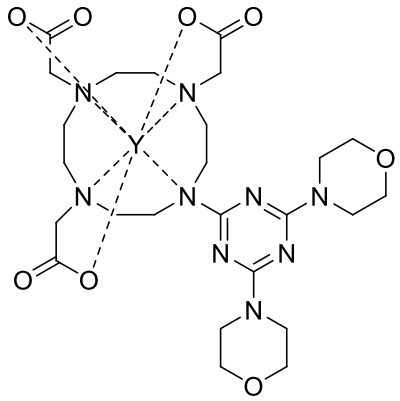

$Y(OTf)_3$ (0.270g, 0.5mmol) was dissolved in MeOH, obtaining a colourless solution. MS (HR ES$^+$) calc. for $C_{25}H_{38}N_9O_8YNa$ (M + Na$^+$) 704.1800 found 704.2403.

Eu(III)-TzMorph$_2$DO3A

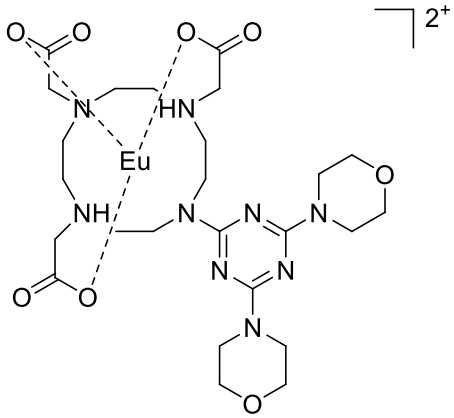

$Eu(OTf)_3$ (108mg, 0.18mmol) was dissolved in water, obtaining a colourless solution. MS (HR ES$^+$) calc. for $C_{25}H_{39}N_9O_8Eu$ (M + H$^+$) 746.2135 found 746.1978.

La(III)-TzMorph$_2$DO3A

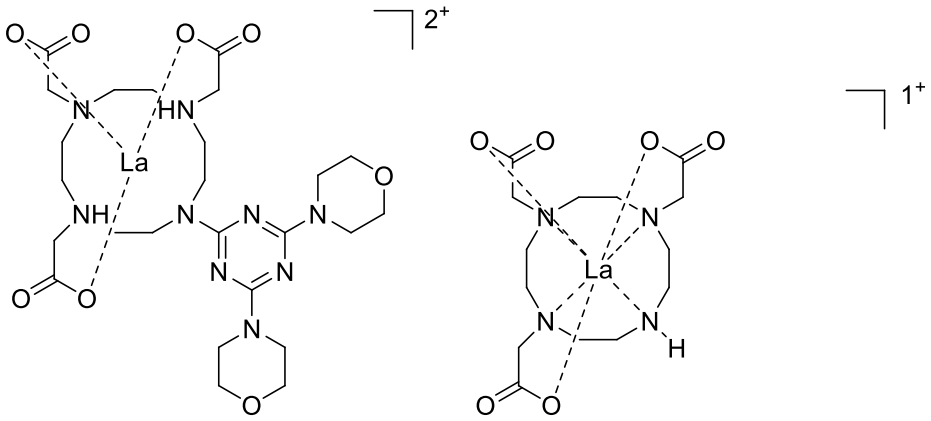

$La(OTf)_3$ (103mg, 0.18mmol) was dissolved in water, obtaining a colourless solution. MS (HR ES$^+$) calc. for $C_{25}H_{38}N_9O_8LaNa$ (M + Na$^+$) 754.1805 found 754.1914.

2.2.3 - Metal complexes with TzMorph$_2$DO3A

All the complexes have been synthesised following the same procedure. TzMorph$_2$DO3A (0.100g, 0.17mmol) were dissolved in water (~3mL), the pH of the solution corrected to reach pH 7, adding a solution of 1M NaOH. The metal salt was dissolved in water (~2mL) and added to the ligand solution. The solution was heated at 40-50°C for five minutes and then cooled to room temperature. The mixture was purified by a short flash column chromatography, getting a clear solution.

Cu(II)-TzMorph$_2$DO3A

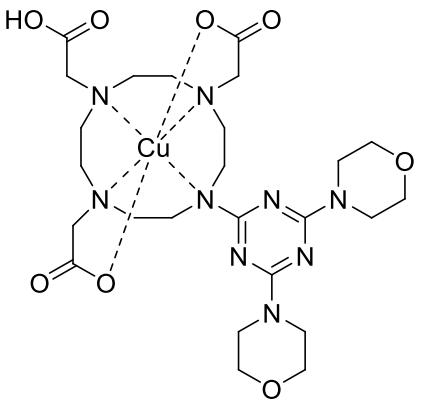

$Cu(OTf)_2$ (64mg, 0.18mmol) was dissolved in water, obtaining a dark blue solution.

MS (HR ES$^-$) calc. for $C_{25}H_{38}N_9O_8Cu$ (M - H$^+$) 655.2140 found 655.1956.

Mn(III)-TzMorph$_2$DO3A

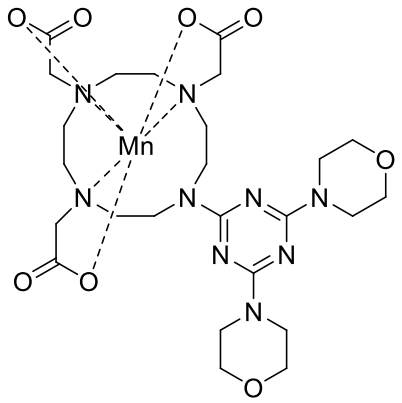

$MnCl_2$ (23mg, 0.18mmol) was dissolved in water, obtaining a pale pink-colourless solution. MS (HR ES^-) calc. for $C_{25}H_{38}N_9O_8Mn$ ($M - H^+$) 647.2224 found 647.2164.

Ni(II)-TzMorph$_2$DO3A

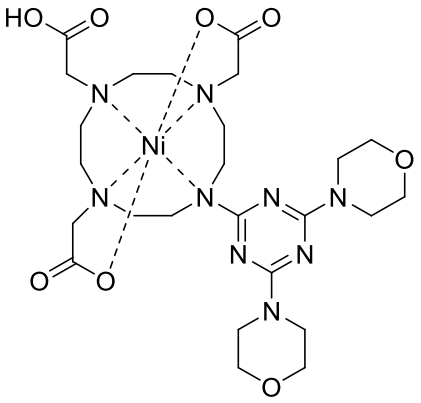

$NiCl_2*6H_2O$ (42mg, 0.18mmol) was dissolved in water, obtaining a purple solution. MS (HR ES^-) calc. for $C_{25}H_{38}N_9O_8Ni$ ($M - H^+$) 650.2197 found 650.2209.

La(III)-TzMorph$_2$DO3A

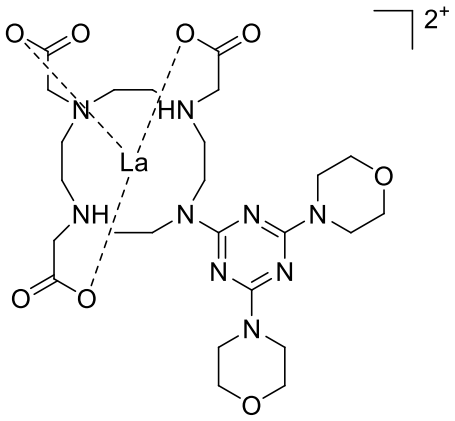

$La(OTf)_3$ (103mg, 0.18mmol) was dissolved in water, obtaining a colourless solution. MS (HR ES$^+$) calc. for $C_{25}H_{39}N_9O_8La$ (M + H$^+$) 732.1986 found 732.0903.

Y(III)-TzMorph$_2$DO3A

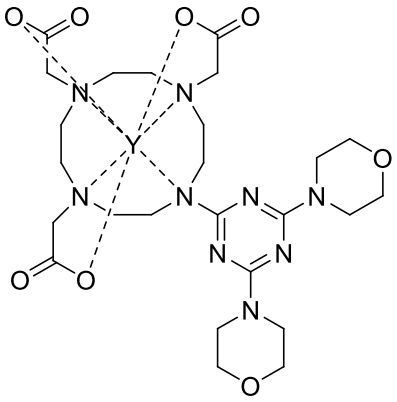

$Y(OTf)_3$ (97mg, 0.18mmol) was dissolved in water, obtaining a colourless solution. MS (HR ES$^+$) calc. for $C_{25}H_{39}N_9O_8Y$ (M + H$^+$) 682.1981 found 682.2074.

Eu(III)-TzMorph$_2$DO3A

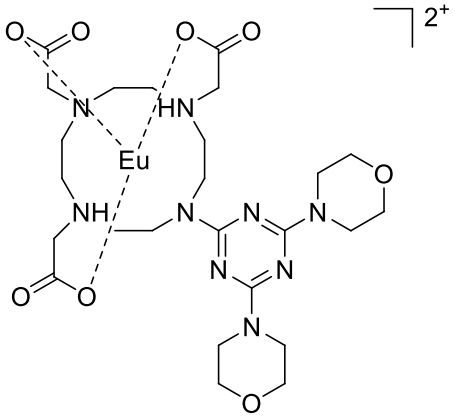

$Eu(OTf)_3$ (108mg, 0.18mmol) was dissolved in water, obtaining a colourless solution. MS (HR ES$^+$) calc. for $C_{25}H_{39}N_9O_8Eu$ (M + H$^+$) 746.2135 found 746.2148.

Gd(III)-TzMorph$_2$DO3A

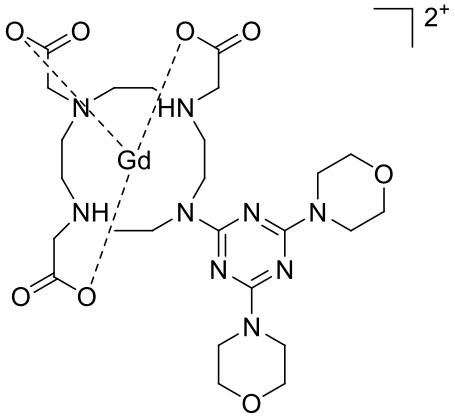

$Gd(OTf)_3$ (109mg, 0.18mmol) was dissolved in water, obtaining a colourless solution. MS (HR ES$^+$) calc. for $C_{25}H_{39}N_9O_8Gd$ (M + H$^+$) 751.2163 found 751.2228.

VO(II)-TzMorph$_2$DO3A

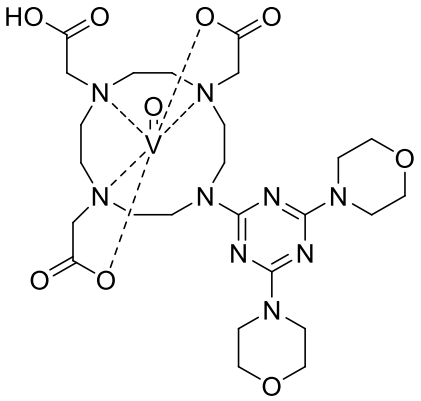

$VOSO_4*xH_2O$ (29mg, 0.18mmol) was dissolved in water, obtaining a green solution. MS (HR ES^-) calc. for $C_{25}H_{38}N_9O_9V$ ($M - H^+$) 659.2233 found 659.2238.

Co(II)-TzMorph$_2$DO3A

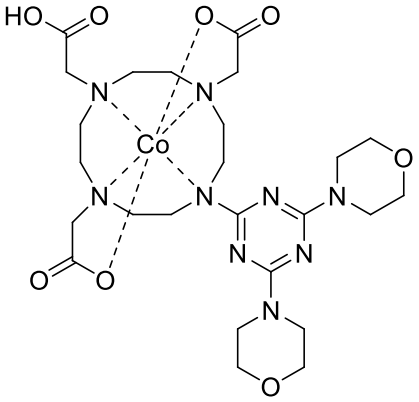

$Co(NO_3)_2*6H_2O$ (53mg, 0.18mmol) was dissolved in water, obtaining a pink solution. MS (HR ES^-) calc. for $C_{25}H_{38}N_9O_8Co$ ($M - H^+$) 651.2176 found 651.2234.

Ce(III)-TzMorph$_2$DO3A

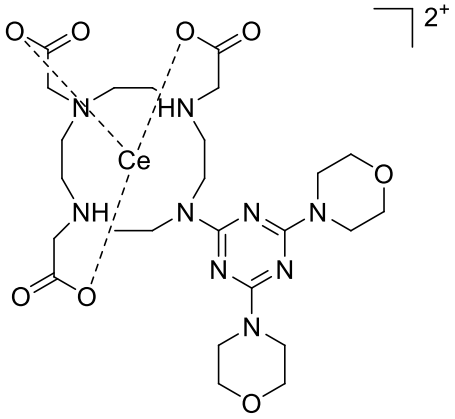

$Ce(NO_3)_3*6H_2O$ (77mg, 0.18mmol) was dissolved in water, obtaining a colourless solution. MS (HR ES$^+$) calc. for $C_{25}H_{38}N_9O_8CeNa$ (M + Na$^+$) 755.1796 found 755.1584.

Yb(III)-TzMorph$_2$DO3A

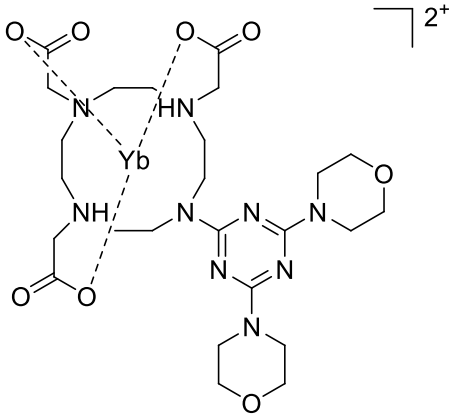

$YbCl_3*6H_2O$ (69mg, 0.18mmol) was dissolved in water, obtaining a colourless solution. MS (HR ES$^+$) calc. for $C_{25}H_{38}N_9O_8Yb$ (M + H$^+$) 767.2345 found 767.2401.

Lu(III)-TzMorph$_2$DO3A

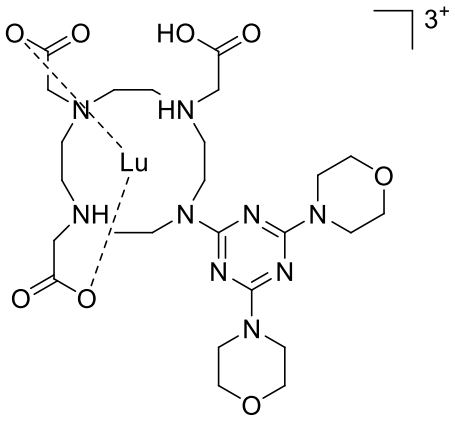

$LuCl_3*6H_2O$ (69mg, 0.18mmol) was dissolved in water, obtaining a colourless solution. MS (HR ES$^+$) calc. for $C_{25}H_{38}N_9O_8Lu$ (M + H$^+$) 768.2348 found 768.2506.

2,4-Dichloro-6-(piperidin-1-yl)-1,3,5-triazine (TzPipCl$_2$)

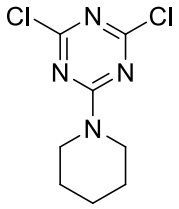

The compound was prepared based on a modified literature method.[3] Cyanuric chloride (10g, 54.2mmol) was dissolved in acetone (30mL), mixture of piperidine (4.61g, 54.2mmol) and K_2CO_3 (7.87g, 56.9mmol) in water (70mL) was slowly added dropwise at -10°C. After the addition, the reaction was allowed to stir at room temperature for 1h. The precipitate was filtered off and washed with water until the pH 7. The white solid was dried *in vacuo* (10.74g, 46.1mmol, 85%). ^{1}H NMR (400 MHz, $CDCl_3$, ppm) δH: 1.01 – 1.18 (m, 6H), 3.16 – 3.29 (m, 4H).

2,2'-((4-Chloro-6-(piperidin-1-yl)-1,3,5-triazin-2-yl)azanediyl)diethanol (TzPipDEACl)

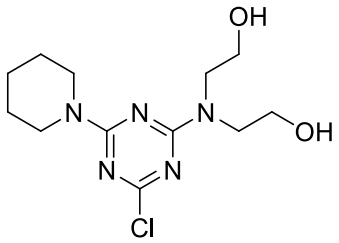

$TzPipCl_2$ (5g, 21.4mmol) was dissolved in acetone (50mL) and added to water (50mL) to form a slurry. Diethanolamine (2.26g, 21.4mmol) was dissolved in acetone (50mL) and added dropwise to the stirred mixture. Sodium bicarbonate (1.81g, 21.4mmol) was added portion wise so as to keep the pH neutral. The mixture was left under stirring at room temperature for 18 hours. The white solid was filtered off and dried *in vacuo* (3.00g, 1.0mmol, 46%). ^{1}H NMR (400 MHz, $CDCl_3$, ppm) δH: 1.55 – 17.1 (m, 8H), 3.68 – 3.91 (m, 10H).

tert-butyl 2,2',2''-(10-(4-(bis(2-hydroxyethyl)amino)-6-(piperidin-1-yl)-1,3,5-triazin-2-yl)-1,4,7,10-tetraazacyclododecane-1,4,7-triyl)triacetate (TzPipDEA-DO3A)

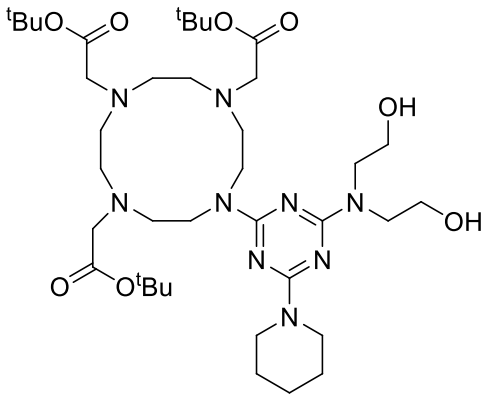

DO3A (1.00g, 1.68mmol), TzPipDEACl (0.506g, 1.68mmol) and K_2CO_3 (0.464g, 3.36mmol) were mixed in dry acetonitrile (40mL) under and atmosphere of nitrogen. The mixture was refluxed for three days. Then the mixture was cooled to room temperature and the solvent removed. The residue was dissolved in chloroform and washed with water, dried over $MgSO_4$ and finally the solvent removed *in vacuo* (1.00g, 1.28mmol, 76%). ^{1}H NMR (400 MHz, $CDCl_3$, ppm) δH: 1.43-1.44 (m, 27H), 1.47-1.56 (m, 6H),

1.58-1.72 (m, 2H), 2.62-2.89 (m, 6H), 2.90-3.16 (m, 6H), 3.17-3.56 (m, 8H), 3.57-3.97 (m, 12H); MS (HR ES$^+$) calc. for $C_{38}H_{70}N_9O_8$ (M + H$^+$) 780.5347 found 780.5366.

2,2',2''-(10-(4-(bis(2-hydroxyethyl)amino)-6-(piperidin-1-yl)-1,3,5-triazin-2-yl)-1,4,7,10-tetraazacyclododecane-1,4,7-triyl)triacetic acid (TzPipDEA-DO3A)

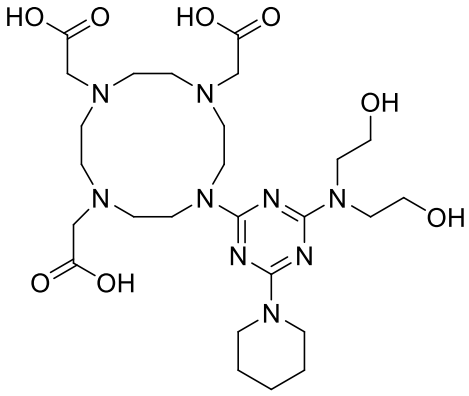

TzPipDEA-DO3A (1.00g, 1.28mmol) was dissolved in dichloromethane (20mL) and trifluoroacetic acid (5.85g, 51.31mmol) was added. The solution was stirred at room temperature for 48 hours, obtaining a yellow-brown solution. The solvent were removed *in vacuo*, and the residue solid was dissolved in methanol (~10mL), this was repeated at least three times, yielding an off pale brown oil. The oil was treated with Et_2O, yielding a white solid (0.710g, 1.16mmol, 90%). ^{1}H NMR (400 MHz, D_2O, ppm) δH: 1.35 - 1.68 (br m, 8H), 2.87 – 4.11 (br m, 32H); ^{13}C NMR (100 MHz, DMSO-d^6 ppm) δC: 172.55, 170.27, 168.72, 165.67, 164.60, 163.93, 158.98, 118.14, 59.56, 58.34, 53.93, 52.95, 52.13, 51.08, 48.76, 47.14, 45.91, 44.95, 44.15, 37.90, 34.94, 25.78, 24.82, 24.45, 23.85, 21.82; MS (HR ES$^+$) calc. for $C_{26}H_{46}N_9O_8$ (M + H$^+$) 612.3469 found 612.3474. IR (νmax, cm^{-1}) 3117 (s), 3012 (s), 2358 (s), 2249 (s), 1593 (s), 1438 (s), 1035 (s), 921 (s), 896 (s), 883 (s), 867 (s), 850 (s), 821 (s), 804 (s), 781 (s), 765 (s), 736 (s), 717 (s), 702 (s), 682 (s), 653 (s), 636 (s), 617 (s).

2.2.4 - Metal complexes with TzPipDEA-DO3A

All the complexes have been synthesised following the same procedure. TzPipDEA-DO3A (0.100g, 0.16mmol) were dissolved in water (~3mL), the pH of the solution corrected to reach pH 7, adding a solution of 1M NaOH. The metal salt was dissolved in water or MeOH (~2mL) and added to the ligand solution. The solution was heated at 40-50°C for five minutes and then cooled to room temperature. The mixture was purified by a short flash column chromatography, getting a clear solution.

Cu(II)-TzPipDEA-DO3A

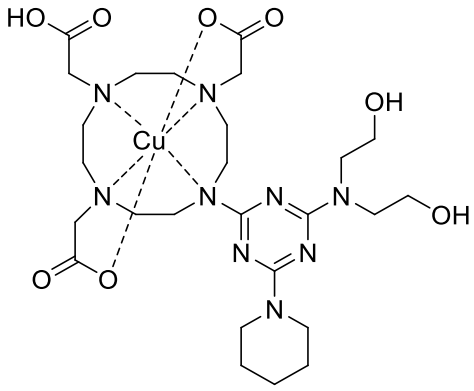

$Cu(OTf)_2$ (62mg, 0.17mmol) was dissolved in water, obtaining a dark blue solution.

MS (HR ES^+) calc. for $C_{26}H_{45}N_9O_8Cu$ ($M + H^+$) 673.2609 found 673.2620.

Mn(III)-TzPipDEA-DO3A

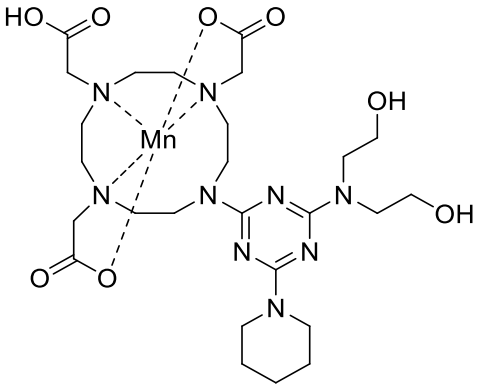

$MnCl_2*4H_2O$ (34mg, 0.17mmol) was dissolved in water, obtaining a colourless solution.

MS (HR ES^+) calc. for $C_{26}H_{43}N_9O_8MnNa$ ($M + Na^+$) 687.2513 found 687.1889.

Eu(III)-TzPipDEA-DO3A

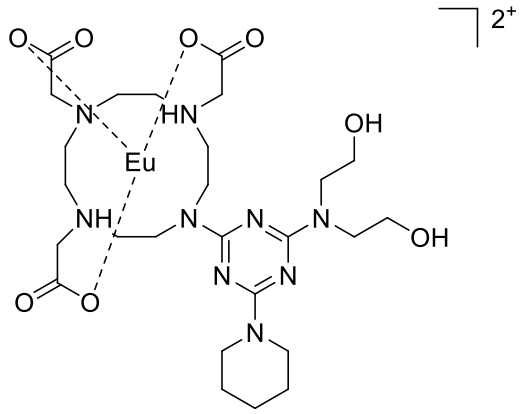

$Eu(OTf)_3$ (103mg, 0.17mmol) was dissolved in water, obtaining a colourless solution. MS (HR ES^+) calc. for $C_{26}H_{43}N_9O_8Eu$ ($M + H^+$) 762.2448 found 762.1774.

Y(III)-TzPipDEA-DO3A

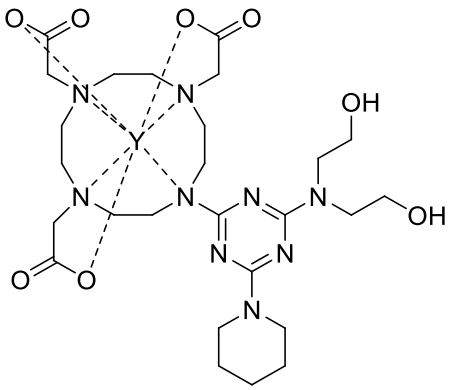

$Y(OTf)_3$ (92mg, 0.17mmol) was dissolved in water, obtaining a colourless solution. MS (HR ES^+) calc. for $C_{26}H_{42}N_9O_8Y$ ($M + H^+$) 698.2293 found 698.2293.

Gd(III)-TzPipDEA-DO3A

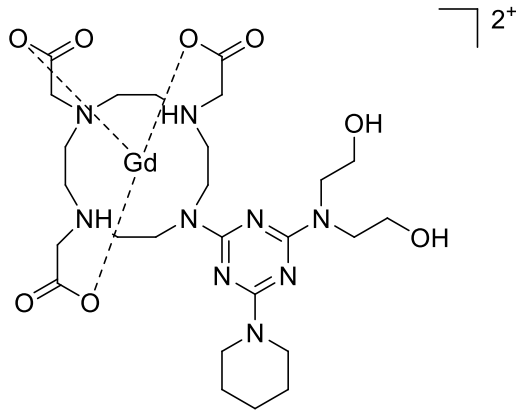

$Gd(OTf)_3$ (104mg, 0.17mmol) was dissolved in water, obtaining a colourless solution. MS (HR ES^+) calc. for $C_{26}H_{43}N_9O_8Gd$ ($M + H^+$) 767.2397 found 767.2482.

VO(II)-TzPipDEA-DO3A

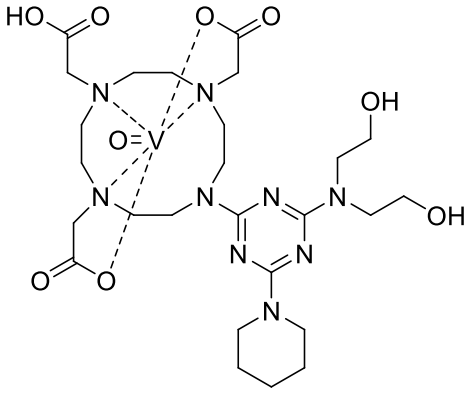

$VOSO_4*xH_2O$ (28mg, 0.17mmol) was dissolved in water, obtaining a green solution. MS (HR ES^+) calc. for $C_{26}H_{44}N_9O_9V$ ($M + H^+$) 677.2702 found 677.2687.

La(III)-TzPipDEA-DO3A

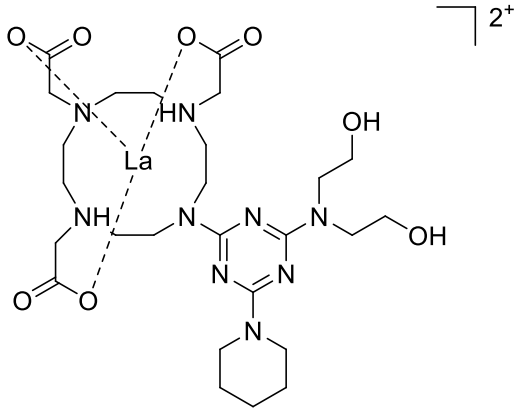

$La(OTf)_3$ (101mg, 0.17mmol) was dissolved in water, obtaining a colourless solution. MS (HR ES^+) calc. for $C_{26}H_{43}N_9O_8La$ ($M + H^+$) 748.2300 found 748.1564.

Ca(II)-TzPipDEA-DO3A

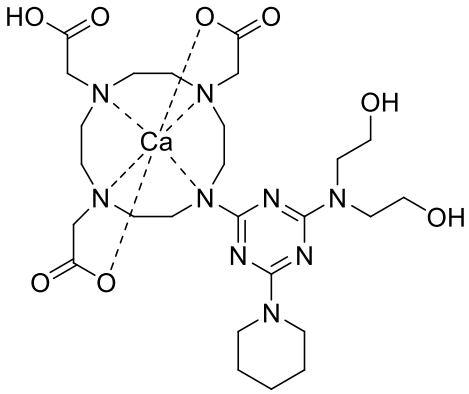

$CaCl_2*2H_2O$ (26mg, 0.17mmol) was dissolved in water, obtaining a colourless solution. MS (HR ES^+) calc. for $C_{26}H_{43}N_9O_8Ca$ ($M + H^+$) 649.2901 found 649.1355.

2.2.5 - Benzothiale ligands and complexes

2-(4-bromophenyl)-1,3-benzothiazole

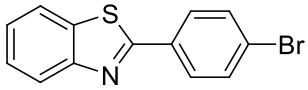

The compound was prepared by literature methodology.[4] 2-aminothiophenol (1.03g, 8.22mmol) and 4-bromobenzaldehyde (1.50g, 8.22mmol) were dissolved in DMSO (20mL) and heated at 200°C for three hours. The mixture was cooled to room temperature and left under stirring overnight. To the mixture was added water, obtaining a precipitate. The solid was filtered and then recrystallised in a solution of acetic acid - water (1:4), filtered again and washed with a solution of $NaHCO_3$. The residue was recrystallised in hot ethanol and then cooled to room temperature to be filtered (1.97g, 6.82mmol, 83%). ^1H NMR (400 MHz, DMSO-d^6, ppm) δH: 7.47 (t, 1H, J = 7.4Hz, -CHCHCS-), 7.55 (t, 1H, J = 7.5Hz, -CHCHCN-), 7.76 (d, 2H, J = 8.4Hz, -CHCHCBr), 8.02 (d, 2H, J = 8.4Hz, -CHCHBr), 8.06 (d, 1H, J = 8.1Hz, -CHCS-), 8.14 (d, 1H, J = 7.9Hz, -CHCN-); MS (HR EI^+) calc. for $C_{13}H_8BrNS$ (M^+) 288.9561 found 288.9347.

2-(4-phenol)-1,3-benzothiazole

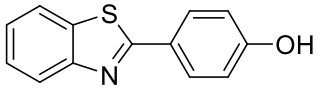

The compound was prepared by literature methodology.[4] 2-aminothiophenol (1.54g, 12.2mmol) and 4-hydroxybenzaldehyde (1.50g, 12.2mmol) were dissolved in ethanol (20mL) and refluxed for 24 hours. The mixture was cooled to room temperature and added water, obtaining a precipitate. The solid was filtered and then recrystallised in hot ethanol and then cooled to room temperature to be filtered (1.89g, 8.32mmol, 68%). ^{1}H NMR (400 MHz, acetone-d^{6}, ppm) δH: 7.02 (d, 2H, J = 8.8Hz, -CHCHCOH), 7.41 (t, 1H, J = 8.0Hz, -CHCHCS-), 7.51 (t, 1H, J = 7.6Hz, -CHCHCN-), 7.98 (d, 1H, J = 7.8Hz, -CHCS-), 8.00 (d, 1H, J = 2.1Hz, -CHCHCOH), 8.02 (d, 1H, J = 2.1Hz, -CHCHCOH), 8.04 (d, 1H, J = 7.4Hz, -CHCN-), 9.37 (br s, 1H, -OH), ; MS (LR EI^{+}) calc. for $C_{13}H_{9}NOS$ (M^{+}) 227.04 found 227.04.

2-(4-fluorophenyl)-1,3-benzothiazole

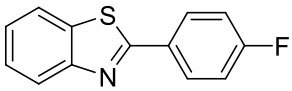

The compound was prepared by literature methodology.[4] 2-aminothiophenol (2.33g, 18.6mmol) and 4-fluorobenzaldehyde (2.31g, 18.6mmol) were dissolved in ethanol (20mL) and refluxed for 24 hours. The mixture was cooled to room temperature and added water, obtaining a precipitate. The solid was filtered and then recrystallised in hot ethanol and then cooled to room temperature to be filtered (0.814g, 3.55mmol, 19%). ^{1}H NMR (400 MHz, acetone-d^{6}, ppm) δH: 7.36 (m, 2H, -CHCHCF), 7.47 (t, 1H, J = 7.2Hz, -CHCHCS-), 7.56 (t, 1H, J = 8.0Hz, -CHCHCN-), 8.05 (d, 1H, J = 8.1Hz, -CHCS-), 8.10 (d, 1H, J = 7.9Hz, -CHCN-), 8.21 (m, 2H, -CHCHCF); MS (LR EI^{+}) calc. for $C_{13}H_{9}FNS$ (M^{+}) 229.03 found 229.03.

2-(4-amino)-1,3-benzothiazole

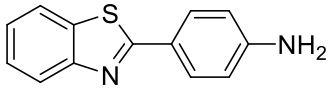

The compound was prepared by literature methodology.[4] 2-aminothiophenol (0.913g, 7.29mmol) and 4-aminobenzoic acid (1.00g, 7.29mmol) were added at polyphosphoric acid (~30mL). The mixture was heated to 180°C for five hours, turning the mixture in a green-black solution. The reaction was cooled down to room temperature and neutralised with a solution of 10% Na_2CO_3; the yellow solid was filtered off and dried *in vacuo* (1.24g, 5.49mmol, 75%). ^{1}H NMR (400 MHz, DMSO-d^6, ppm) δH: 5.93 (s, 2H, -NH), 6.66 (d, 2H, J = 8.6Hz, -CHCHCNH-), 7.34 (t, 1H, J = 7.0Hz, -CHCHCS-), 7.45 (t, 1H, J = 7.1Hz, -CHCHCN-), 7.76 (d, 2H, J = 8.6Hz, -CHCHCNH-), 7.89 (d, 1H, -CHCHCS), 8.02 (d, 1H, -CHCHCN); MS (LR EI$^+$) calc. for $C_{13}H_9N_2S$ (M^+) 226.06 found 226.04.

N-(4-(benzo[d]thiazol-2-yl)phenyl)-2-chloroacetamide

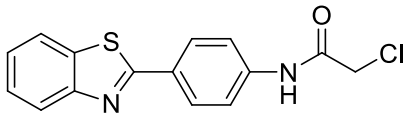

The compound was prepared by literature methodology.[5] 2-(4-amino)-1,3-benzothiazole (2.10g, 9.29mmol) was dissolved in dry dichloromethane, to the mixture was added Et_3N (0.188g, 1.86mmol) to obtain an homogeneous solution. Chloroacetyl chloride (1.58g, 13.93mmol) was dissolved in dichloromethane and added dropwise to the solution at 0°C. The reaction mixture was stirred at 0°C for one hour and then was stirred further for 24 hours at room temperature. The completion of the reaction was monitored by TLC (DCM : MeOH, 8:2). The solid was filtered off and dried *in vacuo* (2.05g, 6.77mmol, 73%). ^{1}H NMR (400 MHz, DMSO-d^6, ppm) δH: 4.34 (s, 2H, -CCHCl), 7.44 (t, 1H, J = 7.0Hz, -CHCHCS-), 7.53 (t, 1H, J = 7.0Hz, -CHCHCN-), 7.82 (d, 2H, J = 8.8Hz, -CHCHCNH-), 8.03 (d, 1H, J = 7.7Hz, -CHCHCS-), 8.08 (d, 2H, J = 8.7Hz, -

CHCHCNH-), 8.14 (d, 1H, J = 7.9Hz, -CHCHCN-), 10.83 (s, 1H, -CNHCO-); MS (LR ES$^+$) calc. for $C_{15}H_{11}N_2OS$ (M + H$^+$) 302.02 found 303.07.

N-Benzothiazole-2-yl-succinamic acid

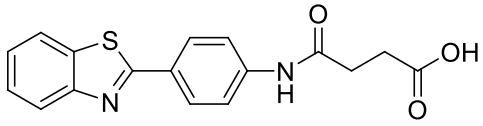

The compound was prepared by literature methodology.[6] 2-(4-amino)-1,3-benzothiazole (0.300g, 1.33mmol) and succinic anhydride (1.33g, 13.29mmol) were refluxed in dry THF (20mL) for 24 hours. The solvent was removed and the solid recrystallised with water, filtered off and dried *in vacuo* (0.200g, 0.61mmol, 46%). ^{1}H NMR (400 MHz, DMSO-d^6, ppm) δH: 1.56 (d, 2H, J = 6.0Hz, -CCHCH-), 1.62 (d, 2H, J = 6.2Hz, -CCHCH-), 6.45 (t, 1H, J = 7.6Hz, -CHCHCS-), 6.54 (t, 1H, J = 7.7Hz, -CHCHCN-), 6.80 (d, 2H, J = 8.6Hz, -CHCHCNH-), 7.04 (m, 3H, -CHCHCNH- and -CHCHCS-), 7.12 (d, 1H, J = 8.0Hz, -CHCHCN-), 9.36 (s, 1H, -CNHCO-); MS (LR ES$^+$) calc. for $C_{17}H_{14}N_2O_3S$ (M + H$^+$) 327.07 found 327.07.

4-(benzo[d]thiazol-2-yl)-N-methylaniline

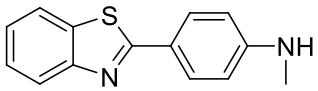

The compound was prepared by literature methodology.[4] 2-aminothiophenol (1.24g, 9.90mmol) and 4-(methylamino)benzoic acid (1.50g, 9.90mmol) were added at polyphosphoric acid (~30mL). The mixture was heated to 180°C for five hours, turning the mixture in a green-black solution. The reaction was cooled down to room temperature and neutralised with a solution of 10% Na_2CO_3; the yellow solid was filtered off and dried *in vacuo* (2.06g, 8.58mmol, 87%). ^{1}H NMR (400 MHz, acetone-d^6, ppm) δH: 2.85 (d, 3H, J = 5.0Hz, -NCH), 5.78 (br, 1H, -NHCH-), 6.73-6.67 (m, 2H, -CHCHCNH-), 7.35 – 7.30 (m, 1H, -CHCHCS-),7.44 (t, 1H, J = 8.2Hz, -CHCHCN-), 7.91 – 7.86 (m, 3H), 7.95 (d,

1H, J = 7.9Hz, -CHCHCN); MS (LR ES$^+$) calc. for $C_{14}H_{12}N_2S$ (M + H$^+$) 241.06 found 241.07.

4-((4-(benzo[d]thiazol-2-yl)phenyl)(methyl)amino)-4-oxobutanoic acid

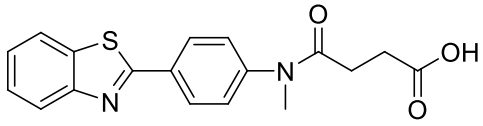

4-(benzo[d]thiazol-2-yl)-N-methylaniline (1.00g, 4.17mmol) and succinic anhydride (0.500g, 5.00mmol) were refluxed in dry THF (30mL) for 24 hours. The solvent was removed and the solid recrystallised with water, filtered off and dried *in vacuo* (1.26g, 3.71mmol, 89%). ^{1}H NMR (400 MHz, D_2O, ppm) δH: 2.19 (br d, 4H, -CC*H*C*H*C-), 2.97 (s, 3H, -CNC*H*-), 6.93 (m, 3H), 7.15 (t, 1H, J = 7.7Hz, -C*H*CHCN-), 7.23 (d, 1H, J = 7.9Hz, -C*H*CHCS-), 7.30 (d, 2H, -CHC*H*CNH-), 7.57 (d, 1H, J = 8.2Hz, -CHCHCN-); ^{13}C NMR (100 MHz, MeOD-d^4 ppm) δC: 177.30, 174.42, 169.32, 155.01, 147.67, 136.37, 134.20, 130.27, 129.67, 128.40, 127.44, 124.09, 123.48, 50.07, 38.36, 30.61, 30.38; MS (LR ES$^+$) calc. for $C_{18}H_{16}N_2O_3S$ (M + H$^+$) 340.07 found 341.10; IR (νmax, cm^{-1}) 2960 (br), 1718 (s), 1625 (s), 1599 (s), 1517 (s), 1483 (s), 1452 (w), 1425 (w), 1386 (s), 1336 (w), 1313 (s), 1249 (w), 1224 (w), 1182 (s), 1122 (s), 1109 (s), 1012 (s), 968 (s), 939 (w), 902 (w), 850 (s), 825 (s), 760 (s), 729 (s), 682 (w), 623 (s), 567 (s), 516 (w), 443 (s).

2-(2-((4-(benzo[d]thiazol-2-yl)phenyl)(methyl)amino)-2-oxoethoxy)acetic acid

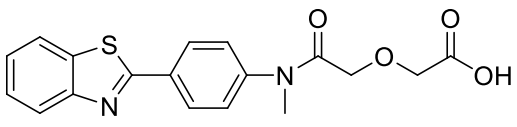

4-(benzo[d]thiazol-2-yl)-N-methylaniline (1.06g, 4.42mmol) and diglycolic anhydride (0.634g, 5.46mmol) were refluxed in dry THF (30mL) for 24 hours. The solvent was removed and the solid recrystallised with water, filtered off and dried *in vacuo* (1.01g, 2.84mmol, 64%). ^{1}H NMR (400 MHz, D_2O, ppm) δH: 3.00 (s, 3H, -CNC*H*), 3.87 – 3.63 (m, 4H), 6.94 (d, 2H, J = 8.2Hz, -CC*H*CH-), 7.02 (br m, 1H, -C*H*CHCS-), 7.20 (t, 1H, J =

7.2Hz, -C*H*CHCN-), 7.35 (br m, 3H), 7.60 (d, 2H, J = 8.2Hz, -CHC*H*CN-); ^{13}C NMR (100 MHz, DMSO-d^6 ppm) δC: 171.82, 168.71, 166.80, 154.41, 135.09, 129.16, 128.70, 128.02, 127.21, 126.12, 124.75, 123.43, 122.21, 111.95, 68.93, 67.93, 37.03, 29.76; MS (LR AP$^+$) calc. for $C_{18}H_{16}N_2O_4S$ (M + H$^+$) 356.07 found 357.16; IR (νmax, cm^{-1}) 3520 (s), 3475 (s), 3311 (s), 3201 (s), 2960 (s), 2679 (s), 2627 (s), 2400 (s), 2360 (s), 2243 (s), 1934 (s), 1703 (s), 1516 (s), 1460 (s), 1249 (s), 1143 (s), 765 (s), 738 (s), 717 (s), 694 (s), 678 (s), 653 (s), 636 (s).

1-((4-(benzo[d]thiazol-2-yl)phenyl)(methyl)amino)-3-chloropropan-2-ol

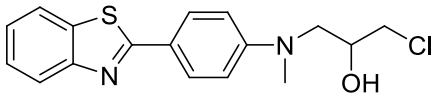

4-(benzo[d]thiazol-2-yl)-N-methylaniline (1.00g, 4.17mmol) and epichlorohydrin (1.92g, 20.83mmol) were dissolved in ethanol (30mL) under nitrogen. The solution was refluxed for three days. The solvent was removed *in vacuo* as well the excess of epichlorohydrin. The solid was purified by chromatography column (DCM : MeOH, 98 : 2), (750mg, 2.26mmol, 54%). ^{1}H NMR (400 MHz, DMSO-d^6, ppm) δH: 3.06 (s, 3H, -CNCH), 3.45 – 3.39 (m, 1H), 3.73 – 3.56 (m, 3H), 3.97 (br m, 1H), 6.85 (d, 2H, J = 8.7Hz, -CCHCH-), 7.36 (t, 1H, J = 7.6Hz, -CHCHCS-), 7.47 (t, 1H, J = 7.7Hz, -CHCHCN-), 7.88 (d, 2H, J = 8.6Hz, -CCHCH-), 7.92 (d, 1H, J = 8.2Hz, -CHCHCS-), 8.04 (d, 2H, J = 7.9Hz, -CHCHCN-). ^{13}C NMR (125 MHz, DMSO-d^6, ppm) δC: 168.3, 154.4, 151.7, 129.0, 126.8, 124.9, 122.4, 122.3, 121.4, 112.0, 69.2, 55.7, 47.8, 39.8. MS (HR ES$^+$) calc. for $C_{17}H_{18}ClN_2OS$ (M + H$^+$) 332.0828 found 332.0829; IR (νmax, cm^{-1}) 3203 (s), 3111 (s), 3049 (s), 2920 (s), 2754 (s), 2630 (s), 2520 (w), 2372 (s), 2102 (s), 1633 (s), 1510 (s), 1458 (s), 1396 (s), 1251 (s), 1145 (s), 1099 (s), 910 (s), 867 (s), 850 (s), 788 (s), 758 (s), 738 (s), 719 (s), 702 (s), 682 (s), 657 (s).

4-(benzo[d]thiazol-2-yl)-N-methyl-N-(oxiran-2-ylmethyl)aniline (Bz-epox)

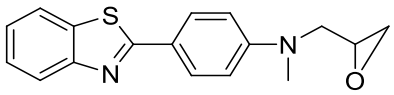

1-((4-(benzo[d]thiazol-2-yl)phenyl)(methyl)amino)-3-chloropropan-2-ol (1.54g, 4.64mmol) was dissolved in MeOH (20mL) under nitrogen and then K_2CO_3 (961mg, 6.96mmol) was added to the solution. The mixture was left under stirring for one hour. The mixture was diluted with Et_2O and washed with water. The aqueous phase was extracted with Et_2O and the organic layers washed with brine, dried with $MgSO_4$, filtered and the solvent removed *in vacuo* (847mg, 2.86mmol, 62%). ^{1}H NMR (400 MHz, $CDCl_3$, ppm) δH: 2.59 – 2.55 (m, 1H), 2.82 (m, 1H), 3.10 (s, 3H, -CNC*H*), 3.19 (s, 1H), 3.49 (dd, 1H, J = 15.5Hz), 3.78 (d m, 1H, J = 16.0Hz), 6.80 (d, 2H, J = 7.7Hz, -CCHC*H*-), 7.33 (t, 1H, J = 7.6Hz, -C*H*CHCS-), 7.45 (t, 1H, J = 7.6Hz, -C*H*CHCN-), 7.84 (d, 1H, J = 7.8Hz, -CHC*H*CS-), 8.00 (d, 2H, J = 8.1Hz, -CC*H*CH-), 8.03 (d, 1H, J = 8.1Hz, -CHC*H*CN-). ^{13}C NMR (125 MHz, $CDCl_3$, ppm) δC: 167.7, 159.3, 150.5, 128.2, 125.4, 125.2, 123.5, 121.0, 120.6, 120.4 110.8, 52.6, 49.3, 44.0, 38.2, 29.3, 28.7. MS (HR EI$^+$) calc. for $C_{17}H_{16}N_2OS$ (M) 296.0983 found 296.0981; IR (νmax, cm^{-1}) 3203 (s), 3116 (s), 3053 (s), 2958 (s), 2860 (s), 2748 (s), 2634 (s), 2490 (s), 2382 (s), 2245 (s), 2011 (s), 1921 (w), 1874 (w), 1803 (w), 1699 (w), 1633 (w), 1519 (w), 1456 (s), 1382 (s), 1246 (s), 1105 (s), 1004 (s), 983 (s), 867 (s), 846 (s), 821 (s), 802 (s), 788 (s), 765 (s), 758 (s), 734 (s), 719 (s), 704 (s), 680 (s), 651 (s).

tert-butyl 2,2',2''-(10-(3-((4-(benzo[d]thiazol-2-yl)phenyl)(methyl)amino)-2-hydroxypropyl)-1,4,7,10-tetraazacyclododecane-1,4,7-triyl)triacetate

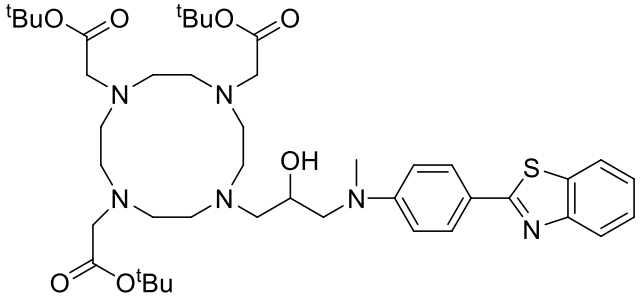

DO3A*HBr (500mg, 0.84mmol) was stirred in acetonitrile (15mL) with K_2CO_3 (174mg, 1.26mmol) for 24 hours. The mixture was filtered off and the solvent was removed *in vacuo*. The residue was dissolved in EtOH (25mL), Et_3N (0.084g, 0.83mmol) and Bz-epox (0.246g, 0.83mmol) were added to the solution. The solution was heated at 50-60°C for 24 hours. The solution was cooled to room temperature and the solvent and the Et_3N removed *in vacuo* (0.600g, 0.74mmol, 89%). ^{1}H NMR (400 MHz, $CDCl_3$, ppm) δH: 1.45 (br s, 27H, ^{t}BuO-), 4.02 – 2.49 (br m, 30H), 6.92 – 6.66 (m, 2H, -CCHC*H*-), 7.33 – 7.28 (m, 1H, -C*H*CHCS-), 7.43 (t, 1H, J = 7.5Hz, -C*H*CHCN-), 7.84 (d, 1H, J = 7.4Hz, -CHC*H*CS-), 8.18 – 7.87 (m, 3H). MS (HR ES$^+$) calc. for $C_{43}H_{67}N_6O_7S$ (M + H$^+$) 811.4792 found 811.4802.

2,2',2''-(10-(3-((4-(benzo[d]thiazol-2-yl)phenyl)(methyl)amino)-2-hydroxypropyl)-1,4,7,10-tetraazacyclododecane-1,4,7-triyl)triacetic acid (Bz-epox-DO3A)

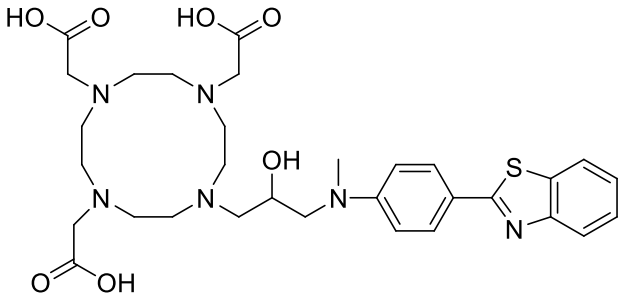

tert-butyl 2,2',2''-(10-(3-((4-(benzo[d]thiazol-2-yl)phenyl)(methyl)amino)-2-hydroxypropyl)-1,4,7,10-tetraazacyclododecane-1,4,7-triyl)triacetate (0.600g, 0.74mmol) was dissolved in dichloromethane (15mL) and trifluoroacetic acid (2.53g, 22.21mmol) was added. The solution was stirred at room temperature for 48 hours. The solvent were removed *in vacuo*, and the residue solid was dissolved in methanol (~10mL), this was repeated at least three times. The oil was treated with Et_2O, yielding an off dark green hygroscopic oil (0.428g, 0.66mmol, 90%). ^{1}H NMR (400 MHz, MeOD-d^4, ppm) δH: 2.60 – 3.28 (br m, 12H), 3.37 – 4.52 (br m, 18H), 6.96 (d, 2H, J = 7.7Hz, -CCHC*H*-), 7.37 – 7.43 (m, 1H, -C*H*CHCS-), 7.52 (t, 1H, J = 7.1Hz, -C*H*CHCN-), 7.90 (d, 1H, J = 8.0Hz, -CHC*H*CS-), 7.95 (d, 1H, J = 7.8Hz -CHC*H*CN-); ^{13}C NMR (100 MHz, MeOD-d^4, ppm) δC: 173.3,

169.8, 128.7, 126.3, 124.6, 121.5, 120.9, 111.9, 111.7, 65.5, 55.9, 55.0, 52.6, 52.3, 51.8, 50.4, 49.4, 48.5, 42.0, 38.5, 14.0. MS (HR ES$^+$) calc. for $C_{31}H_{43}N_6O_7S$ (M + H$^+$) 643.2914 found 643.2897. IR (νmax, cm^{-1}) 3198 (s), 2895 (s), 2368 (w), 2266 (w), 1597 (s), 1514 (s), 1441 (w), 883 (s), 846 (s), 821 (s), 806 (w), 787 (s), 765 (s), 758 (s), 738 (s), 721 (s), 702 (s), 680 (s).

2.2.6 - Metal complexes with Bz-epox-DO3A

All the complexes have been synthesised following the same procedure. Bz-epox-DO3A (0.050g, 0.08mmol) were dissolved in a mix of water and methanol (~3mL), the pH of the solution corrected to reach pH 7, adding a solution of 1M NaOH. The metal salt was dissolved in water (~2mL) and added to the ligand solution. The solution was heated at 40-50°C for five minutes and then cooled to room temperature. The mixture was purified by a short flash column chromatography, getting a clear solution.

Cu(II)-Bz-epox-DO3A

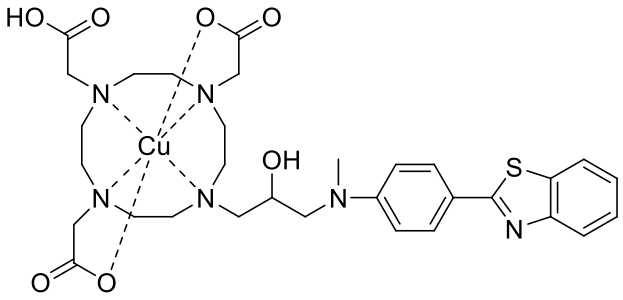

$CuSO_4$*5H_2O (21mg, 0.08mmol) was dissolved in water, obtaining a dark blue solution. MS (HR AP$^+$) calc. for $C_{31}H_{41}N_6O_7SCu$ (M + H$^+$) 704.2053 found 704.2056.

Tb(III)-Bz-epox-DO3A

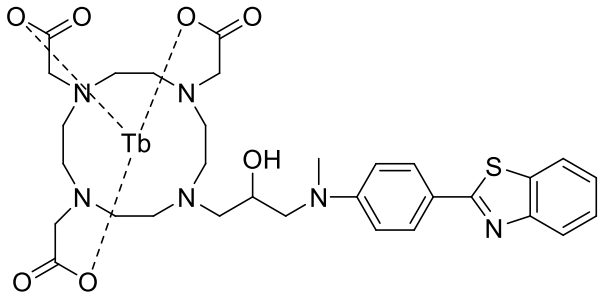

$Tb(OTf)_3$ (50mg, 0.08mmol) was dissolved in water, obtaining a colourless solution.

MS (HR AP^+) calc. for $C_{31}H_{41}N_6O_7STb$ ($M + H^+$) 799.1933 found 799.1933.

Eu(III)-Bz-epox-DO3A

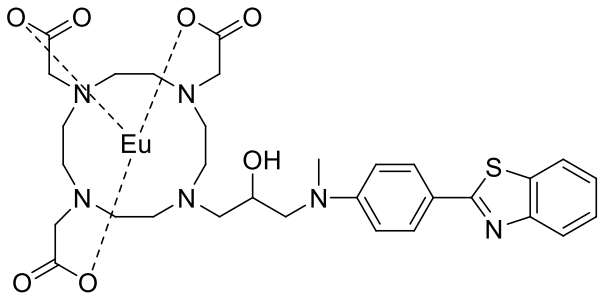

$Eu(OTf)_3$ (49mg, 0.08mmol) was dissolved in water, obtaining a colourless solution.

MS (HR AP^+) calc. for $C_{31}H_{41}N_6O_7SEu$ ($M + H^+$) 791.1878 found 791.1873.

VO(II)-Bz-epox-DO3A

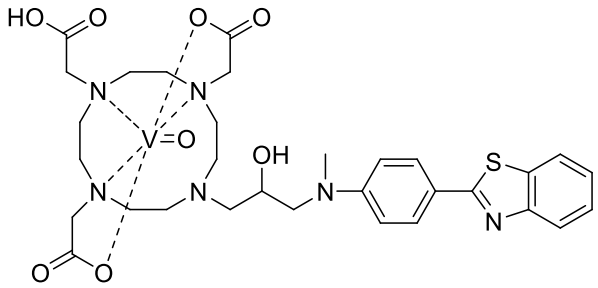

$VOSO_4*xH_2O$ (15mg, 0.08mmol) was dissolved in water, obtaining a blue solution.

MS (HR ES^-) calc. for $C_{31}H_{39}N_6O_8SV$ ($M - H^-$) 706.1990 found 706.2006.

DFO-Ga(III) complex

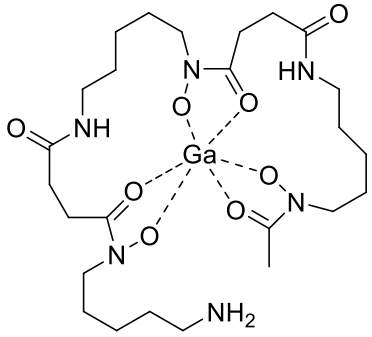

Deferoxamine mesylate (0.100g, 0.15mmol) was dissolved in water (~5mL), $KHCO_3$ (0.061g, 0.61mmol) and $Ga(NO_3)_3*xH_2O$ (0.039g, 0.15mmol) were added to the solution and left under stirring for 24 hours. The solvent was removed *in vacuo.* MS (HR ES^+) calc. for $C_{25}H_{46}N_6O_8Ga$ ($M + H^+$) 627.2633 found 627.2656.

DFO-Ga(III)-Bz-epox

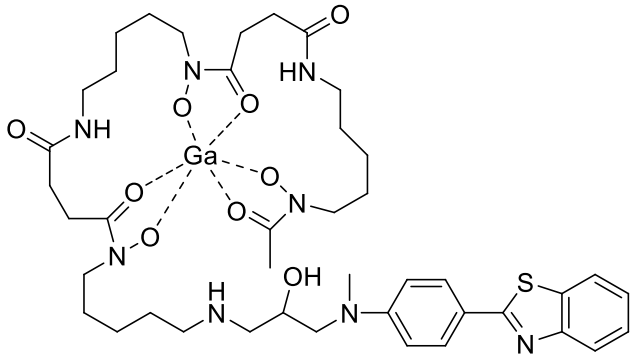

To the mixture obtained from DFO-Ga (0.100g, 0.15mmol of deferoxamine mesylate), Bz-epox (0.046g, 0.15mmol) and Et_3N (0.015g, 0.15mmol) were added to the white mixture and stirred at ~50°C for 48 hours. The mixture was cooled to room temperature and the solid filtered off. The solvent was finally removed *in vacuo.* (0.120g, 0.13mmol, 85%).^{1}H NMR (400 MHz, DMSO-d^6, ppm) δH: 1.14 – 2.40 (br m, 27H), 2.58 – 3.73 (br m, 26H), 6.84 (d, 2H, J = 9.0Hz, -CCHC*H*-), 7.34 (t, 1H, J = 7.7Hz -C*H*CHCS-), 7.45 (t, 1H, J = 7.7Hz, -C*H*CHCN-), 7.90 (m, 3H), 8.03 (d, 1H, J = 6.8Hz -CHC*H*CN-); ^{13}C NMR (100 MHz, DMSO-d^6, ppm) δC: 154.4, 134.2, 128.9, 122.2, 112.0, 58.8, 28.5, 8.5. MS

(HR ES$^+$) calc. for $C_{42}H_{62}N_8O_9SGa$ (M + H$^+$) 923.3616 found 923.3653. IR (νmax, cm^{-1}) 3305 (w), 3203 (w), 3117 (w), 2945 (w), 2870 (w), 2513 (w), 2378 (w), 1516 (w), 1458 (w), 977 (s), 947 (s), 906 (s), 883 (s), 864 (s), 846 (s), 821 (s), 806 (s), 785 (s), 758 (s), 736 (s), 713 (s), 700 (s), 679 (s), 655 (s), 640 (s), 619 (s).

DFO-Eu(III) complex

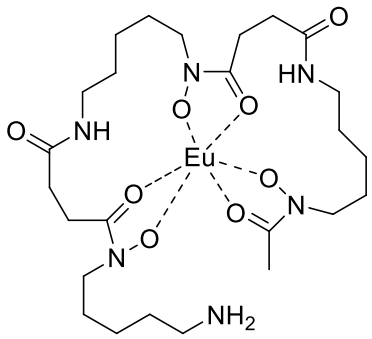

Deferoxamine mesylate (0.100g, 0.15mmol) was dissolved in water (~5mL), $KHCO_3$ (0.061g, 0.61mmol) and $Eu(OTf)_3$ (0.091g, 0.15mmol) were added to the solution and left under stirring for 24 hours. The solvent was removed *in vacuo.* MS (HR ES$^+$) calc. for $C_{25}H_{46}N_6O_8Eu$ (M + H$^+$) 709.2576 found 709.2581.

DFO-Eu(III)-Bz-epox

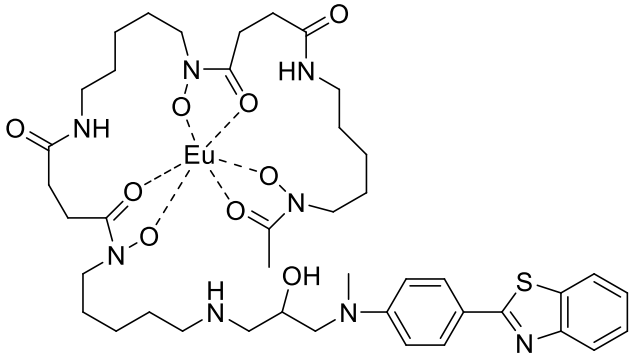

To the mixture obtained from DFO-Eu (0.100g, 0.15mmol of deferoxamine mesylate), Bz-epox (0.046g, 0.15mmol) and Et_3N (0.015g, 0.15mmol) were added to the white mixture and stirred at ~50°C for 48 hours. The mixture was cooled to room temperature and the solid filtered off. The solvent was finally removed *in vacuo.* (0.130g, 0.13mmol,

85%). MS (HR ES$^+$) calc. for $C_{42}H_{62}N_8O_9SEu$ (M + H$^+$) 1005.3559 found 1005.3596. IR (νmax, cm^{-1}) 2515 (w), 2058 (w), 1271 (w), 883 (s), 842 (s), 817 (s), 804 (s), 788 (s), 779 (s), 765 (s), 758 (s), 719 (s), 702 (s), 680 (s), 665 (s), 651 (s).

DFO-Traut's reagent

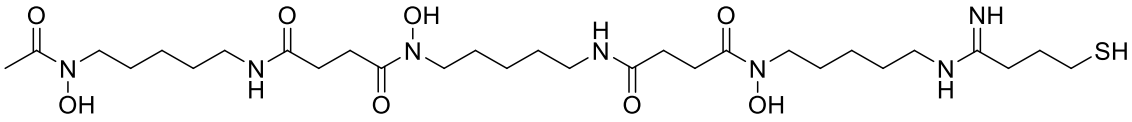

The compound was prepared by literature methodology.[7] Deferoxamine mesylate (0.300g, 0.46mmol) was dissolved in phosphate buffered saline solution (50mL) adjusted at pH 8.0 and 2-iminothiolane hydrochloride (0.126g, 0.92mmol) was added. The reaction was left under stirring for six hours. After the pH was changed to 5, adding small amounts of 0.1M HNO_3. The solution was then extracted with three portions of 1-butanol (~60mL total). The organic fractions were reunited and washed with brine, and then dried on $MgSO_4$. The solvent was removed *in vacuo.* The residue was then dissolved again in 1-butanol, eliminated once again and then the residue finally suspended in a mixture (1:1) of DCM and MeOH. Undissolved inorganic salts were filtered off and the solvent finally removed *in vacuo*, obtaining a brown oil, the oil was recrystalised with Et_2O and then the solvent removed again *in vacuo,* obtaining a brown solid (0.250g, 0.38mmol, 83%).^{1}H NMR (400 MHz, MeOD-d^4, ppm) δH: 1.41 – 1.24 (m, 10H), 1.54 – 1.41 (m, 9H), 1.55 – 1.71 (m, 5H), 1.73 – 2.17 (m, 4H), 1.73 – 2.17 (m, 4H), 2.20 – 2.67 (m, 5H), 2.68 – 2.96 (m, 3H), 3.09 – 3.25 (m, 4H), 3.25 – 3.45 (m, 3H), 3.53 – 3.68 (m, 5H); ^{13}C NMR (100 MHz, MeOD-d^4, ppm) δC: 173.2, 172.1, 65.4, 61.3, 51.5, 48.5, 40.8, 39.3, 39.0, 37.7, 34.4, 31.7, 31.5, 30.0, 29.8, 29.3, 28.5, 27.7, 27.4, 26.4, 25.9, 25.6, 23.5, 23.3, 23.1, 23.0, 22.7, 18.9, 18.6, 12.8. MS (HR ES$^+$) calc. for $C_{29}H_{56}N_7O_8S$ (M + H$^+$) 662.3911 found 662.3910. IR (νmax, cm^{-1}) 3238 (w), 3124 (w), 2791 (s), 2534 (s), 2449 (s), 2389 (s), 2322 (s), 2266 (s), 1978 (w), 1924 (w), 1458 (w), 1178 (w), 779 (s), 758 (s), 738 (s), 719 (s), 680 (s), 652 (s), 638 (s), 619 (s).

1-((4-(benzo[d]thiazol-2-yl)phenyl)(methyl)amino)-3-(1,4,7,10-tetraazacyclododecan-1-yl)propan-2-ol (cyclen-Bz-epox)

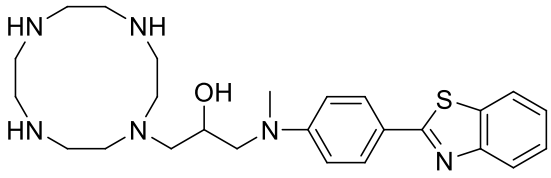

Cyclen (0.059g, 0.34mmol) was dissolved in acetonitrile (10mL) and Bz-epox (0.100g, 0.34mmol) was added to the solution with few drops of THF. The mixture was left under stirring for three days. The solid was filtered off and the solvent was removed *in vacuo*. (0.139g, 0.30mmol, 88%). ^{1}H NMR (400 MHz, MeOD-d^{4}, ppm) δH: 2.42 – 2.91 (br m, 21H), 3.07 (s, 3H), 6.75 (d, 2H, J = 9.0Hz, -CCHC*H*-), 7.25 – 7.31 (m, 1H, -C*H*CHCS-), 7.41 (t, 1H, J = 7.1Hz, -C*H*CHCN-), 7.81 (d, 1H, J = 7.8Hz, -CHC*H*CS-), 7.87 – 7.99 (m, 3H); ^{13}C NMR (100 MHz, $CDCl_3$, ppm) δC: 168.7, 154.4, 151.6, 134.5, 129.1, 126.0, 124.3, 124.2, 122.2, 121.4, 121.3, 112.0, 111.7, 67.6, 65.8, 59.4, 58.1, 56.8, 52.4, 47.1, 46.1, 45.9, 45.6, 39.6, 31.0, 30.3, 22.7, 18.5, 15.3. MS (HR ES^{+}) calc. for $C_{25}H_{37}N_6OS$ (M + H^{+}) 469.2750 found 469.2731. IR (νmax, cm^{-1}) 3306 (w), 3205 (s), 3064 (w), 2956 (s), 2860 (s), 2376 8s), 1917 (w), 1637 (w), 1516 (w), 1458 (w), 881 (s), 850 (s), 825 (s), 804 (s), 779 (s), 765 (s), 758 (s), 736 (s), 719 (s), 696 (s), 678 (s), 648 (s).

Cu(II)-Cyclen-Bz-epox

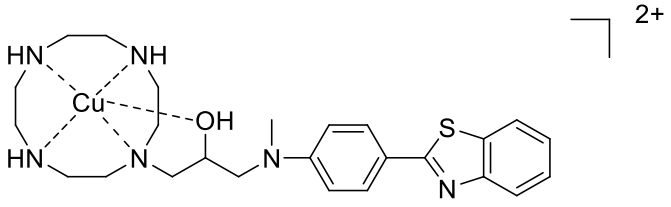

Cyclen-Bz-epox (0.030g, 0.06mmol) was dissolved in MeOH (~3mL); a solution of $CuSO_4$*$5H_2O$ (0.017g, 0.06mmol) was dissolved in MeOH (~2mL) and added to the ligand. The solution was heated to 50°C for five minutes, changing colour in a dark blue solution. The solution was cooled to room temperature and filtered off on a small

chromatography column. MS (HR ES^+) calc. for $C_{25}H_{35}N_6O_1SCu$ ($M + H^+$) 530.1889 found 530.1894.

[1] S. Manohar, S. I. Khan and D. S. Rawat, *Bioorganic & Medicinal Chemistry Letters* 2010, *20*, 322-325.

[2] B. Jagadish, G. L. Brickert-Albrecht, G. S. Nichol, E. A. Mash and N. Raghunand, *Tetrahedron Letters* 2011, *52*, 2058-2061.

[3] T. Peppel and M. Köckerling, *Journal of Coordination Chemistry* 2009, *62*, 1902-1913.

[4] a) C. A. Mathis, B. J. Bacskai, S. T. Kajdasz, M. E. McLellan, M. P. Frosch, B. T. Hyman, D. P. Holt, Y. Wang, G.-F. Huang, M. L. Debnath and W. E. Klunk, *Bioorganic & Medicinal Chemistry Letters* 2002, *12*, 295-298; b) X.-Q. Zhu, M.-T. Zhang, A. Yu, C.-H. Wang and J.-P. Cheng, *Journal of the American Chemical Society* 2008, *130*, 2501-2516.

[5] N. Saini, R. Varshney, A. K. Tiwari, A. Kaul, M. Allard, M. P. S. Ishar and A. K. Mishra, *Dalton Transactions* 2013, *42*, 4994-5003.

[6] K. Cui, X. Lu, W. Cui, J. Wu, X. Chen and Q. Lu, *Chemical Communications* 2011, *47*, 920-922.

[7] P. Galinetto, A. Taglietti, L. Pasotti, P. Pallavicini, G. Dacarro, E. Giulotto and M. S. Grandi, *Journal of Applied Spectroscopy* 2016, *82*, 1052-1059.

CHAPTER 3

1-*N*-2,4,6-TRIAZINE SUBSTITUTED CYCLEN LIGANDS

Many physiological processes, such as immune cell activation, cell migration and cell proliferation, require direct contact between cells, or between cells and extracellular matrix. These interactions are also involved in the development of tumour metastases,[1] tumour cells can break free from the site and can be transferred through the blood or lymphatic system to another tissue to invade, then they must be able to develop their own blood supply (angiogenesis) to survive and in this way the tumour can be spread to different sites.[2] One group molecules responsible for cell adhesion are the integrins. Integrins are heterodimeric glycoproteins containing α and β chains; the α chain has approximately 1100 amino acids and usually consists of two chains joined by a disulfide bond, most of the subunit is an extracellular chain, with a short transmembrane domain and a short cytoplasmic domain. The β chain typically has 800 residues and can be divided into three broad families.[3] The integrin $\alpha_V\beta_3$ is one of the most widely studied, also known as the vitronectin receptor, is responsible for cells binding to proteins in the extracellular matrix (ECM), and has been found to be over expressed in many different tumour cells, including osteosarcomas, neuroblastomas, melanomas, breast, brain and lung cancer and has a role in angiogenesis process.[4] Thus it is clear that the development of $\alpha_V\beta_3$ recognition species are attractive targets for new imaging or therapeutic agents.[5]

The amino acid sequence Arg-Gly-Asp (RGD), known as "universal cell recognition site", is one of the most frequently used integrin binding sequence motifs. The crystal structure of the $\alpha_V\beta_3$ complexed with a *cyclo*-RGD ligand was resolved by Arnaout's group in 2002,[6] and showed that ligation intimately involved the RGD sequence. Hence, the development of antagonists based on this sequence can be used to inhibit or, in the case of imaging agent development, locate the $\alpha_V\beta_3$ receptor.

Cyclo RGD petites are very expensive and already extensively used in imaging inflammation,[7] so the current research has focused on the design of alternative vectorising agents.

Cyanuric chloride (2,4,6-trichloro-1,3,5-triazine) has always received much attention due its low cost allowing a wide range of applications to be found.[8] The ability to progressively substitute the chloro substituents with a range of groups, through sequential nucleophilic aromatic substitution (S_NAr) reactions, enables the controlled synthesis of mono-, di- and tri-substituted compounds.[8] These have been widely studied to create a library of complex ligand structures able to incorporate an ample range of functional groups and the capacity to control their physicochemical properties to fit the desired purpose.[8] Triazines have also been extensively used as building blocks for pesticides and herbicides,[9] and in the manufacture of melamine resins[10] or crosslinking agents. 2,4,6-Triazine derivatives have also found extensive medicinal applications as antimicrobials,[11] antivirals,[12] antituberculosis drugs,[13] and antimalarials,[14] but most extensively as non-proliferative chemotherapeutic (anti-cancer) agents.[15]

Dipyridamole (Persantine©) is used as an antiplatelet drug to prevent strokes, inhibit thrombus formation and as a vasodilator (Figure 3.1). It is also an inhibitor of human equilibrative nucleoside transporters (hENTs) and its similarity to cyanuric chloride, makes it an attractive target for hENT targeting. In the current work the tri-substituted triazine moiety is used by incorporating the piperidine and diethanolamine moieties and allowing the third chlorine free for further substitution with a metal binding site.

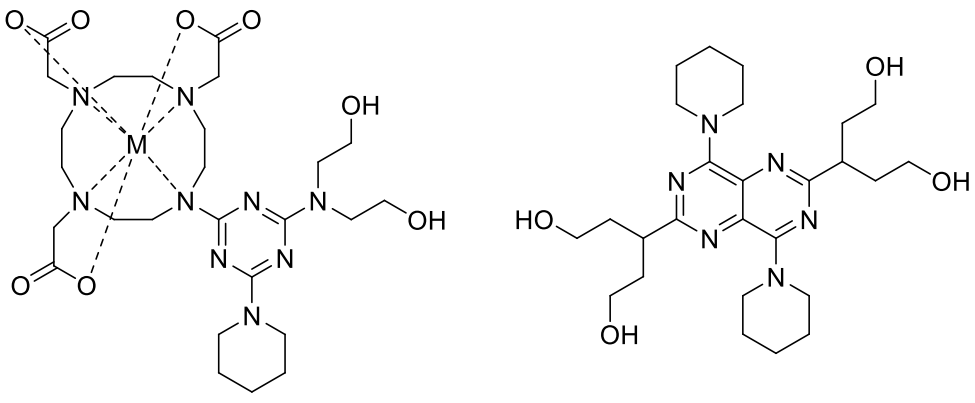

Figure 3.1: the targeting molecule (left) and Dipyridamole (right)

Present examples of chemotherapeutic agents containing the 1,3,5-triazine core are hexamethylmelamine (HMM, Altretamine©) and 2-amino-4-morpholino-*s*-triazine (Figure 3.2), both clinically used to treat lung, breast and ovarian cancer.[16] Although the precise mechanism by which Altretamine© works is unknown some hypotheses have been presented; the most evaluated theory considers the compound as an alkylating antineoplastic agent, with the capacity to damage the tumour cells through the production of formaldehyde as an alkylating species via oxidative p450 action on the parent drug.[17]

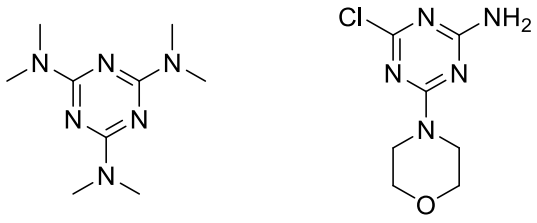

Figure 3.2: HMM (left) and 2-amino-4-morpholino-*s*-triazine

Kumar's group also reported a list of di- and tri-substituted s-triazine derivatives with anticancer activity.[18] Tri-substituted s-triazine derivatives, bearing anilino, benzoxazole and morpholino groups, showed the best activity against the cancer cell lines tested compared to the di-substituted s-triazine compounds that do not bear the morpholine, revealing the importance of morpholino group. The anticancer activity of morpholino group has been proved recently targeting phosphatidylinositol 3-kinase (PI3K) in tumours.[19] PI3K has been proved as the key regulator of the cell growth, metabolism and survival; the activation of the PI3K pathway in cancerous tissues has encouraged interest in identifying potent and selective inhibitors of PI3K pathways.[20] One of the best inhibitors currently synthesised is ZSTK474 (Figure 3.3), due to its capacity to bind the Val828 by a hydrogen bond of the oxygen of one morpholine and Pro758 by the difluoromethyl group.[21] At present, due to its high *in vivo* activity against human cancer xenografts, this compound has entered in clinical trials and is used as the benchmark for new molecules.

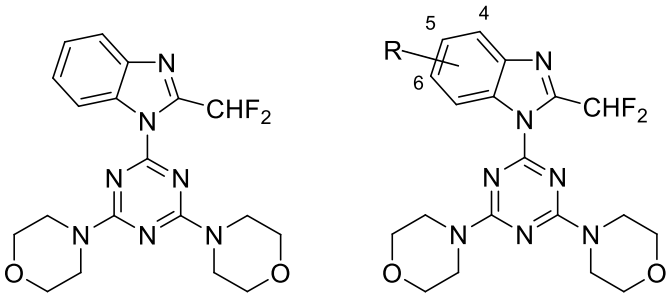

Figure 3.3: ZSTK474 compound and analogues

The triazine structure of the compound makes it ‘editable’ by the use of different nucleophiles. Work by Rewcastle's group synthesised different analogues (Figure 3.4) and evaluated the binding properties to PI3K and the inhibition of phosphorylation or cell growth.[22] Analogues of ZSTK474 can be synthesised for application as new ^{18}F-PET probes. The presence of morpholine and difluoromethyl moieties are essential to bind PI3K and the possibility to modify the triazine core makes it attractive for imaging probes. ZSTK474 derivatives have been synthesised using different approaches by Makino's group,[23] the first was to substitute one of the morpholines with a piperazine, leaving a reaction point for a further functionalisation. The compound showed a weaker binding affinity to the PI3K, revealing how the morpholine promotes the affinity via hydrogen bonding. To compensate the loss of stability two more compounds have been synthesised, one of them retaining the piperazine core but adding an appropriate electron-donating substituent like a hydroxy group at the 4-position of the benzimidazole and another, retaining the two morpholines on the triazine and adding a fluoroethyl group at the 4-position of the benzimidazole (Figure 3.4)

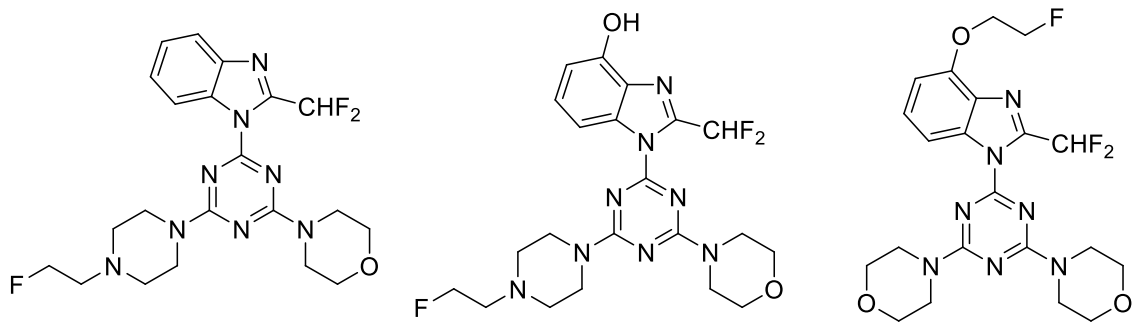

Figure 3.4: compounds synthesised by Makino's group

The stability showed by the second molecule was comparable to the ZSTK474 and made it eligible for radiolabeling studies as a PI3K probe. The compound exhibited the rapid blood clearance that is one of the important characteristics for tumour imaging probes, but unfortunately also a low tracer accumulation was observed.

Morpholines were chosen as a simple model analogues of more complicated species (e.g. amino acids), whilst still imparting some water solubility, hydrogen bonding potential and affording often crystalline intermediates. Due to the facile sequential displacement of its chlorine atoms, cyanuric chloride was used as a core to prepare many compounds, by reacting different amino compounds in the presence of base.[8] The replacement of the chlorine atoms may be controlled via changes in temperature, where the substitution of the first chlorine atom occurs at 0-5°C, the second occurs approximately at room temperature and the third requires temperatures at 70-100°C in order to activate the last chlorine (Figure 3.5)

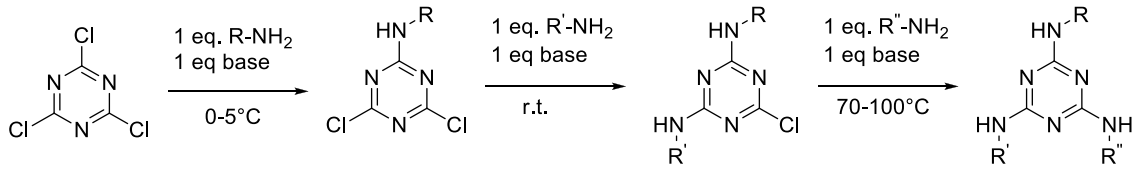

Figure 3.5: general synthesis of mono, bis and tri substituted s-triazines

The starting material DO3A*HBr was prepared using published method,[24] using the macrocycle to coordinate the metal. Before synthesising the dipyridamole analogues and to understand better the triazine chemistry a di-morpholine triazine moiety, following the preparation reported by Hughes (Cardiff University, PhD thesis, 2012) has been synthesised to react with the DO3A core. The protected macrocycle was then reacted with 2-4-dimorpholino-s-triazine in acetonitrile under reflux and an inert atmosphere for three days, yielding the trisubstituted triazine ($TzMorph_2DO3A$) as a colourless oil. Finally the product was dissolved in DCM and deprotected adding TFA and leaving the reaction under stirring for two days. The completion of the reaction was followed by ^1H NMR by the loss of the peaks at 1.43-1.46 ppm, revealing the deprotection of the carboxylic acid groups. (Figure 3.6)

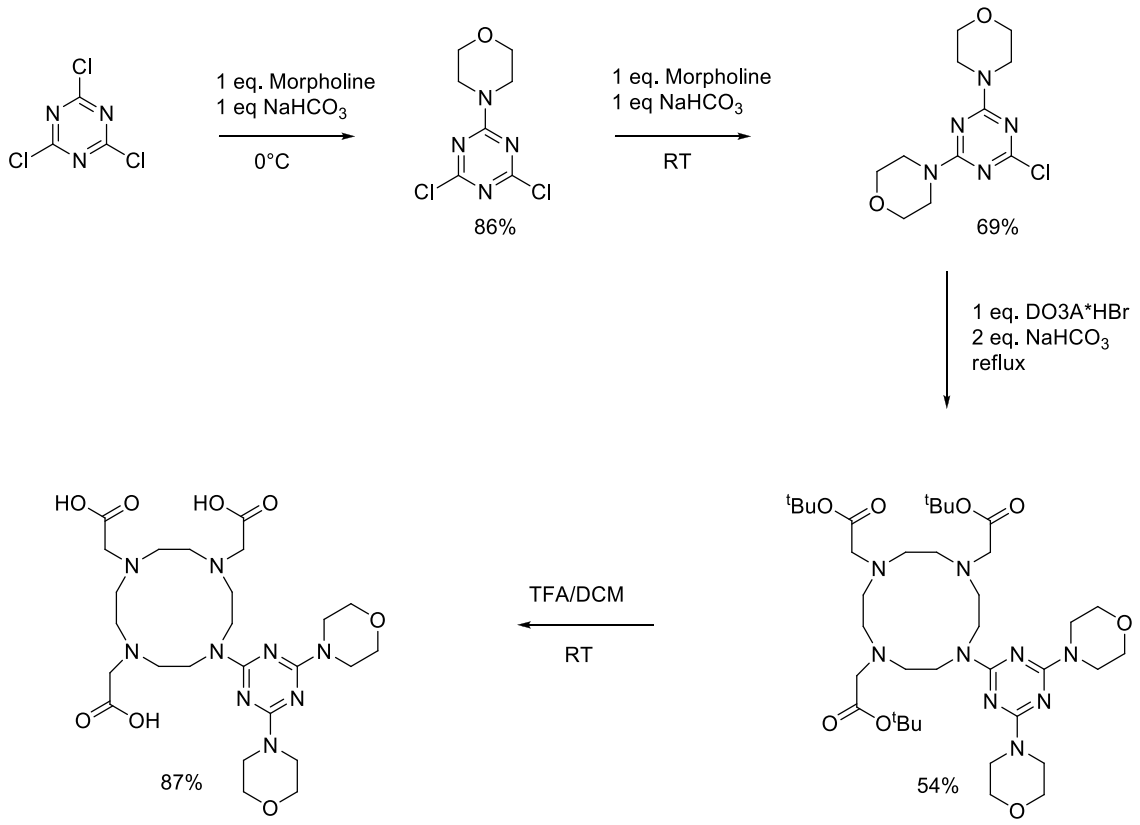

Figure 3.6: synthesis of TzMorph$_2$DO3A ligand

A wide range of metals have been used to explore and understand better the coordination chemistry of this ligand. To synthesise the complexes two different procedures have applied.

The first one required that TzMorph$_2$DO3A (0.17mmol) was dissolved in ca. 3mL of water and the pH of the solution corrected to reach pH 7, adding a solution of 1M NaOH. The metal salt, typically as a chloride, triflate or nitrate, was dissolved in ca. 2mL of water and added to the ligand solution. The solution was heated at 40-50°C for five minutes and then cooled to room temperature. The mixture was purified by flash chromatography on a short column, to afford a clear solution (Figure 3.7).

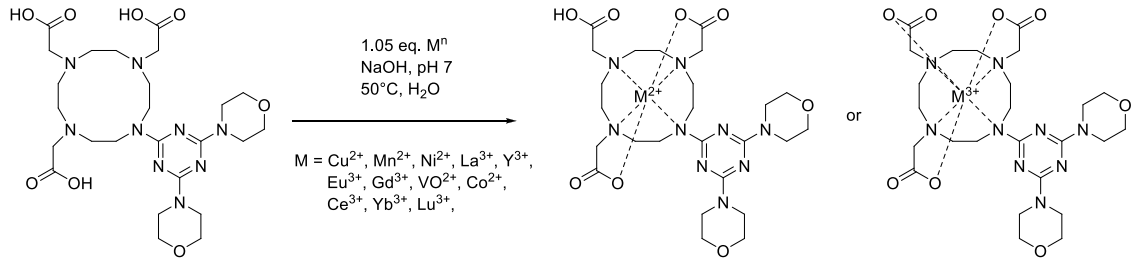

Figure 3.7: first method synthesis of TzMorph$_2$DO3A complexes

In the second method TzMorph$_2$DO3A (0.50mmol) was dissolved in ca. 3mL of MeOH. The metal salt was dissolved in ca. 2mL of MeOH and added to the ligand solution. The pH of the solution corrected to basic pH adding Et_3N until there was the formation of a precipitate and the solid was separated by centrifuge (Figure 3.8).

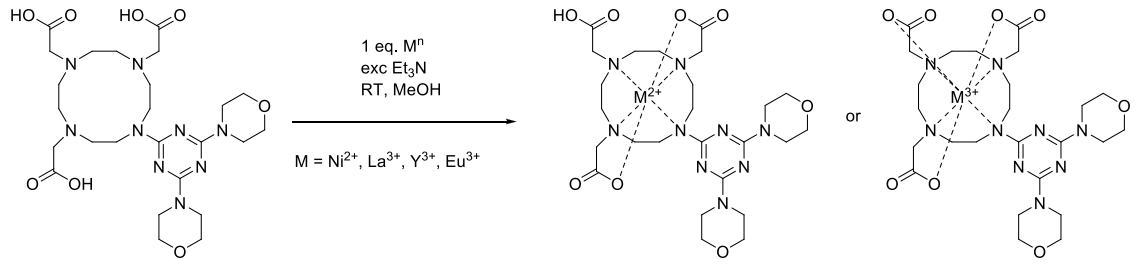

Figure 3.8: second method synthesis of TzMorph$_2$DO3A complexes

All the complexes have been characterised by ESI-MS. Several examples afforded crystals suitable for x-ray crystallography. The structures obtained will be reported and discussed below.

Electronic spectroscopy has also been used to determine ligand field parameters.

3.4.1 - Determination of the empirical formula

The last step of the synthesis the ligand $TzMorph_2DO3A$, TFA has been used to remove the protection groups; all the successive compounds were prepared assuming that the ligand does not present any residual molecule of acid. This ensures that the ligand is always used in excess, driving reactions to completion.

However, it is likely that given the basicity of cyclen $TzMorph_2DO3A$ will be initially isolated as a TFA salt. To determine the presence of the amount of TFA present and hence the empirical formula of the ligand a metal titration was undertaken (Job's method).

Aliquots of 100 µL ligand solution (0.1M) was added to a fixed volume of nickel equimolar solution in nine volume ratios and the absorbance of the solutions has been recorded. The ratio of the solutions and the absorbance registered at 541 nm are reported in the table and the graph below (Figure 3.9)

The maximum amount of product is formed when the proportions of reactants employed corresponds to the empirical formula. For n = 0 ($TzMorph_2DO3A\text{-}TFA_n$) a ratio of 1:1 would appear at 100 µL added volume (total volume = 200 µL). The data show that the maximum absorbance corresponds with the ratio metal : ligand equal to 4 : 6, this means that the data is consistent for $TzMorph_2DO3A\text{-}TFA_n$ with $n = 3$.

Sample	Volume ratio of M : Ligand	Absorbance (A) at 541 nm
A	1 :9	0.0689
B	2 : 8	0.1098
C	3 : 7	0.2637
D	4 : 6	0.3096
E	5 : 5	0.2465
F	4 : 6	0.1084
G	3 : 7	0.1683
H	2 : 8	0.0632
I	1 :9	0.0611

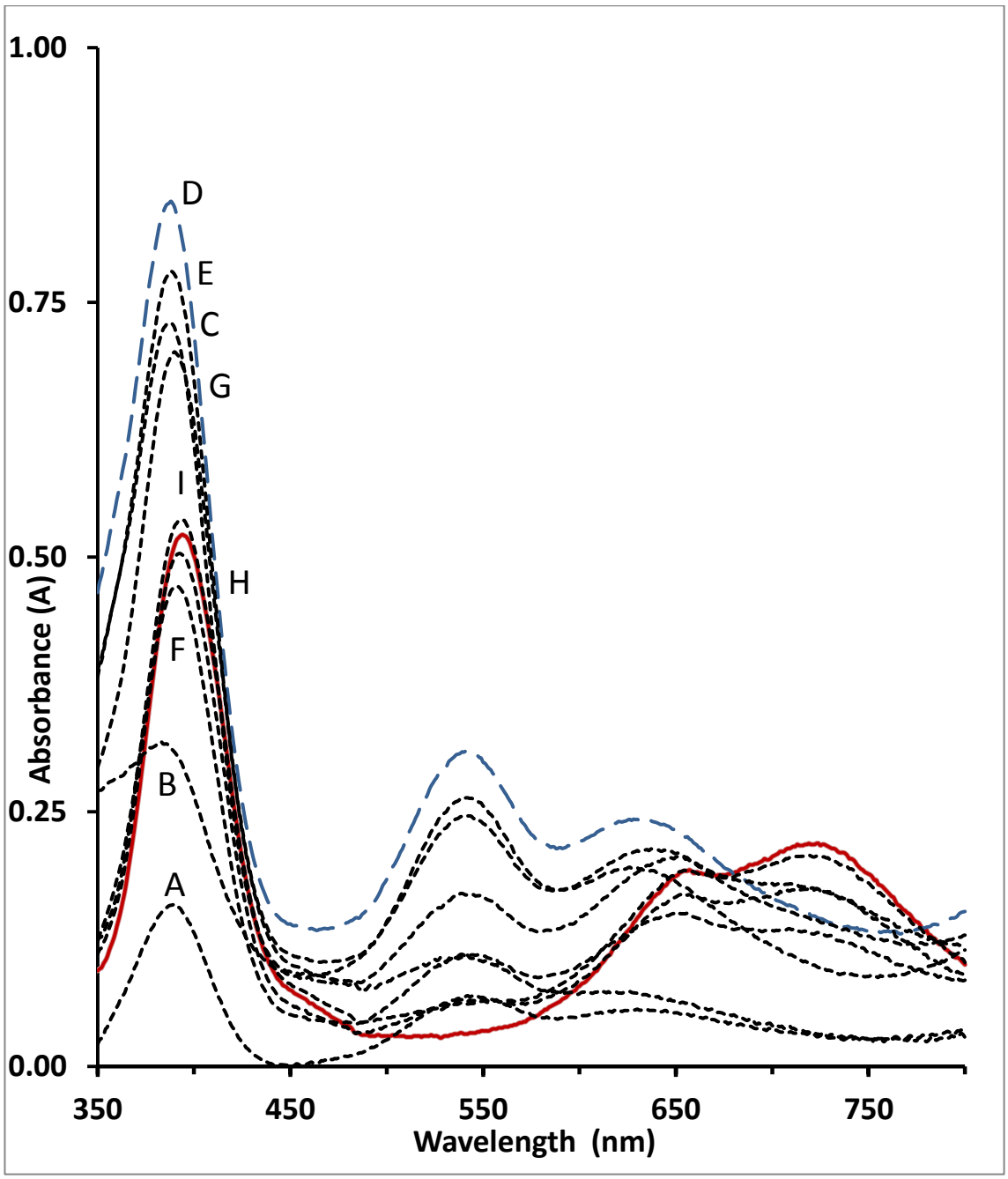

Figure 3.9: UV spectra with different ratios metal : ligand. The blue line represents the sample D, with a ratio 4:6. The red line represents the pure Ni(II) spectrum.

3.4.2 - UV measurements

UV measurements of solution of Cu(II), Co(II) and Ni(II) have been conducted to determine the nature of the complexes in solution. To a 0.02 M solution of $TzMorph_2DO3A\text{-}TFA_3$, adjusted at pH 7 adding a solution 2M of NaOH, has been added an equimolar solution of the metal and an UV spectrum in the range of 350 - 1300 nm has been recorded. The data obtained will be discussed for every metal analysed in the below section.

3.4.3 - Copper(II)-TzMorph$_2$DO3A

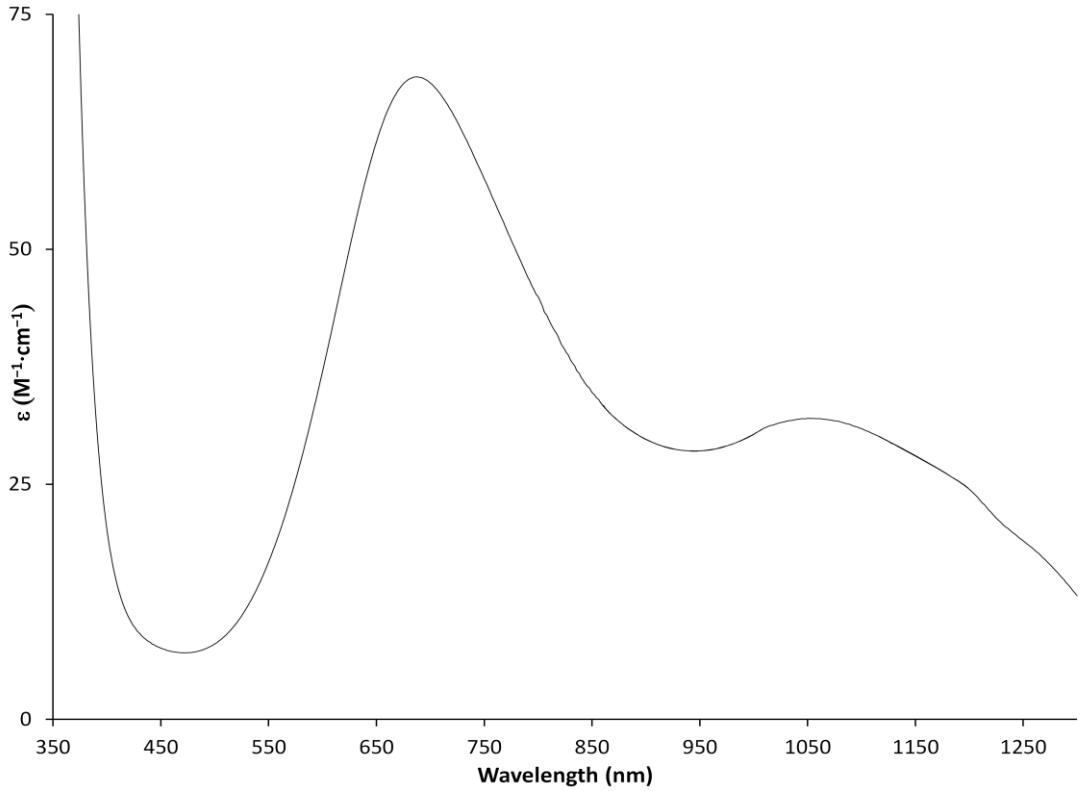

Figure 3.10 - Electronic spectrum of 0.01M Na[Cu-TzMorph$_2$DO3A] in H2O. The sample was prepared from TzMorph$_2$DO3A-TFA$_3$ + $CuCl_2.6H_2O$ after adjusting the pH to 7 with 2M NaOH.

The electronic spectrum of Na[Cu(TzMorph$_2$DO3A)in H2O is displayed in figure 3.10. The Cu(II) complex is assigned as 5 coordinated trigonal bipyrimidal system. This is evidenced by the presence of two features at 688 and 1050 nm in the electronic spectrum (Figure 3.10). This suggests that this is an N_3O_2 trigonal bipyrimidal system from three cyclen nitrogen and two pendant carboxylate derived donors. From an examination of many 4,5, and 6 coordinate complexes,[25] this assignment is in good agreement with other 5 coordinate donor compounds. For example Cu(bipy)$_2$OAc (10,860 and 15,150 cm^{-1}) and Cu(Me$_6$tren)Br$_2$ (10,400 and 13,400 cm^{-1}).[25]

3.4.4 - Nickel(II)-TzMorph$_2$DO3A

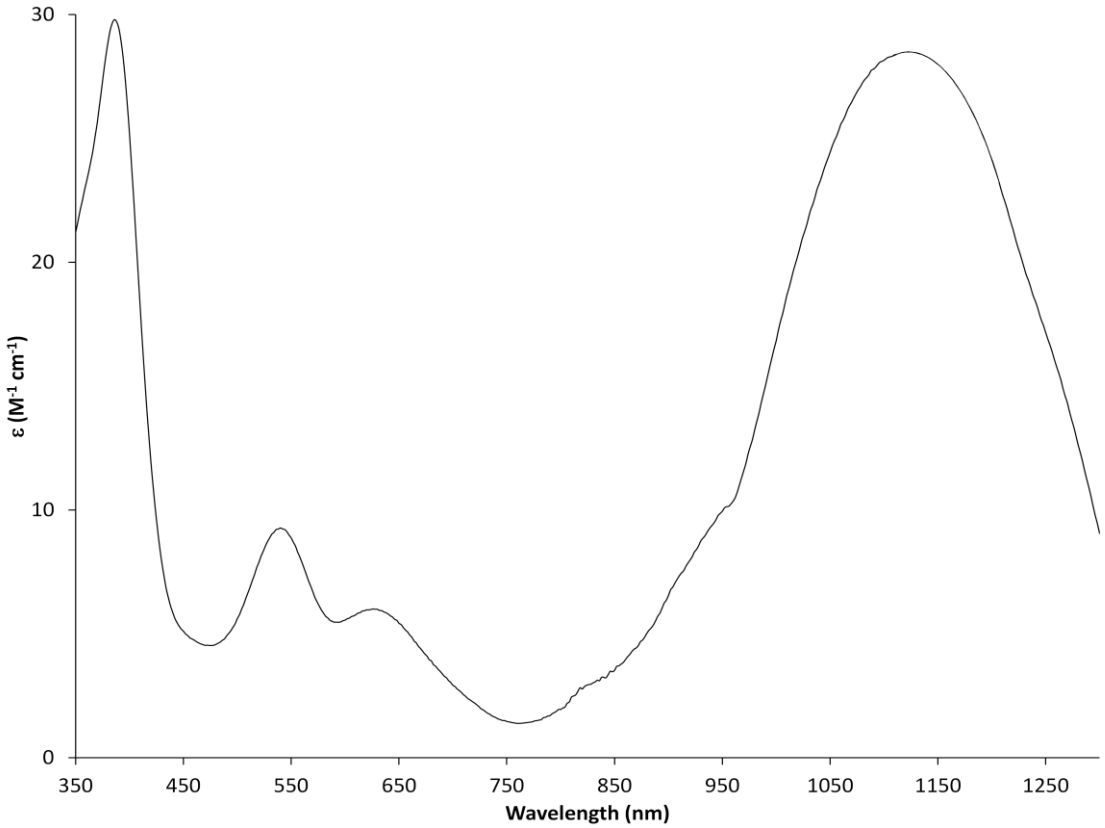

Figure 3.11- Electronic spectrum of 0.01M Na[Ni-TzMorph$_2$DO3A] in H_2O. The sample was prepared from TzMorph$_2$DO3A-TFA_3 + $NiCl_2.6H_2O$ after adjusting the pH to 7 with 2M NaOH.

The electronic spectrum of the Ni(II) complex of TzMorph$_2$DO3A is shown in figure 3.11. Here it is apparent that complex is a distorted 6 coordinate species. The low extinction coefficient values observed for the transitions are in the range of 6 – 30, indicative the origin of these transitions are d – d in nature. However there is clearly an addition feature at 540 nm. The bands observed are tentatively assigned in the table below. Analysis of this data yields a ligand field splitting value of 8928 cm^{-1} and a Racah B ($B = (v_2 + v_3 - 3 v_1)/15$) parameter of 1010 cm^{-1}. These calculations are of course crude approximations since they assume octahedral symmetry, which is unlikely to be attainable in complexes of TzMorph$_2$DO3A. The assignment of v_2 as the peak at 624 nm and not 540 nm was made on the basis that this affords a Racah B parameter of 1010 cm^{-1} whilst using the 540 nm peak would yields a nonsensical value of 1176 cm^{-1} as it is higher than that of the free ion (1042 cm^{-1}). The high Racah B value obtained implies a poorly covalent complex with a highly ionic character, logical for an N_3O_3 chromophore with 3 anionic

donors. It is worth noting that the Δ_o value obtained is only a little higher than that of the $[Ni(OH_2)_6]^{2+}$ ion (B = 8,500cm^{-1}) and we may assume that the macrocyclic and chelate effects account for the stability of the complex The weak, formally forbidden $^1E_{2g} \leftarrow {}^3A_{2g}$ transition may be tentatively assigned to the weak feature at 820 nm. However this is somewhat speculative due to the difficulty of obtaining a good NIR background in aqueous solution.

It is possible speculate that the additional feature at 540 nm resembles that obtained in Lifsshitz salts in which an octahedral-square planar equilibrium or mixture exist.[26] Hence the band at 540 nm may be due to a square planar N_2O_2 component arising from the dissociation of two amine and one carboxylate donor in the strained triazine-cyclen macrocycle. Given the constraints of the macrocyclic ring in this system it is likely that the N-donor and their corresponding carboxylate donors at ring position 4 and 10 are those that remain coordinated (the triazine is at ring position 1).

Transition assignment	λ (nm)	λ (cm-1)
$\nu_1 = {}^3T_{2g} \leftarrow {}^3A_{2g}$ (Δ_o)	1120	8928
$\nu_2 = {}^3T_{1g}$ (F) $\leftarrow {}^3A_{2g}$	624	16025
$\nu_3 = {}^3T_{1g}$ (P) $\leftarrow {}^3A_{2g}$	386	25906

Racah B ($\nu_2 + \nu_3 - 3\ \nu_1$)/15)	1010

Table 1 - Spectral assignemnt of Na[Ni-TzMorph$_2$DO3A] in H_2O and associated ligand field parameters.

3.4.5 - Cobalt(II)-TzMorph$_2$DO3A

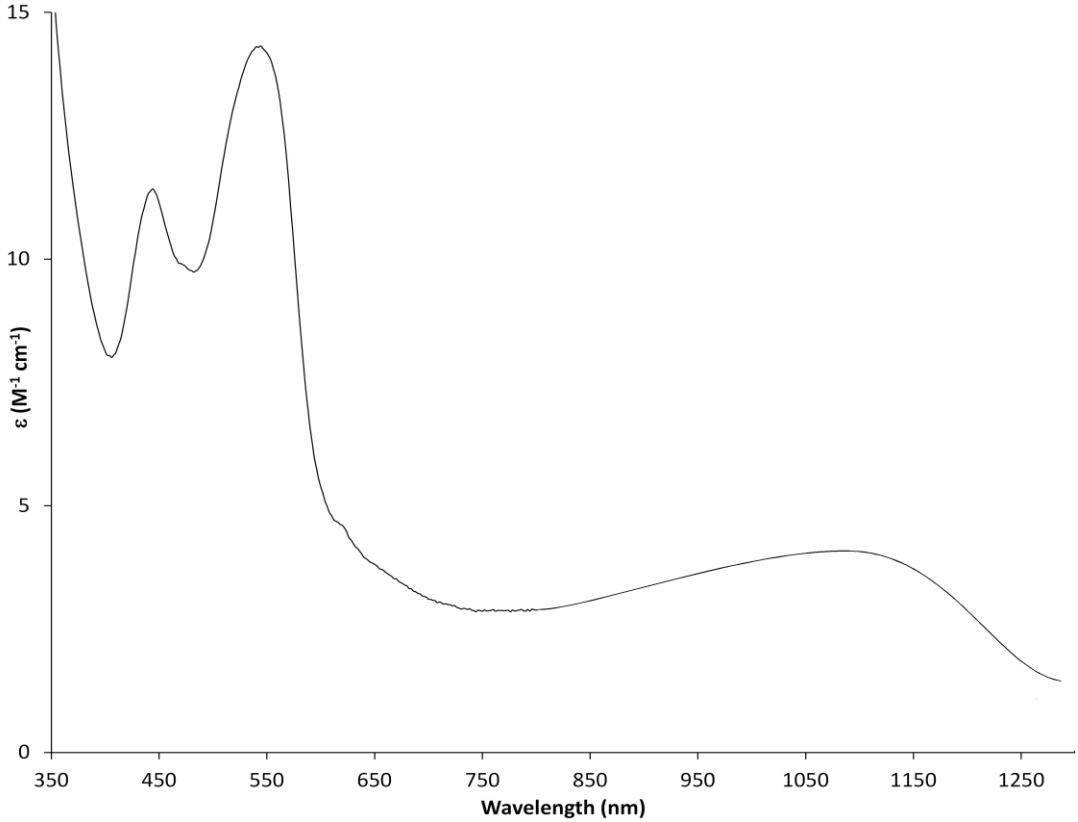

Figure 3.12 - Electronic spectrum of 0.01M Na[Co-TzMorph$_2$DO3A] in H_2O. The sample was prepared from TzMorph$_2$DO3A-TFA$_3$ + $CoCl_2.6H_2O$ after adjusting the pH to 7 with 2M NaOH.

The electronic spectrum of Na[Co-TzMorph$_2$DO3A] in H_2O is illustrated in figure 3.12. The weak nature of the transitions implies that the bands observed are d - d in origin and that the complex is a high spin low symmetry d^7 (*i.e.* Co(II)) species. The ground state term for high-spin d^7 is $^4T_{1g}$ with spin allowed transitions to $^4T_{2g}$ (low energy feature), $^4A_{2g}$ and $^4T_{1g}$(P) level (high energy features). Since the complex envelope shape of the higher energy feature is indicative of low symmetry and the $^4A_{2g}$ transition is often weak (formally a two electron transition) is not possible to rigorously derive, from this data alone, Δ and B for this species. However using the method of Lever[27] it could be possible to use the transition energy ratio method to approximate Δ and B. Taking v_1 as 1105 nm and v_3 as the more intense high energy feature (440 nm) we obtain a Dq/B value of 1.38, v_3/B = 35.7 and Dq= 1.45 B. Hence it could be possible to approximate Δ = 9090 cm^{-1} and B = 660 cm^{-1}.While this Δ value seems reasonable for this type of trianionic ligand, the B value is somewhat low in comparison to the d^7 free ion at 985 cm^{-1} or the $[Co(OH_2)_6]^{2+}$

complex at 850 cm^{-1}.[28] This inconsistency may arise from the assumption that this complex is octahedral in solution, which given its distorted geometry is unlikely.

3.5.1 – D-BLOCK METAL COMPLEXES OF TZMORPH$_2$DO3A

3.5.1.2 - Copper(II) and Nickel(II) complexes of TzMorph$_2$DO3A

Through the vapour diffusion of acetone into water solutions of the Ni(II) and Cu(II) complexes of TzMorph$_2$DO3A it has been possible to isolate light blue needle-like crystals for the Cu(II) species and light purple long columns for the Ni(II) complex suitable for the crystallographic studies.

Their relevant crystal parameters and details of data collection are presented in the supporting information.

H[Ni(II)-TzMorph$_2$DO3A] - The data reveal that the nickel compound forms a 1:1 metal : ligand ratio, with the molecule crystallising in the orthorhombic space group Pbc2$_1$ (Figure 3.13). The asymmetric unit contains two independent molecules (Z = 2) as well as one acetone molecule for complex that gives to the structure a C_2 symmetry.

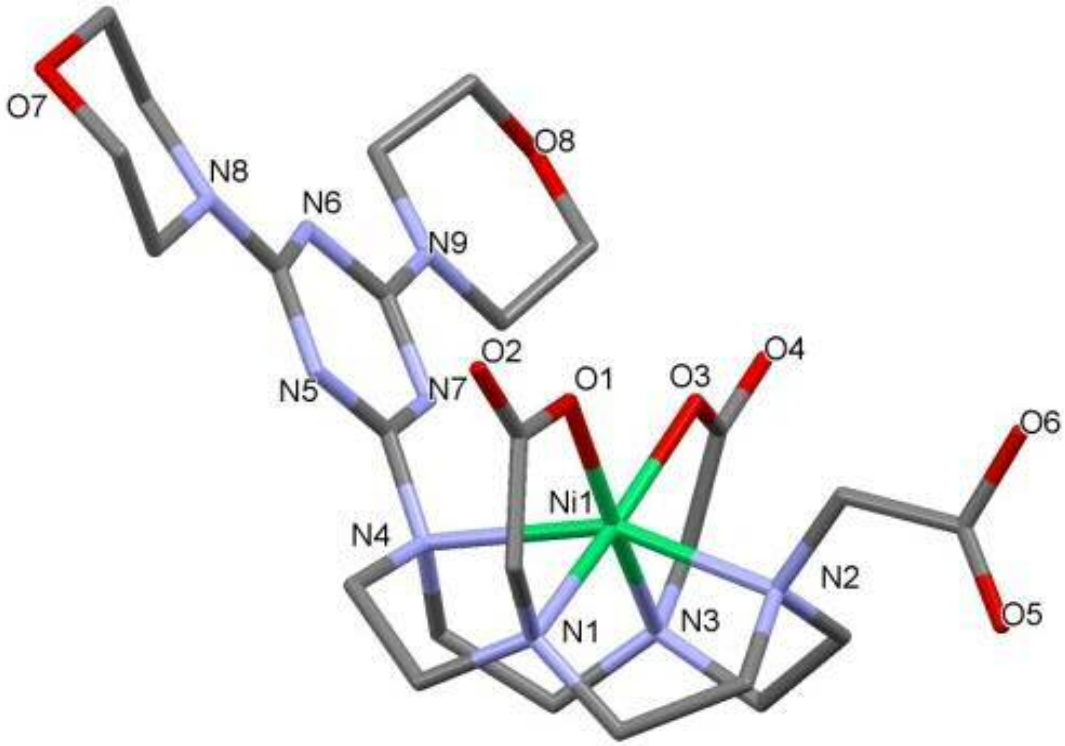

Figure 3.13: H[Ni(II)-TzMorph$_2$DO3A] complex structure

The metal centre is six coordinate with a geometry resembling a distorted octahedron, being the Ni(II) a d^8 ion, the structure could suggest that the metal assumes a high spin configuration in the solid state. Figure 3.14, to show better the coordination structure the triazine core has been removed.

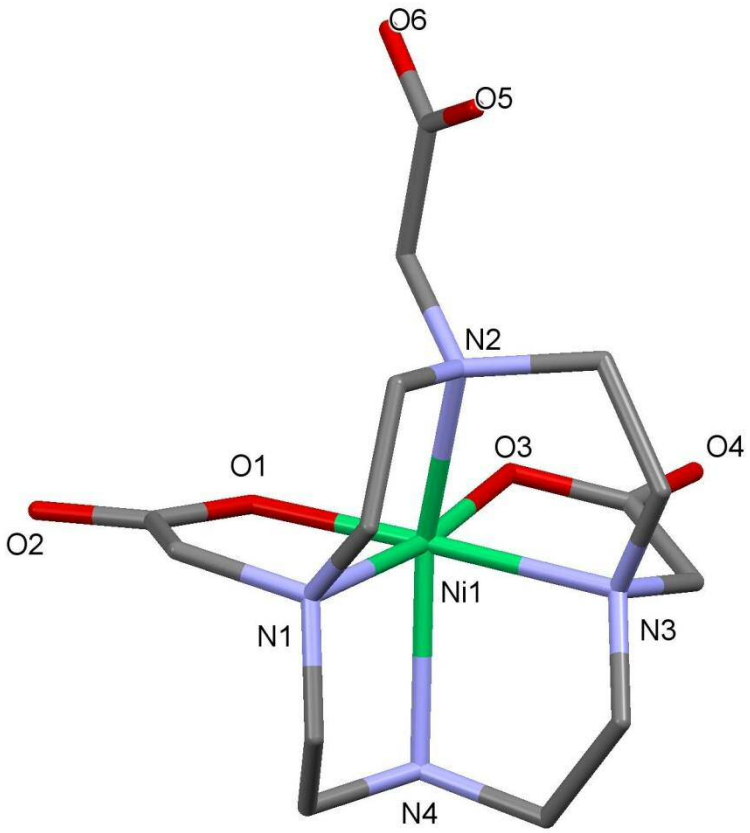

Figure 3.14: H[Ni(II)-TzMorph$_2$DO3A] with triazine core omitted for clarity

The structure also displays an approximate mirror plane through the triazine core, with each morpholine group in a pseudo-chair conformation and essentially sp^2 geometry at the morpholino N atom. The Ni(II) centre is coordinated by all four of the nitrogens in the macrocyclic ring while the two remaining coordination sites are occupied by the 4,10-pendant acid groups adjacent to the triazine ring, leaving the third one, opposite to the triazine core, unbound.

Considering the bond length between the metal and the axial nitrogen bearing the non bonding acid it is possible to see that it is 2.144(3) Å, longer than the length found for the equatorial Ni1 - N1 and Ni1 - N3 bonds, 2.098(3) and 2.103(3) Å respectively. The lengths found for these bonds are in accordance with the average trend that can be

observed in the Ni octahedral species (Ni - N = 2.07 - 2.11 Å) than in square planar species (Ni - N = 1.88 - 1.91 Å).[29] The length of Ni - O bonds was found to be 2.000(3) and 2.016(3) Å respectively, shorter than other Ni complexes encountered in literature.[29] This distance is given by the two acid groups borne on the macrocycle, considering the coordination provide by an acetate group is possible to see that the bonds lengths are similar to those of the Ni - N bonds better resembling a perfect octahedral geometry.[30] The stronger distortion observed in the structure can instead be explained by the chelate effect of the two acid groups, which constrains the equatorial bonds in a more rigid and distorted geometry. [30]

Significantly, the crystal structure also reveals that the Ni - $N_{triazine}$ bond to be elongated at 2.370(3) Å which is a consequence of the highly electron triazine substituent. As the triazine core is very electron deficient, the amine is a relatively poor donor and a weaker Ni - N bond results.

H[Cu(II)-TzMorph$_2$DO3A]- The copper (II) complex crystallises in the orthorhombic space group Pbca and contains 8 molecules in the unit cell (Z = 8). (Figure 3.15)

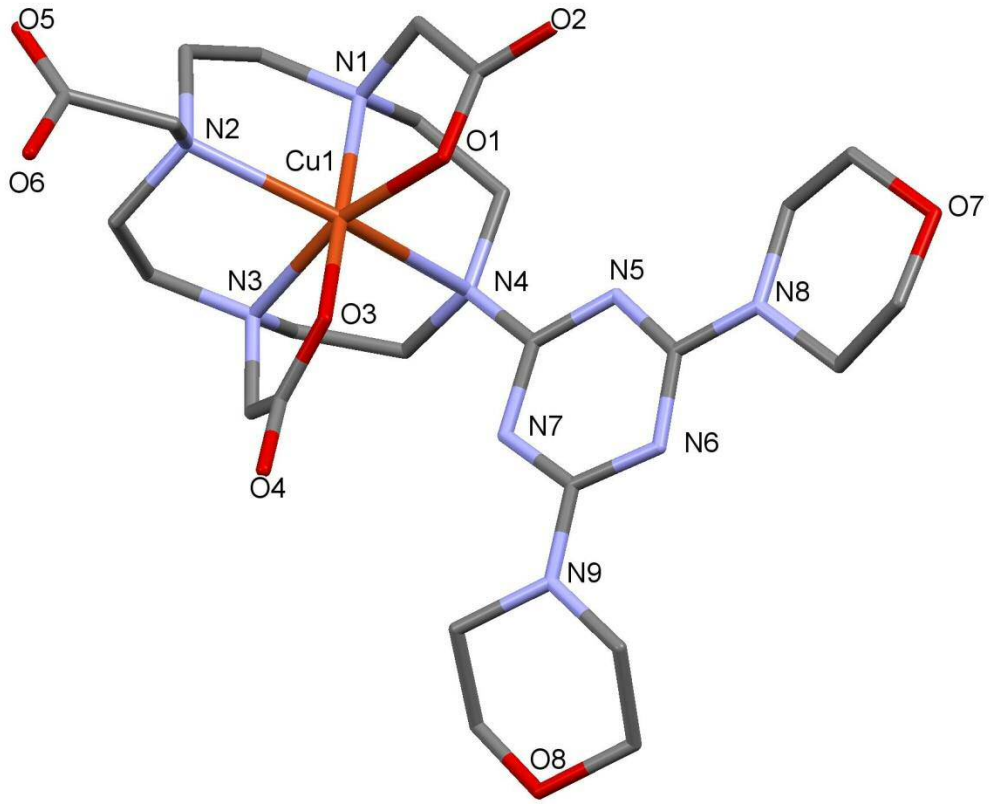

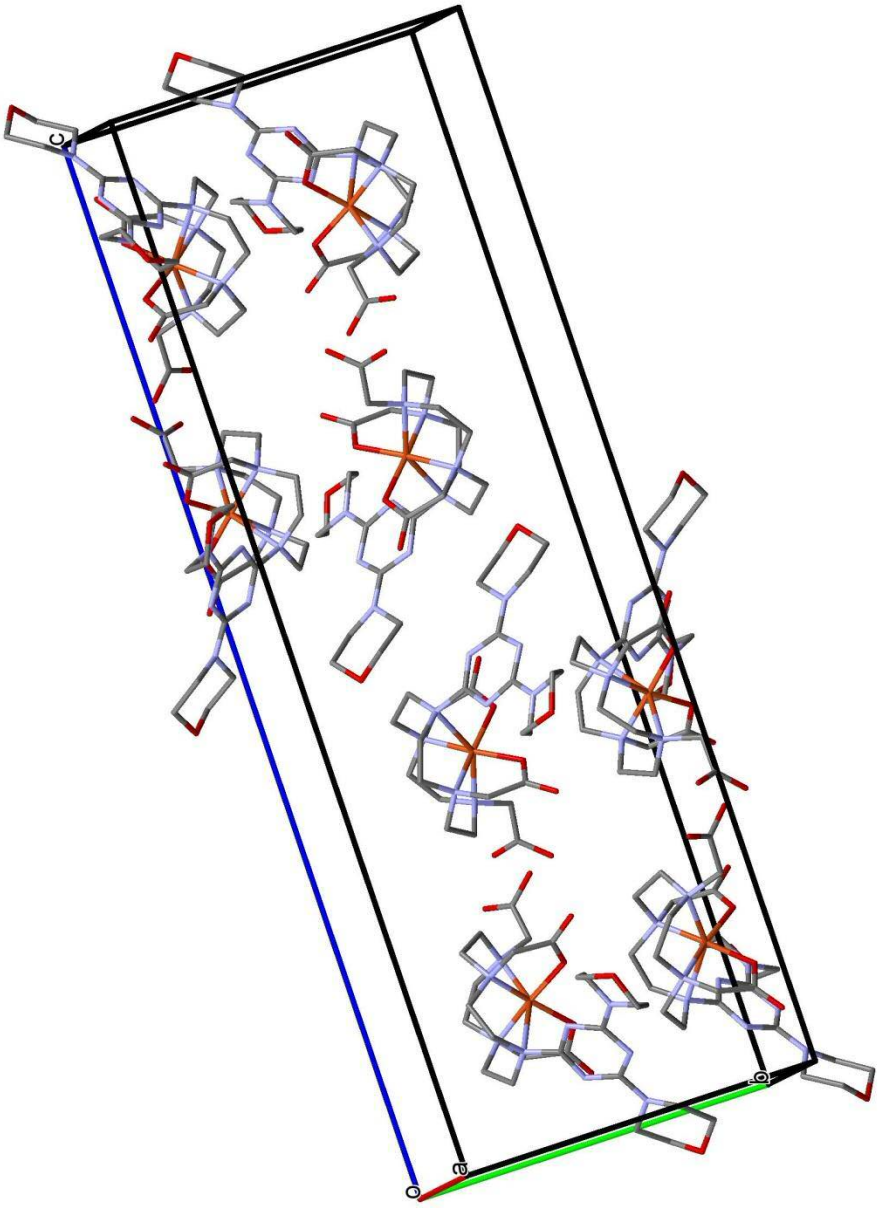

Figure 3.15: H[Cu(II)-TzMorph$_2$DO3A] complex structure (top) and unit cell (bottom)

The copper (II) presents a distorted octahedral N_4O_2 geometry through the four macrocyclic nitrogens and two (opposite) carboxylate arms, while the other carboxylic acid group is turned away from the Cu atom. This conformation is not unusual for the

copper chemistry, in literature indeed the two most common geometries for a copper complex coordinated by cyclen or derivates are the octahedral and the square pyramidal geometry. [31]

As expected for a Cu(II) complex in the octahedral geometry there is a tetragonal distortion with four relatively short bonds and two longer bonds; 2.056(3) and 2.090(3) Å for the macrocyclic ring and 1.936(2) and 1.942(2) Å for the carboxylate arms involved in the coordination and disposed in the equatorial plane; comparable bond distances found in the literature.[31e, 32]

There is no significant difference in the metal - nitrogen bond lengths that not bear the carboxylate arm involved in the coordination as well; the length results 2.318(3) Å compared to 2.391 and 2.390 Å found in a DO3A - copper complex in literature.[32] Finally, in a similar manner to the Ni(II) complex the M - $N_{triazine}$ distance is the longest (2.585(3) Å) and in an axial position, due to the lower electron density at this amine.

At the supramolecular level it is possible to identify an interesting H-bond networking (Figure 3.16). H-bonds can be found between O8 of the morpholine moiety, and H9 of the ethanol molecule in the crystal lattice, with a distance of 2.062(3) Å. The carboxylate oxygen O2 is also involved in coordination with two molecules of water (protons H10A/B) incorporated in the crystal, with a length of 1.917(3) Å. Finally, the second carboxylate group O4 directly binds the metal (with a length of 1.722(3) Å),with H6 of the carboxylate group in the axial position and therefore not involved in the coordination.

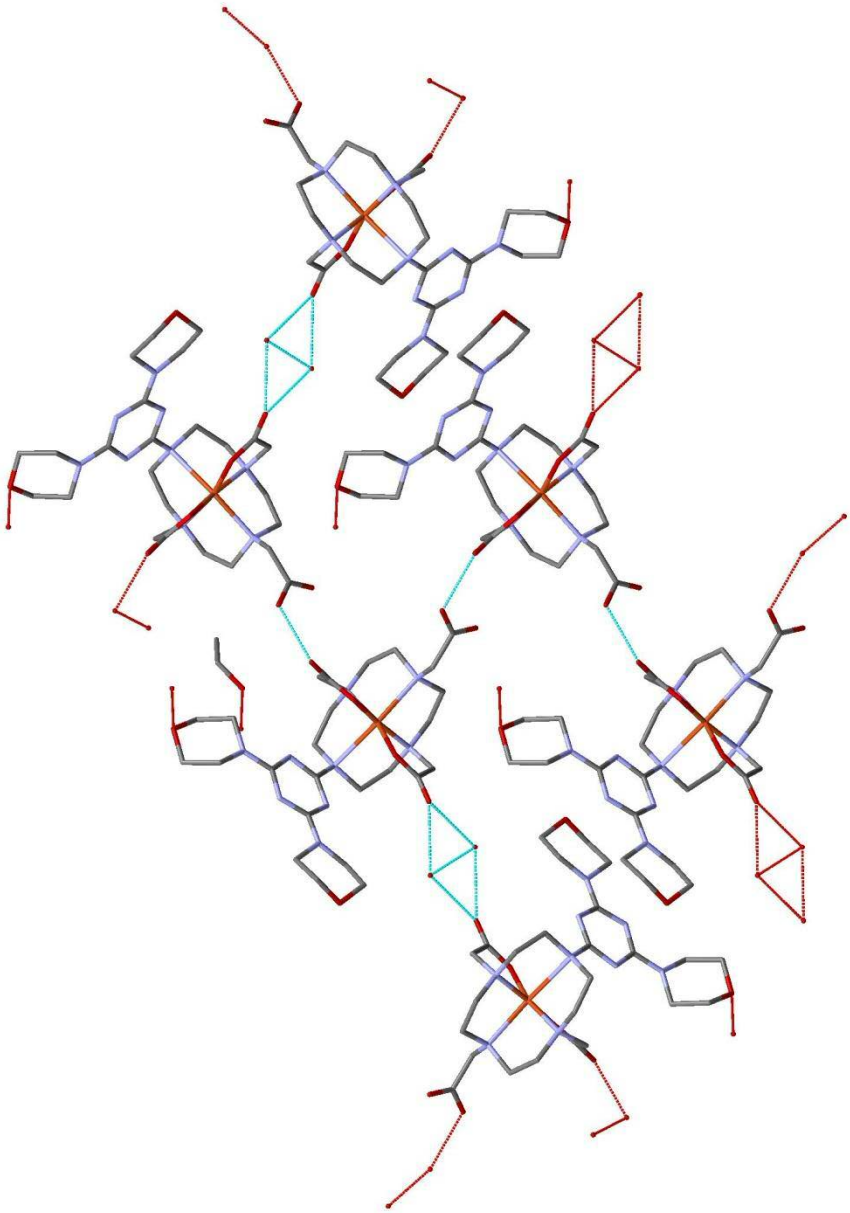

Figure 3.16: H-bond network in H[Cu(II)-TzMorph$_2$DO3A] complex

3.5.1.3 - Manganese(II) complexes of $TzMorph_2DO3A$

Two different manganese-containing complexes were isolated depending upon the solvent systems used for the crystallisation.

$Na_2Mn_2[Mn(II)_2\text{-}(TzMorph_2DO3A)_2](TFA)_2$ - The slow evaporation of an aqueous solution of Mn(II)-$TzMorph_2DO3A$ leads to colourless plates with the structure reported in the figure 3.17. As shown the structure presents two manganese and one sodium atom in the asymmetric unit cell, bringing the metal : ligand ratio to 2 : 1, with the molecule crystallising in the triclinic space group P-1.

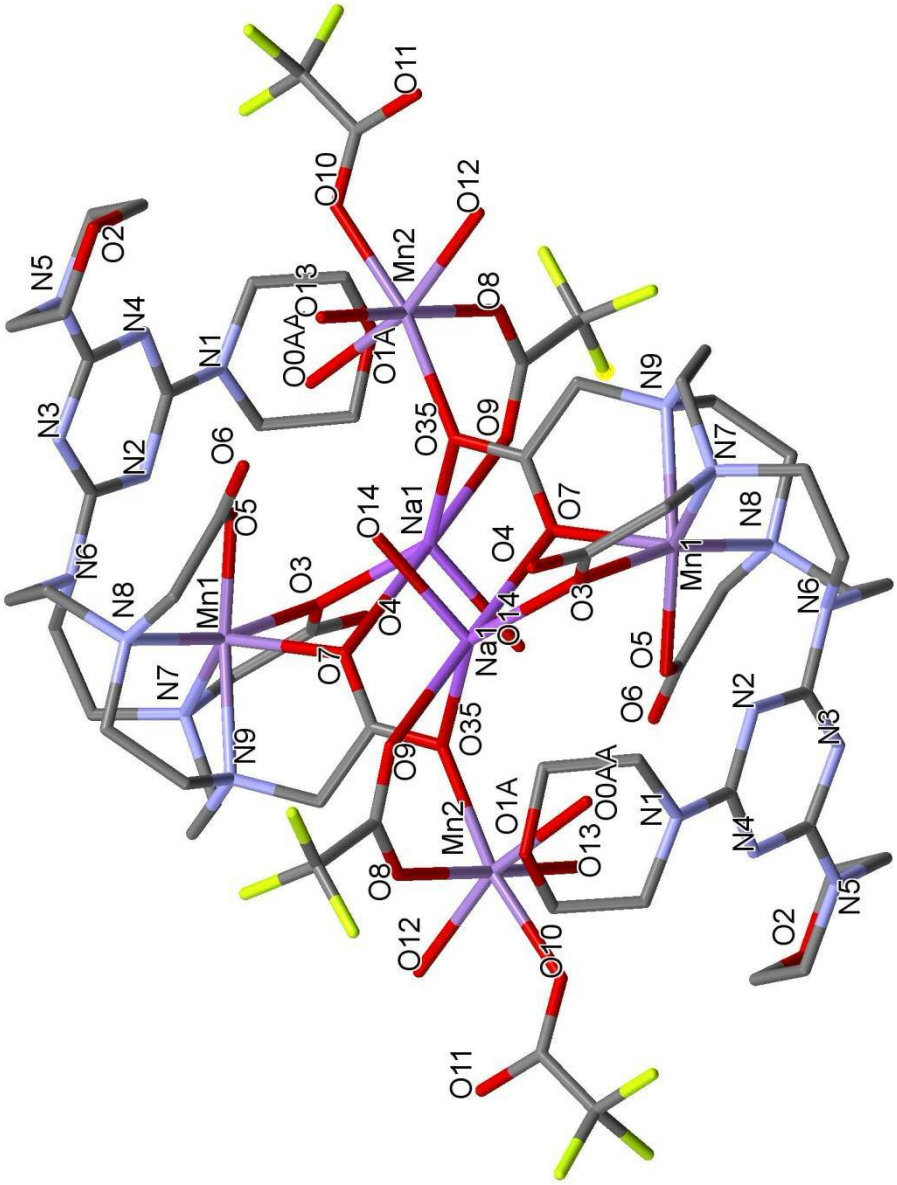

Figure 3.17: $Na_2Mn_2[Mn(II)_2\text{-}(TzMorph_2DO3A)_2](TFA)_2$ complex structure

The structure displays six-coordinate manganese centres with a N_3O_3 donor set in a distorted trigonal prismatic molecular geometry (Figure 3.18), with one face occupied by three nitrogens of the macrocycle and the other face coordinated with three oxygens from the carboxylate arms. The unbound nitrogen is the one bearing the triazine moiety, again reflecting the influence of the triazine core on the donor properties of this ring

nitrogen. Considering the oxygen set, all the carboxylate arms are involved in the coordination contrary to that shown in the nickel or copper complexes where only two carboxylate arms were included in the coordination set, with the acid group opposite to the triazine moiety turned away from the metal centre.

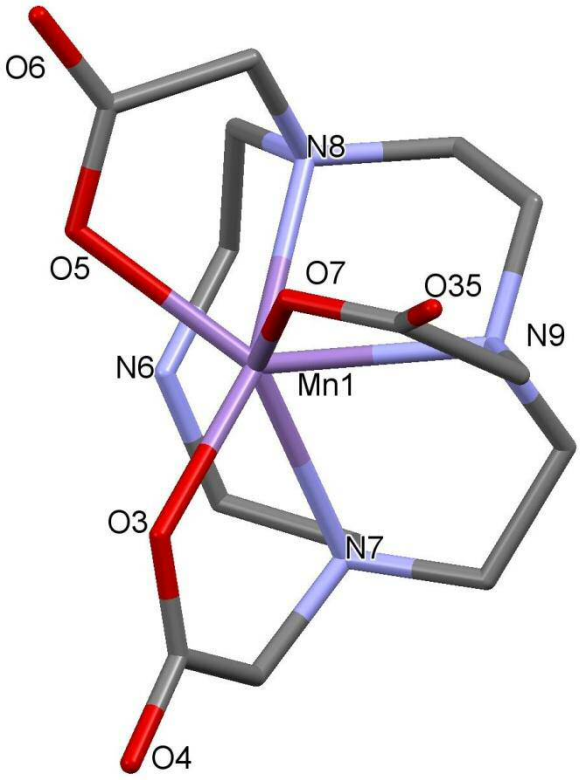

Figure 3.18: $Na_2Mn_2[Mn(II)_2\text{-}(TzMorph_2DO3A)_2](TFA)_2$ with triazine core omitted for clarity

The Mn – N and Mn – O bond lengths are 2.323(2), 2.349(2) and 2.296(2) Å and 2.315(2), 2.138(19) and 2.207(19) Å respectively; all the distances fall in the range of previously reported Mn-O and Mn-N bonds in high-spin 6-coordinate species.[33] Contrary to other literature 7 or 8 coordinate structures this structure lacks weak coordination bonds that fall in the range of 2.77 - 2.91 Å.[34]

The carboxylate arms on the N7 and N9 are those coordinated to the Na atom through O3 and O7, and the metal centre is also a bridge between the second complex structure contained in the unit cell; the bond O35 - Na1 the sodium connects the two ligand molecules together. Finally the Na completes its coordination sphere with a

molecule of water and a trifluoroacetate anion; the trifluoroacetate is connected to the second manganese centre present in the structure as well, bridging the two metals.

The X-ray data also revealed a second manganese atom, completely free from the coordination of the macrocycle. It is possible to recognise a different geometry for this metallic centre, if the Mn coordinated to the macrocycle assumes a distorted trigonal prismatic geometry, for the second one is clearly a distorted octahedral geometry, with the equatorial axis formed by three molecules of water and the O8 provided by the trifluoroacetate anion. The axial bond distances are 2.248(2) and 2.218(2) Å and are occupied by a second trifluoroacetate molecule, not involved in any other bond and through the bond Mn2 - O35 with a carboxylate arm of the macrocycle.

The crystal lattice is supported by a network of hydrogen bonds, particularly between a water molecule coordinated to Mn2 (centred around O13), and O4 of a carboxylate group on the ligand. The proton involved in H-bonding was calculated to be 1.889 Å from O4, with this orientation allowing generation of a linear mono-dimensional layer (Figure 3.19).

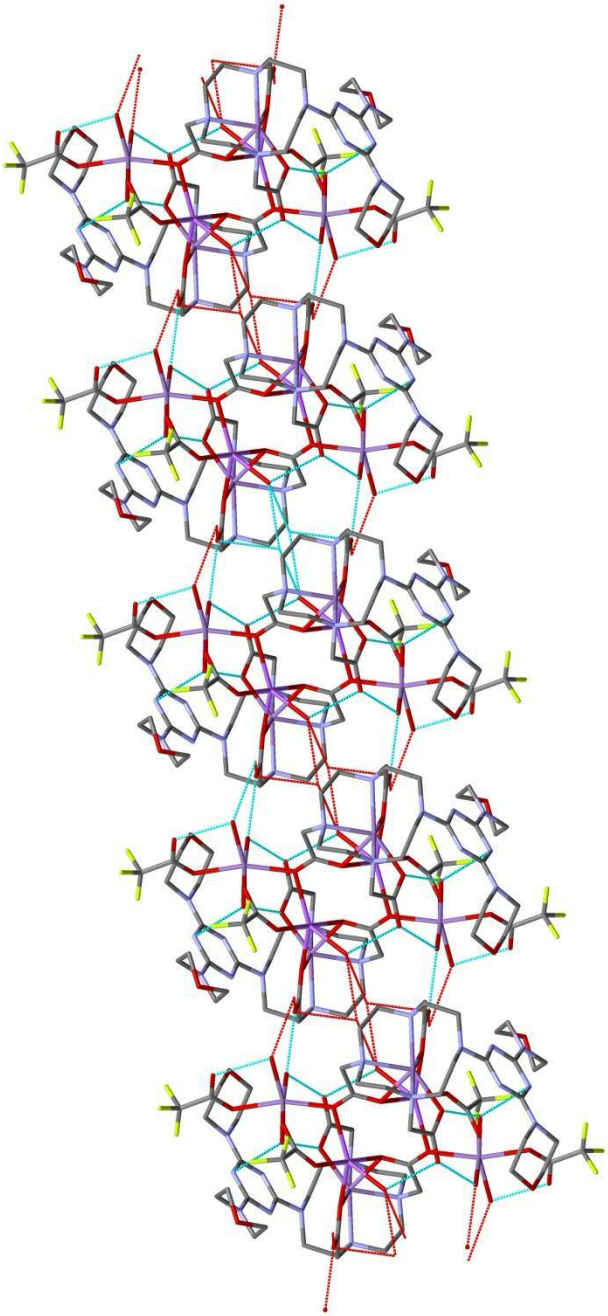

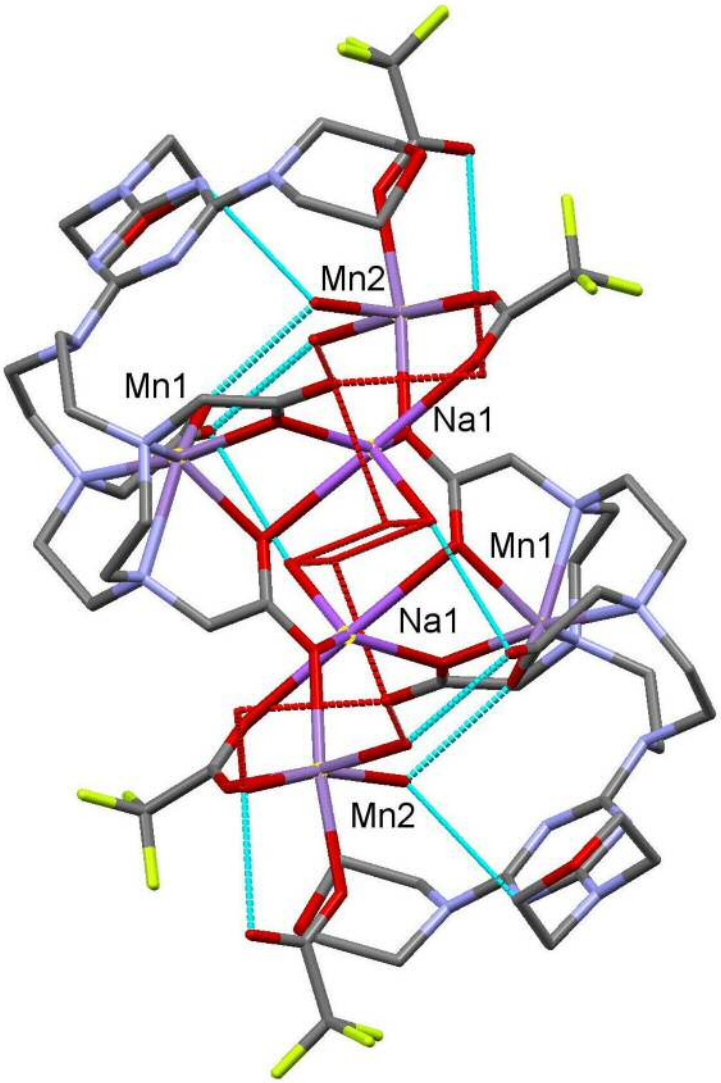

Figure 3.19: $Na_2Mn_2[Mn(II)_2\text{-}(TzMorph_2DO3A)_2](TFA)_2$ complex H-bond network (lateral and front view)

$Mn_5[Mn(II)_4\text{-}(TzMorph_2DO3A)_4]Cl_6$ - The slow diffusion of acetone vapour into a concentrated aqueous solution of Mn(II)-$TzMorph_2$DO3A gave long needles of a different manganese complex.

The crystals are tetragonal (Z = 2, two molecules for unit cell) in the space group I-4 with S_4 symmetry. This compound has crystallised as cluster with a metal : ligand ratio of 9 : 4 (Figure 3.20)

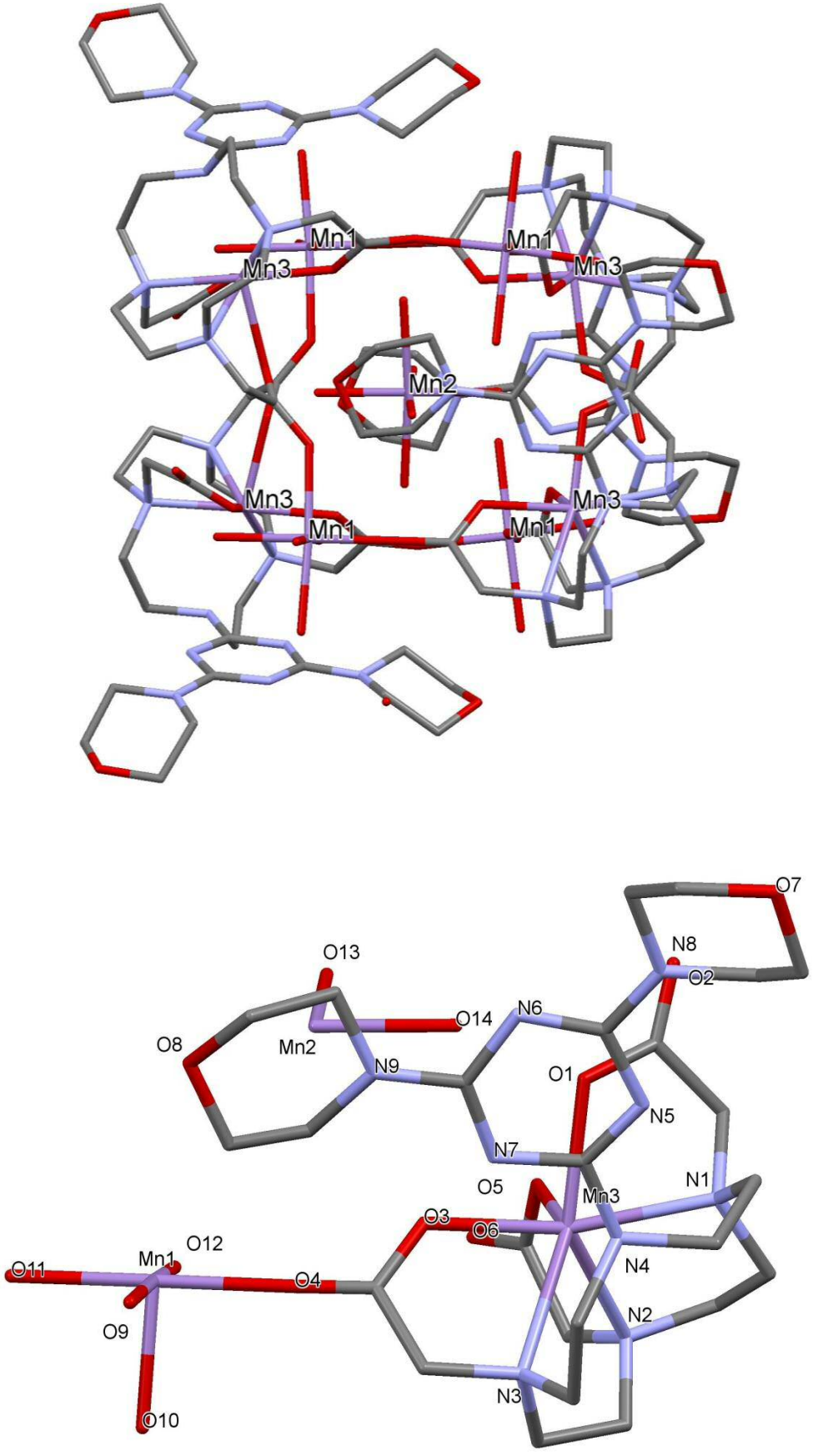

Figure 3.20: $Mn_5[Mn(II)_4\text{-}(TzMorph_2DO3A)_4]Cl_6$ complex structure (top) and asymmetric unit (bottom), chlorine atoms omitted for clarity

The cluster has a Mn central atom in a slightly distorted octahedral geometry with the full coordination sphere occupied by water molecules. Contrary to complex with eight donors found in literature that present an octahedral geometry[34a] the asymmetric unit shows how the metal linked to the ligand presents the same N_3O_3 set donor found in the first crystal structure, a distorted trigonal prismatic geometry, with one of the face occupied by the oxygens and the other by the nitrogens, with the nitrogen bearing the triazine complete free from coordination.

Also the lengths observed for the metal - nitrogen and metal - oxygen bonds are comparable to the ones found in the literature with compounds similar to the one synthesised,[33] with the distances Mn - N 2.397(5), 2.407(5) and 2.281(5) Å respectively and the bonds Mn - O 2.225(4), 2.233(4) and 2.143(4) Å.

Finally there is another manganese atom acting as a bridge between two different ligand molecules. The metal presents a slightly distorted octahedral geometry, with one axial axis occupied by O6, the carboxylate arm borne on the N2, opposite to the triazine core and the O4 as equatorial axis, the carboxylate arm on the N3, next to the triazine moiety; finally the six coordination sphere is occupied by four molecules of water.

An interesting difference observed between the two crystallisation techniques is the difference in crystal polymorphs, which appears to be largely due to the H-bonding network. The slow evaporation method gave a largely supramolecular network which is absent in the crystal obtained via diffusion. In this case, the H-bond network is restricted to the central metal and the carboxylate arms of the ligand (Figure 3.21).

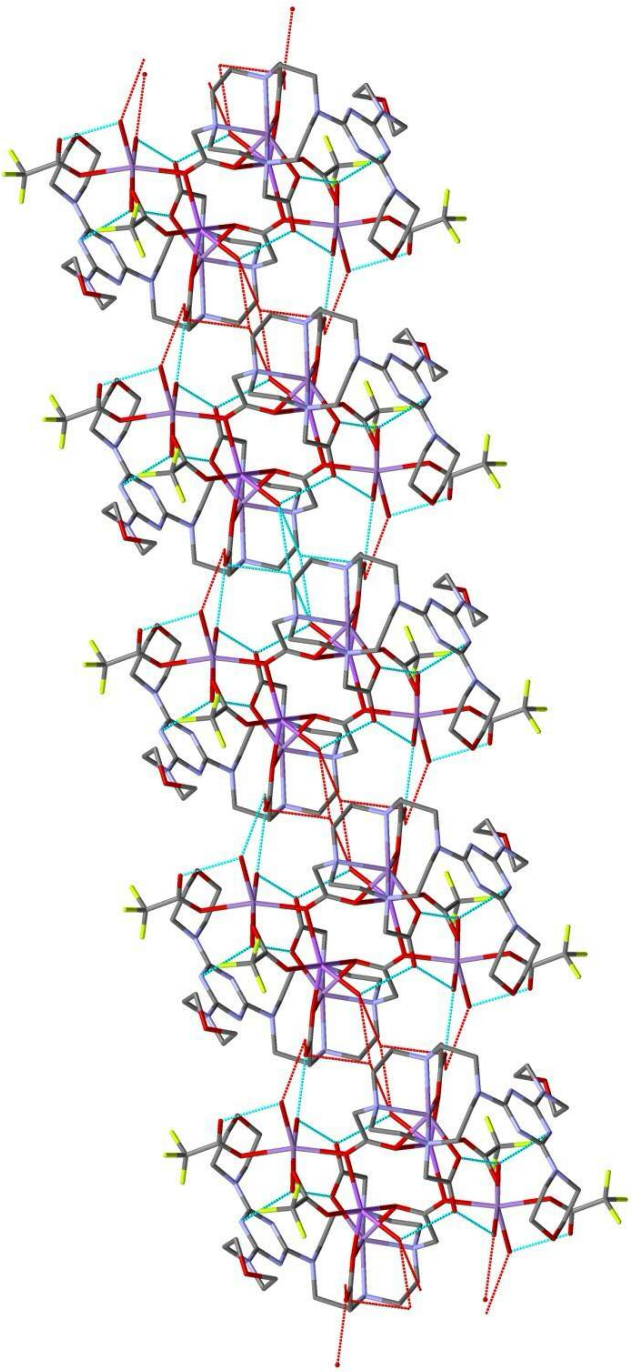

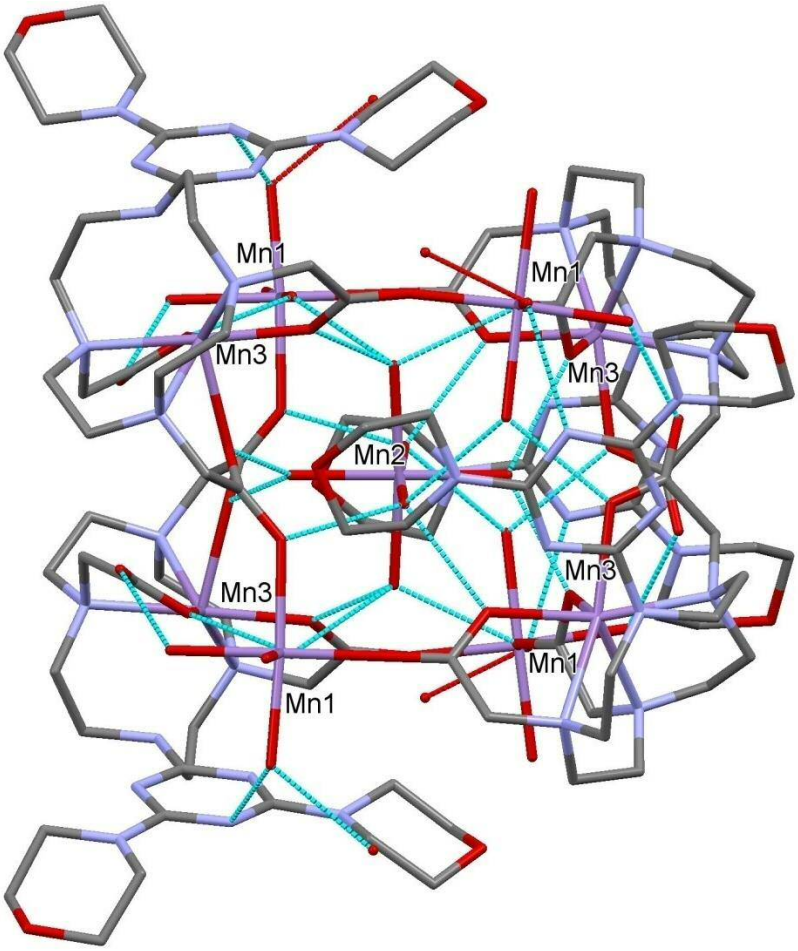

Figure 3.21: $Na_2Mn_2[Mn(II)_2\text{-}(TzMorph_2DO3A)_2](TFA)_2$ complex H-bond network presents the supramolecular network (top); $Mn_5[Mn(II)_4\text{-}(TzMorph_2DO3A)_4]Cl_6$ complexes H-bond networks presents only an intramolecular network (bottom).

3.5.1.4 - Vanadyl(IV) complex of $TzMorph_2DO3A$

H[V(IV)(=O)-$TzMorph_2$DO3A] - Through the vapour diffusion of acetone into an aqueous solution of H[V(IV)(=O)-$TzMorph_2$DO3A] it was possible to isolate light purple needle shaped crystals suitable for crystallographic studies. The analysis showed a monoclinic crystal system in the space group C2/c with three independent molecules in the asymmetric unit (Z = 3) and a total of twenty-four per unit cell.

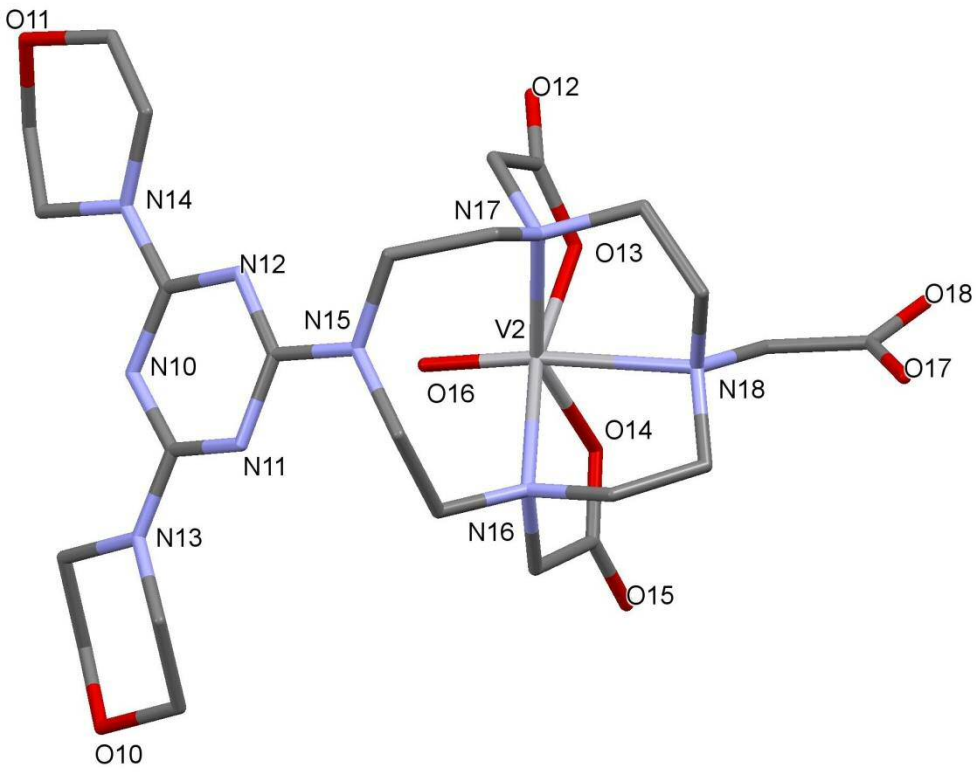

Figure 3.22: H[V(IV)(=O)-$TzMorph_2$DO3A] complex structure

As reported above the structure presents three independent molecules, all with a ratio metal : ligand equal to 1 : 1 (Figure 3.22).

The vanadium assumes a distorted octahedral geometry with a N_3O_3 donor set disposed in the facial fashion using all three cyclen donors but leaving the N-triazine moiety uncoordinated. The axial ligand site is occupied by the carbonyl bond (1.600(5) Å) and the bond V - N18 (2.397(6) Å), nitrogen that bears a carboxylate arm not involved in the coordination sphere and is longer than those normally found in literature cyclen vanadyl(IV) complexes (average of 2.16 Å for the V - N bond).[35]

This observation may be explained by the coordination of the equatorial set provided by the acid group that constrains the metal within the plane of the ring.

The equatorial set is composed of two of the two cyclen ring nitrogens, N16 and N17 and two oxygens, O14 and O13, from the carboxylate arms borne on these nitrogens.

The octahedral geometry in this complex is strongly distorted, especially considering the bond angles of the compound (see table 2).

N17-V2-O13	77.09	O14-V2--N18	79.78	O13-V2-O16	99.42
N17-V2-N16	106.75	O13-V2-N18	90.74	O14-V2-O16	101.40
N16-V2-O14	81.38	N16-V2-N18	78.36	N16-V2-O16	91.70
O14-V2-O13	90.23	N17-V2-N18	78.36	N17-V2-O16	102.46

Table 2: H[V(IV)(=O)-TzMorph$_2$DO3A] complex angles (°)

3.5.2 - LANTHANIDE COMPLEXES OF TZMORPH$_2$DO3A

After the chemistry of d-block elements had been explored, attention was devoted to the lanthanide elements, it has been possible to synthesise lanthanum(III), europium(III), gadolinium(III), cerium(III), ytterbium(III) and lutetium(III) complexes.

3.5.2.1 - Europium(III) and Gadolinium(III) complexes of TzMorph$_2$DO3A

The europium(III) and gadolinium(III) complexes of TzMorph$_2$DO3A are similar in chemistry, reactivity and structures and for these reasons they can be considered together. For both of the complexes suitable X-ray crystals have been obtained by slow evaporation of a mixture solution of water and methanol, collecting colourless plates for the Eu(III) and colourless blocks for the Gd in the triclinic system (Z = 1, one molecule for unit cell) and space group P-1, with a metal : ligand ratio of 1:1. Furthermore the structures are dimeric which is a common feature for lanthanide complexes and carboxylate bridged tetrameric structures of Tb(III) and Eu(III) have also been reported.[36] Thus these complexes contrast the predominately monomeric complexes formed by the d-block metal the d-block metals.[37] (Figure 3.23).

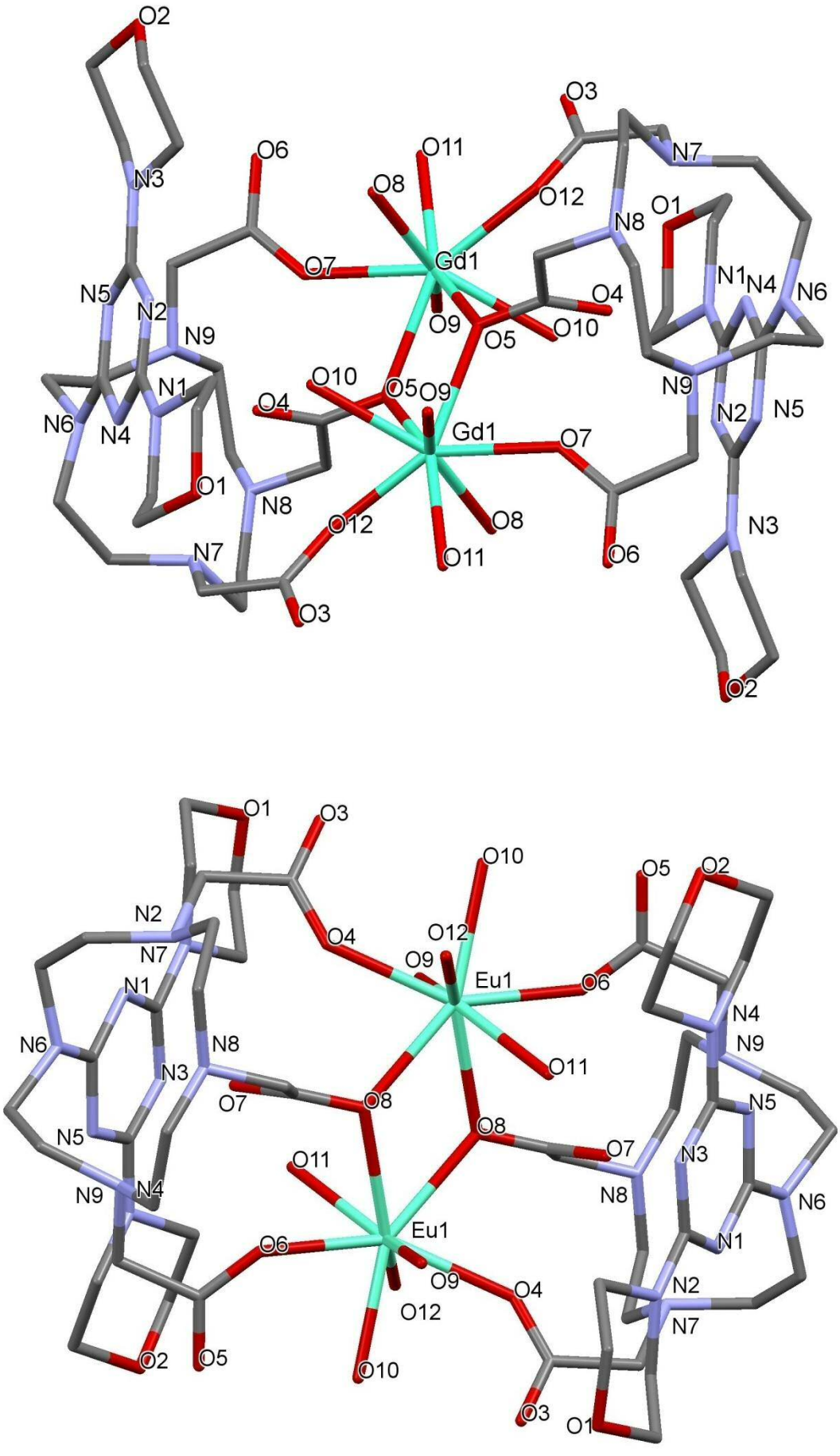

Figure 3.23: $\{H_4[Gd(III)_2(TzMorph_2DO3A)_2]\}^{4+}$ complex structure (top) and $\{H_4[Eu(III)_2(TzMorph_2DO3A)_2]\}^{4+}$ complex structure(bottom) with counteranions omitted for clarity

Both of the complexes show a highly unusual coordination mode with all of the macrocyclic nitrogens donors uncoordinated. This is in strong contrast to the bonding mode displayed by the d-block complexes or in the literature for other Eu(III) and Gd(III) complexes in which the metal centre is universally bound by the macrocyclic *N*-donors.[38] The metal cation is only coordinated by the carboxylate arms on the cyclen ring, with water molecules completing the 8 coordinate sphere. The carboxylate arm on the 'opposite' cycle ring position to the to the triazine core is involved in a μ^2-bridging mode between the two metals centres via a single carboxylate derived O-donor.

The europium(III) complex has a distorted square antiprismatic geometry, a very common geometry for carboxylate-substituted lanthanide complexes of cyclen, normally with the metal centre coordinated by the four nitrogens of the macrocycle ring and the three oxygens of the carboxylic acid.[39] The complex obtained, instead, displays a coordination sphere occupied by four water molecules, than the metal - nitrogen bonds, with three of them on a face of the square antiprism. The residual position is occupied by a metal - oxygen bond, namely the O6 borne on the N9 with a length of 2.374(3) Å. The other face instead is occupied by a water molecule and three oxygen atoms; the carboxylate arm on the N7 that has a bond distance equal to 2.367(3) Å, these distances are in the range that has been found in the literature about this kind of complexes.[36, 39-40]

Finally the two residual sites in the coordination sphere are occupied by carboxylate arm on the N8, the one opposite to the triazine core bridging the two metal centres.

The O8-Eu1-O8 angle is 64.36(10)°, while Eu1-O8-Eu1 is 115.64(10)°; also the length of the bonds is symmetrical, with two opposite M-O bonds long 2.429(2) Å and the residual two 2.505(2) Å. It is eventually possible to calculate the distance between the two metal centres as 4.177(3) Å (Figure 3.24).

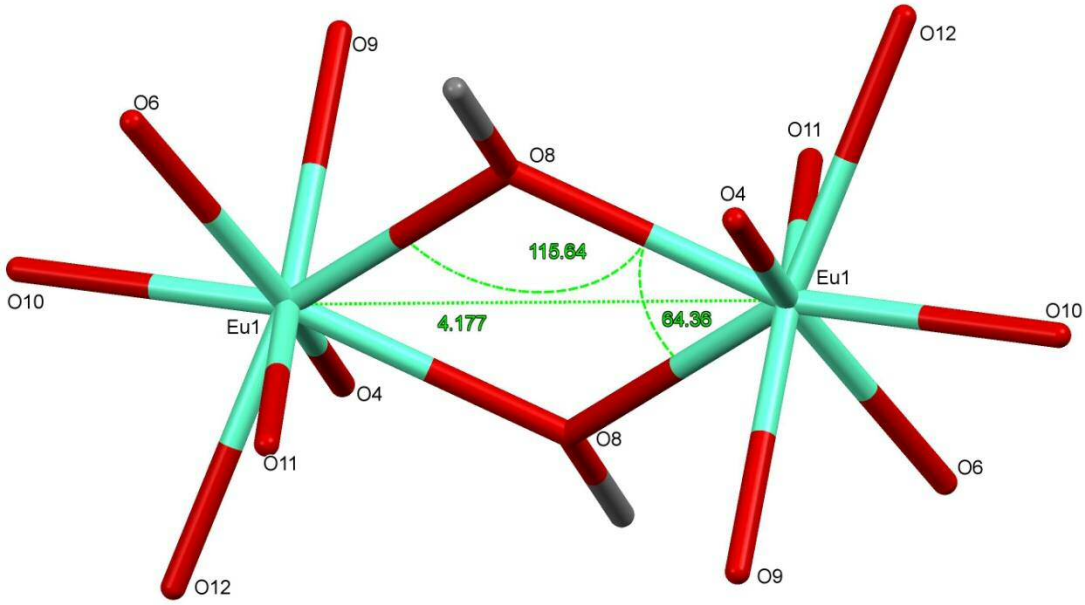

Figure 3.24: the planar trapezoid in $\{H_4[Eu(III)_2(TzMorph_2DO3A)_2]\}^{4+}$ complex

The gadolinium(III) is similar to the europium(III) complex with a distorted square antiprismatic geometry, and three water molecules occupying one of the face of the antiprism which is completed by the bond with the O12, oxygen on the N7 of the cyclen ring. The other face of the antiprism instead is taken by a residual molecule of water, the Gd1-O7 bond and the carboxylate pendants borne on the two N8 of the macrocycles. Analysing the length of these bonds, they result respectively 2.375(16) Å for Gd1-O7 and 2.362(15) Å for Gd1-O12, in line with that has been found in the literature with an average of 2.35 Å for a Eu-DO3A based complex.[41]

As for the europium complex (Figure 3.24), the moiety formed by the two metal centres and the two O5, as bridges assumes a planar trapezoid conformation. Calculating bond distances and angles result that the angle O5-Gd1-O5 is 64.33(6)°, while the angle formed by Gd1-O5-Gd1 equal to 115.67(6)°, considering the length of the bonds emerges that are longer than ones had been found in literature and perfectly symmetrical, resulting 2.424(15) Å for the shortest and 2.500(15) Å for the longest side. Finally the distance between the gadolinium atoms has been calculated and found to be 4.169(15) Å, similar to that observed for the europium(III) complex. (Figure 3.25).

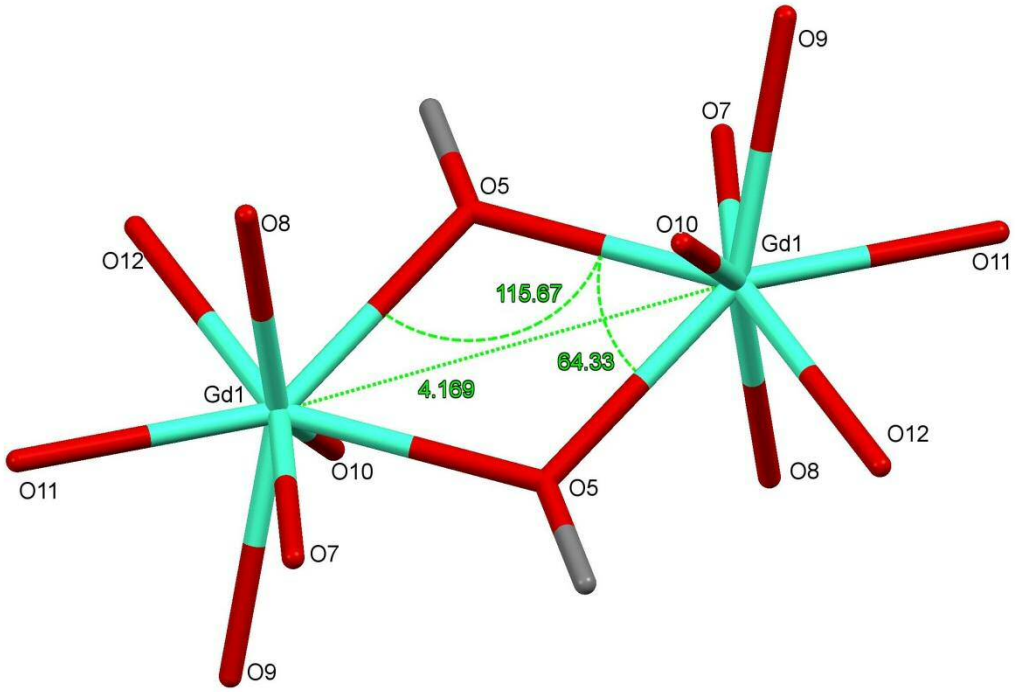

Figure 3.25: the planar trapezoid in $\{H_4[Gd(III)_2(TzMorph_2DO3A)_2]\}^{4+}$ complex

3.5.2.2 - Lanthanum(III) complexes of $TzMorph_2DO3A$

For the La(III) complexes of $TzMorph_2DO3A$ it has been possible to grow two types of complexes as single crystals suitable for x-ray analysis.

$\{Na_2H_4[La(III)_2(TzMorph_2DO3A)_2]\}^{2+}$ - Through the slow evaporation of aqueous solution of La(III)-$TzMorph_2DO3A$ have been obtained colourless plate crystals suitable for a X-rays crystallography analysis.

The structure shows a metal : ligand ratio equal to 1 : 1, similar to the gadolinium or europium compound; in the crystalline system $P2_1/n$ equivalent to the monoclinic crystal system has been found the presence of two molecule for every unit cell (Z = 2).

Like all the lanthanides analysed so far is possible to recognise some common features; the macrocyclic nitrogens remain uncoordinated and the metal cations are bound by the oxygens on the carboxylate arms, with the O6 as bridge between the two lanthanum(III) centres (Figure 3.26).

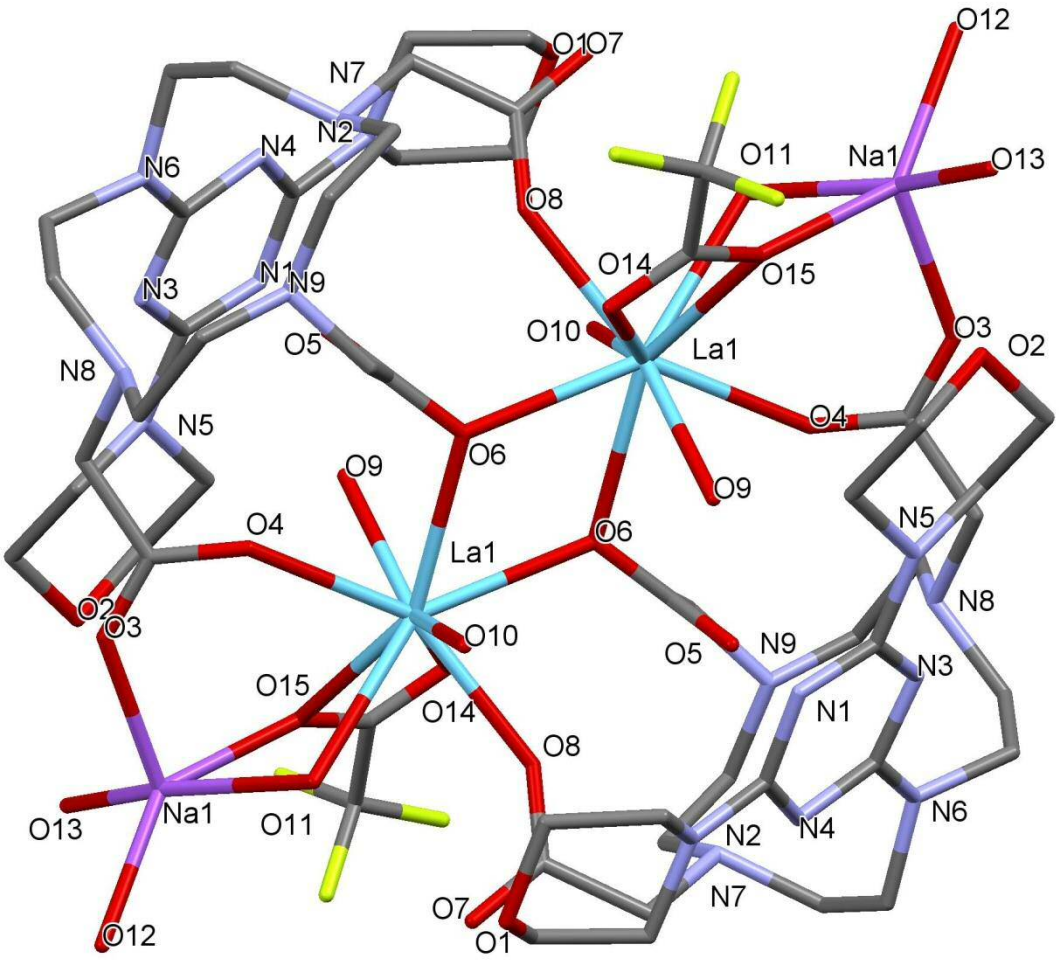

Figure 3.26: $\{Na_2H_4[La(III)_2(TzMorph_2DO3A)_2]\}^{2+}$ complex structure with counteranions omitted for clarity.

The lanthanum assumes a distorted tricapped trigonal prismatic geometry, that is common for lanthanide complexes,[42] with the coordination sphere completely occupied by the oxygens. Two spots are taken by the O6 provided by every ligand, as previously reported, the atom operates as bridge between the two metal centres forming a planar trapezoid conformation, with the La-O-La angle equal to 117.11(14)° and the O-La-O 62.93(15)°, while the bond lengths La-O 2.589(4) Å and 2.565(4) Å respectively and the length La-La 4.397(2) Å, shorter than it has been found in literature[43] (Figure 3.27).

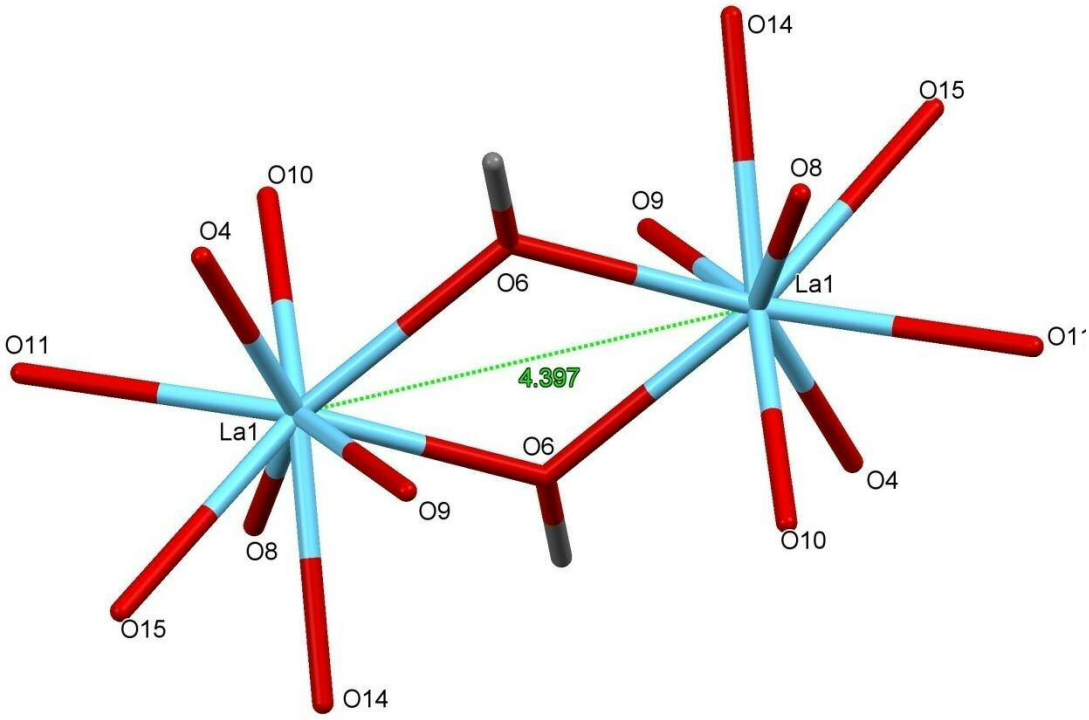

Figure 3.27: the planar trapezoid of $\{Na_2H_4[La(III)_2(TzMorph_2DO3A)_2]\}^{2+}$ complex

One face of the distorted tricapped trigonal prism is then completed by one molecule of triflic acid, with the oxygen labelled O15 coordinating also a sodium atom; then a molecule of sodium hydroxide and the O8, an oxygen provided by one of the carboxylate arms of the macrocycle.

The second face of the prism is instead occupied by two molecules of water, the oxygen O4 of the carboxylate arm and the O6, provided by the carboxylate arm opposite to the triazine core and involved, as previously reported, in the coordination sphere capping the trigonal prism.

The bond lengths found are reported in the table 3 showing that on average the distances found are longer that the ones reported in the literature.[42-44]

Table 3: La-O bond distances (Å)

La1-O4	2.463(4)	La1-O8	2.447(4)	La1-O11	2.662(4)
La1-O6	2.566(4)	La1-O9	2.509(4)	La1-O14	2.705(4)
La1-O6^{i}	2.589(4)	La1-O10	2.507(4)	La1-O15	2.617(4)

The formation of the La(III) complex differed from other syntheses, where it was found that the pH necessary to precipitate the complex was reached by addition of Et3N. The resultant crude complex was recrystallised from methanol by slow evaporation of the solvent, to produce colourless hexagonal prism crystals suitable for X-rays analysis.

The unit cell presents six molecule for unit (Z = 6) in a 1 : 1 ratio between the metal and the ligand and disposed in the R-3c:H crystal system.

Some features show how the complex is completely different to the lanthanide compounds presented so far (Figure 3.28).

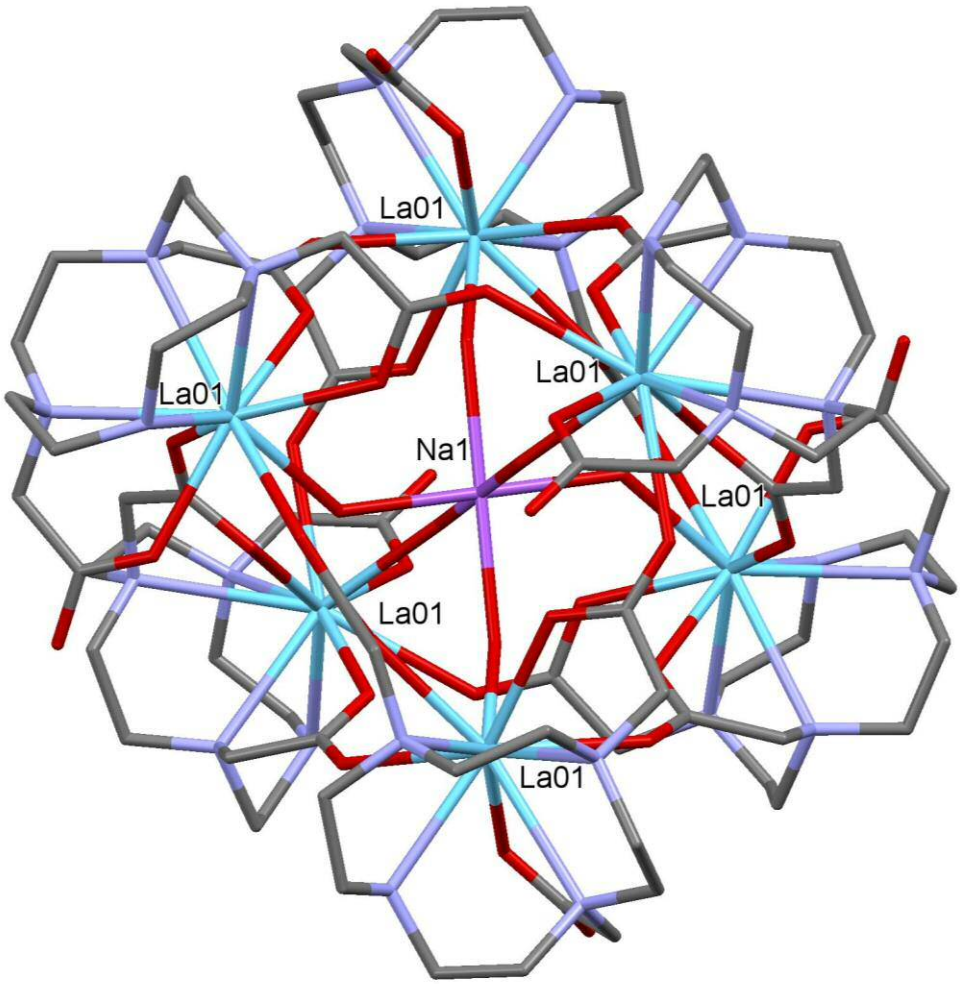

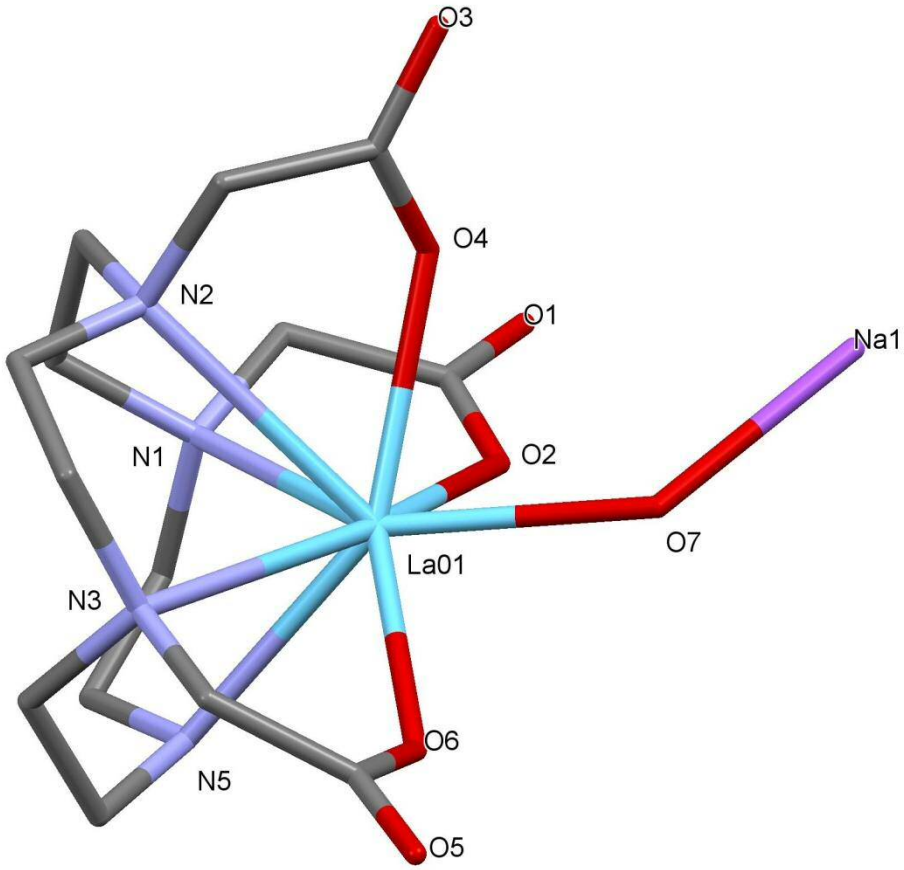

Figure 3.28: $\{NaH_6[La(III)_6(TzMorph_2DO3A)_6]\}^{7+}$ complex structure (top) and asymmetric unit (bottom), counteranions omitted for clarity

The complex is not obviously a dimer and there is no characteristic planar trapezoid orientation of the oxygens donors and the metal centres. An interesting characteristic is that the metal is bound within the ligand cavity, with all the 4 ring nitrogen and 3 carboxylate donors coordinating the La(III) centre. Most interestingly the structure reveals the loss of the triazine core. We interpret this observation as the strongly Lewis acidic La(III) cation renders the triazine core even more electron deficient and susceptible to nucleophilic attack by water or hydroxide (the complex was prepared at elevated pH values) at the *ipso*-carbon position. This is not observed in the above Ln(III) complexes since the *N*-triazine donor is not bound to the metal centre.

The metal centre has a coordination number of ten in a distorted bicapped square antiprismatic geometry. The capping bonds are formed by the lanthanum and the N2, a nitrogen of the cyclen ring, and O1, a carboxylate arm that is used as bridge between two metal centres, measuring 2.917(5) Å and 2.749(4) Å respectively, these result much

longer than the common capping bond found in literature with an average length of 2.56 Å.[42] One face of the square antiprism is occupied by N5, the nitrogen that had borne the triazine core, O6 and O2, borne on the macrocycle and O7 supplied by sodium hydroxyde found in the centre of the compound and coordinated to all six lanthanides. Finally the other antiprism face is occupied by the remaining nitrogen donors of cyclen ring, O4 from the last carboxylate arm left and O3 provided by a different carboxylate arm of a ligand molecule.

It is possible to see that the change in geometry leaves the metal-oxygen bond distances in the same range of measurements (2.47 - 2.55 Å) compared to the above structures. Contrary to what has been found in the literature, the range of metal - nitrogen bond lengths are longer in for this material; 2.80 - 2.91 Å for the nitrogens bearing a carboxylate arm. It is also interesting to note that the length between the metal and the nitrogen that was bearing the triazine core is shorter, M - N5 is 2.707(6) Å, than the common distance found in the literature,[42, 44b] but also the release of the triazine changed the length of the bond completely, indeed for all the compounds until now discussed the M - $N_{triazine}$ bond was the longest one of the M - $N_{macrocycle}$ bonds. This is due to the electron withdrawing effect of the triazine core. With the release of this moiety of the molecule it is possible to measure a stronger binding effect that results in a shorter bond length.

It has been proved that changing the pH of the solution adding an excess of base like Et_3N has the effect to modify the coordination geometry of the compound and to release the triazine core as leaving group, in particular this feature could be used in future to develop new compound investigating the role of the pH in the release of the triazine core or using different leaving groups to understand their behaviour at assorted pH.

3.5.2.3 - Lutetium(III) complex of $TzMorph_2DO3A$

Crystals suitable for a solid state analysis have been grown by slow evaporation of a concentrate aqueous solution of Lu(III)-$TzMorph_2DO3A$.

The data show that the lutetium compound forms a 1 : 1 metal : ligand ratio, with the molecule crystallising in the triclinic space group P-1 and with two independent molecule (Z = 2) in the unit cell (Figure 3.29).

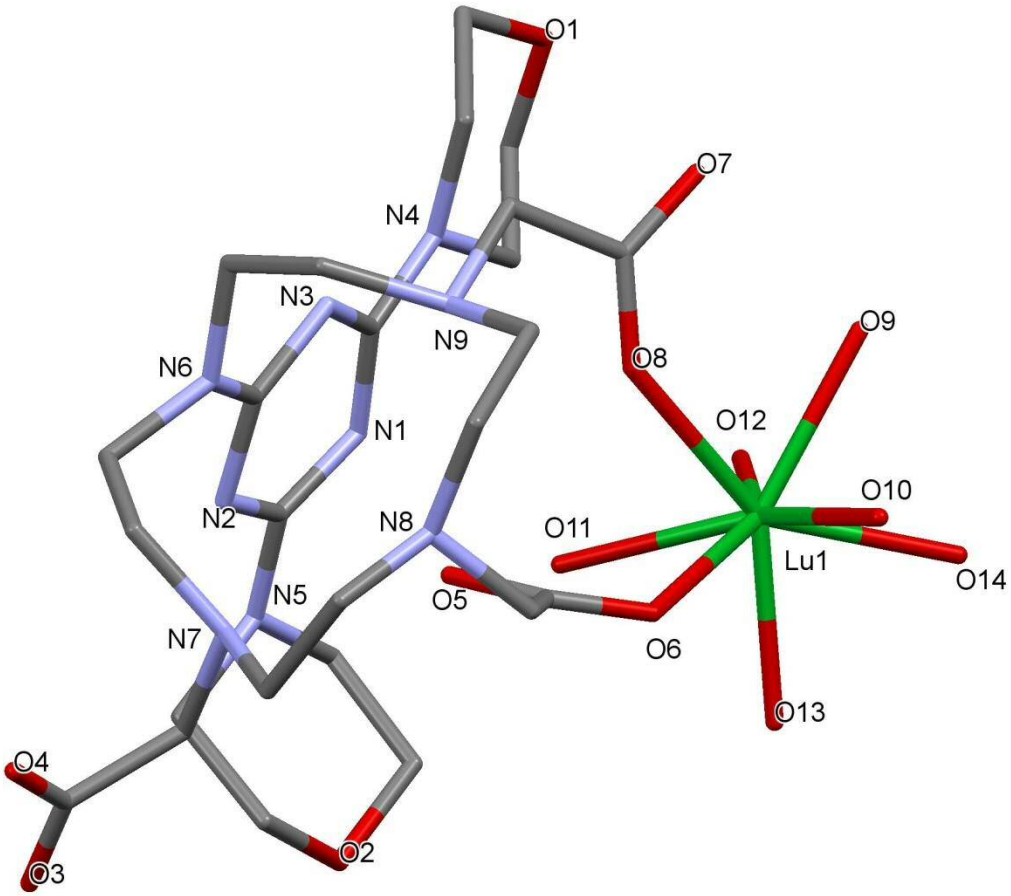

Figure 3.29: H_2[Lu(III)-$TzMorph_2DO3A$]Cl_2 complex structure.

The Lu(III) presents a distorted square antiprismatic geometry, and like several of the complexesdescribed above the macrocyclic nitrogens are uncoordinated. This is different also considering the kind of bonds found in the literature about lutetium(III) complexes, with the metal centre always being coordinated through the macrocyclic N-donors.[45] A peculiar characteristic of this compound is that, even if it is a M(III), the coordination is provided only by two carboxylate arms on the cyclen ring, 2.311(4) and 2.312(4) Å respectively, and with a comparable Lu-O length found in the literature (2.2-2.3 Å).[45a, b] The eight donor coordination sphere is occupied by the two oxygens

provided by the acid groups and completed by six molecules of water arranged in a distorted square antiprismatic geometry. One face is occupied by four oxygens: O9, O10, O12 and O14 all from molecules of water; the second face instead is occupied by two oxygens provided by molecules of water (O11 and O13) and two provided by the carboxylate arms, O6 and O8. Finally an interesting characteristic of this compound is is the the charge on complex. Since the the Lu(III) is coordinated only by two carboxylate groups this leaves a positive charge to balance. Furthermore the structure presents two amine groups of macrocycle protonated, N7 and N9 (the hydrogens in the figure 3.28 have been removed for clarity), bringing the total positive charge to be balanced to +3. Considering the secondary coordination sphere in the structure there are one fully occupied Cl^- and two 50% occupied Cl^- able to provide a -2 negative charges. The final positive charge is balanced by the free carboxylate arm that is deprotonated, but not involved in the first coordination sphere of the compound, leaving the complex neutral. This behaviour is unique amonst the complexes in this study.

3.5.3 - LIGAND AND COMPLEXES DIPYRIDAMOLE MIMIC SYNTHESIS

After exploring the chemistry of M-TzMorph$_2$DO3A a mimic ligand of dipyridamole has been synthesised. Adopting the same conditions used to develop the symmetrical di-morpholine triazine core it has been possible to synthesise an asymmetrical triazine core, employing piperidine and diethanolamine as nucleophilic substituents. The final steps were the addition of the cyclen core and then the release of the protection group by the addition of TFA. The synthetic path is reported below in figure 3.29, instead all the details about the conditions used and the full characterisation of the ligand are described in the experimental section.

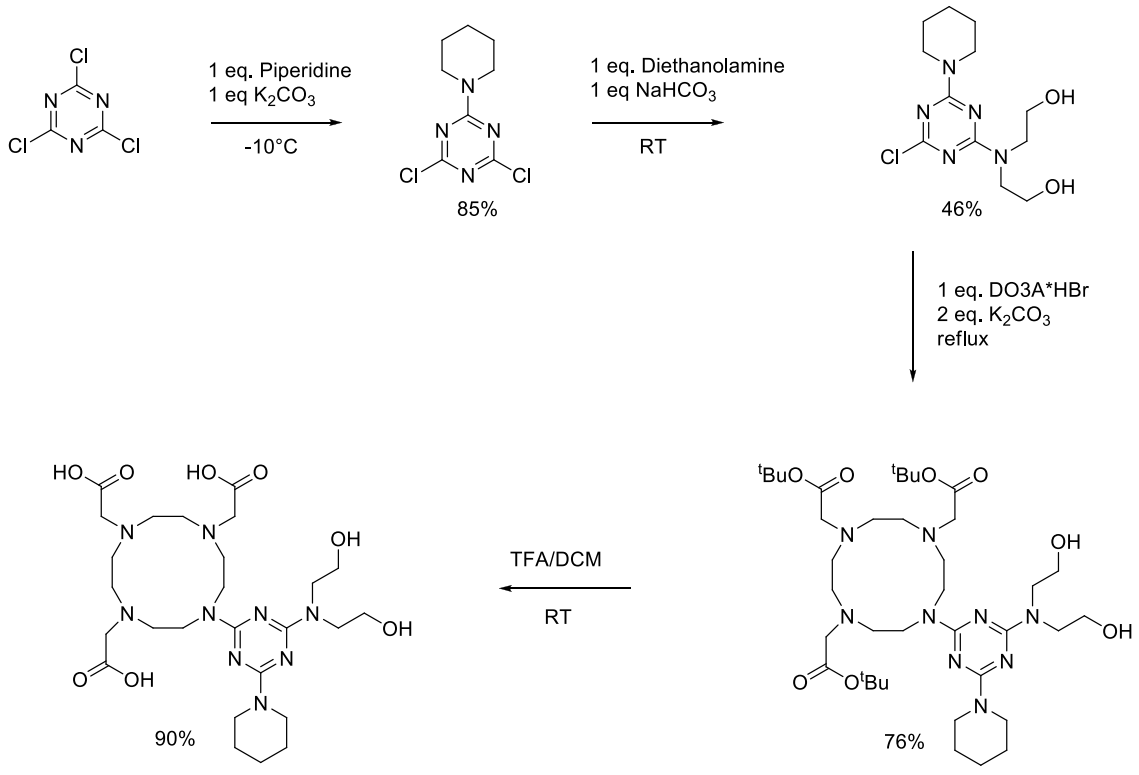

Figure 3.30: synthesis of TzPipDEA-DO3A ligand

To synthesise the complexes TzPipDEA-DO3A (0.16mmol) was dissolved in ca. 3mL of water and the pH of the solution corrected to reach pH 7, adding a solution of 1M NaOH. The metal salt, typically as a chloride, triflate or nitrate, was dissolved in ca. 2mL of water and added to the ligand solution. The solution was heated at 40-50°C for five minutes and then cooled to room temperature. The mixture was purified by flash chromatography on a short column, to afford a clear solution, then the compounds

have been characterised by mass spectroscopy and all the results are reported in the experimental section (Figure 3.31).

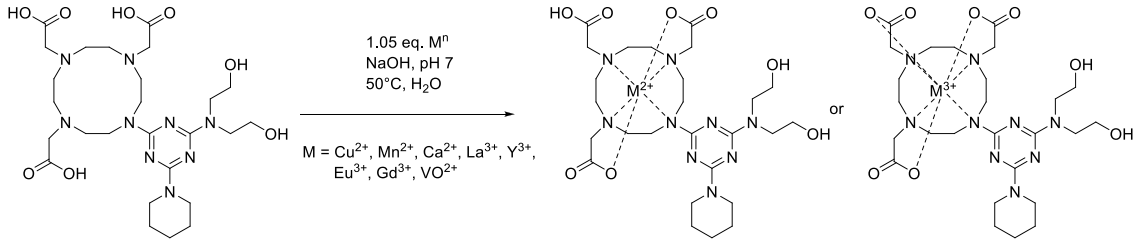

Figure 3.31: method synthesis of TzPipDEA-DO3A complexes

In this chapter has been described the formation of twelve novel complexes using the metals Cu(II), Mn(II), Ni(II), La(III), Y(III), Eu(III), Gd(III), VO(II), Co(II), Ce(III), Yb(III) and Lu(III) with the ligand $TzMorph_2DO3A$. Furthermore it has been investigated by spectroscopy, using the Job's method, the empirical formula of the ligand, resulting with the presence of three molecules of TFA. Always through a UV spectroscopy studiey has been investigated the structure of three complexes (Cu(II), Co(II) and Ni(II)) in solution. Analysing the data and comparing with the literature results that the copper compound presents a trigonal bipyramid structure, suggesting that the metal centre is coordinate by a N_3O_2 system.

The nickel complex instead, shows as an evident distorted six coordinate species, with a N_3O_3 donor system, it is not impossible to exclude that the species could exist in equilibrium or mixture with a square planar N_2O_2 donor system, due to the presence of a band at 540 nm. Finally the Co(II) complex has been hypothesised that presents an octahedral geometry system in solution based on N_3O_3 donors.

Single crystal X-ray diffraction data was collected successfully for several metals. The data can be analysed dividing the metals in similar group.

The d-block metals Ni(II), Cu(II), Mn(II) and V(IV) in solid state present some communal characteristic, the metal is inside the macrocycle, coordinated by the nitrogen of the cyclen ring and by the carboxylate gropus as pendant donors. Furthermore all the metals present a longer M-$N_{triazine}$ bond (or even not coordinated), this is due to the triazine core of the compound, being the moiety very electron deficient this affect the donor capacity of the amine, resulting in a weaker M-N bond.

The lanthanide complexes (Eu(III), Gd(III) and La(III)) instead present a dimeric structure, forming a perfect planar trapezoid between the metal centres, moreover the metal is outside the macrocycle, not coordinated at all by the nitrogens, feature absolutely inusual and not found in literature. The only two exceptions to these general characteristic are the Lu(III) complex, that does not present the dimeric structrure and it

is coordinated by only two carboxylate arms, and the La(III) complex obtained synthesising the complex at basic pH. In this last structure the lanthanide is found inside the cage coordinated by the cyclen ring too, but more important the structure does not show the presence of the triazine core anymore; working at pH around 11 indeed could be the cause to make the triazine core acting like leaving group.

Finally a new dipyridamole mimic ligand has been synthesised and fully characterised (TzPipDEA-DO3A), moreover seven novel complexes has been obtainted using the metal Cu(II), Mn(II), Ca(II), La(III), Y(III), Eu(III), Gd(III) and VO(II) and characterised by MS. Further studies could be conducted on this versitile new ligand to understand the coordination chemistry of these novel complexes and to deveop their radiochemistry.

[1] J. S. Desgrosellier and D. A. Cheresh, *Nat Rev Cancer* 2010, *10*, 9-22.

[2] C. J. Avraamides, B. Garmy-Susini and J. A. Varner, *Nat Rev Cancer* 2008, *8*, 604-617.

[3] D. Cox, T. Aoki, J. Seki, Y. Motoyama and K. Yoshida, *Medicinal Research Reviews* 1994, *14*, 195-228.

[4] R. Haubner, D. Finsinger and H. Kessler, *Angew. Chem. Int. Ed. Engl* 1997, *36*, 1374-1389.

[5] a) X. Chen, S. Liu, Y. Hou, M. Tohme, R. Park, J. R. Bading and P. S. Conti, *Molecular Imaging & Biology* 2004, *6*, 350-359; b) X. Chen, R. Park, Y. Hou, V. Khankaldyyan, I. Gonzales-Gomez, M. Tohme, J. R. Bading, W. E. Laug and P. S. Conti, *European Journal of Nuclear Medicine and Molecular Imaging* 2004, *31*, 1081-1089; c) C. Zhang, M. Jugold, E. C. Woenne, T. Lammers, B. Morgenstern, M. M. Mueller, H. Zentgraf, M. Bock, M. Eisenhut, W. Semmler and F. Kiessling, *Cancer Research* 2007, *67*, 1555-1562.

[6] J.-P. Xiong, T. Stehle, R. Zhang, A. Joachimiak, M. Frech, S. L. Goodman and M. A. Arnaout, *Science* 2002, *296*, 151-155.

[7] I. Ina, R. Dominik, S. Jochen, O. Michaela van, D. Ulrike, K. B. Andreas and S. Samuel, *Current Cancer Drug Targets* 2014, *14*, 371-379.

[8] a) J. R. Dudley, J. T. Thurston, F. C. Schaefer, D. Holm-Hansen, C. J. Hull and P. Adams, *Journal of the American Chemical Society* 1951, *73*, 2986-2990; b) J. T. Thurston, J. R. Dudley, D. W. Kaiser, I. Hechenbleikner, F. C. Schaefer and D. Holm-Hansen, *Journal of the American Chemical Society* 1951, *73*, 2981-2983.

[9] H. Sabik, R. Jeannot and B. Rondeau, *Journal of Chromatography A* 2000, *885*, 217-236.

[10] B. Klaus and S. Clemens, *Current Organic Synthesis* 2012, *9*, 342-356.

[11] a) F. Almalioti, J. MacDougall, S. Hughes, M. M. Hasson, R. L. Jenkins, B. D. Ward, G. J. Tizzard, S. J. Coles, D. W. Williams, S. Bamford, I. A. Fallis and A. Dervisi, *Dalton Trans* 2013, *42*, 12370-12380; b) S. N. Gavade, V. L. Markad, K. M. Kodam, M. S. Shingare and D. V. Mane, *Bioorganic & Medicinal Chemistry Letters* 2012, *22*, 5075-5077.

[12] B. Liu, Y. Lee, J. Zou, H. M. Petrassi, R. W. Joseph, W. Chao, E. L. Michelotti, M. Bukhtiyarova, E. B. Springman and B. D. Dorsey, *Bioorganic & Medicinal Chemistry Letters* 2010, *20*, 6592-6596.

[13] V. R. Avupati, R. P. Yejella, V. R. Parala, K. N. Killari, V. M. R. Papasani, P. Cheepurupalli, V. R. Gavalapu and B. Boddeda, *Bioorganic & Medicinal Chemistry Letters* 2013, *23*, 5968-5970.

[14] P. Chellan, K. M. Land, A. Shokar, A. Au, S. H. An, D. Taylor, P. J. Smith, K. Chibale and G. S. Smith, *Organometallics* 2013, *32*, 4793-4804.

[15] D. R. Shah, R. P. Modh and K. H. Chikhalia, *Future Medicinal Chemistry* 2014, *6*, 463-477.

[16] K. Arya and A. Dandia, *Bioorg Med Chem Lett* 2007, *17*, 3298-3304.

[17] G. Damia and M. D'Incalci, *Clinical Pharmacokinetics* 1995, *28*, 439-448.

[18] G. Jagadeesh Kumar, H. V. S. Sriramkumar Bomma, E. Srihari, S. Shrivastava, V. G. M. Naidu, K. Srinivas and V. Jayathirtha Rao, *Medicinal Chemistry Research* 2013, *22*, 5973-5981.

[19] M. S. Miller, J.-A. Pinson, Z. Zheng, I. G. Jennings and P. E. Thompson, *Bioorganic & Medicinal Chemistry Letters* 2013, *23*, 802-805.

[20] L. C. Cantley, *Science* 2002, *296*, 1655-1657.

[21] A. Berndt, S. Miller, O. Williams, D. D. Le, B. T. Houseman, J. I. Pacold, F. Gorrec, W.-C. Hon, P. Ren, Y. Liu, C. Rommel, P. Gaillard, T. Ruckle, M. K. Schwarz, K. M. Shokat, J. P. Shaw and R. L. Williams, *Nat Chem Biol* 2010, *6*, 117-124.

[22] G. W. Rewcastle, S. A. Gamage, J. U. Flanagan, R. Frederick, W. A. Denny, B. C. Baguley, P. Kestell, R. Singh, J. D. Kendall, E. S. Marshall, C. L. Lill, W. J. Lee, S. Kolekar, C. M. Buchanan, S. M. Jamieson and P. R. Shepherd, *J Med Chem* 2011, *54*, 7105-7126.

[23] A. Makino, T. Arai, M. Hirata, M. Ono, Y. Ohmomo and H. Saji, *Nucl Med Biol* 2016, *43*, 101-107.

[24] B. Jagadish, G. L. Brickert-Albrecht, G. S. Nichol, E. A. Mash and N. Raghunand, *Tetrahedron Letters* 2011, *52*, 2058-2061.

[25] A. B. P. Lever, *Inorganic electronic spectroscopy*, Elsevier, 1984.

[26] E. Wiberg, N. Wiberg and A. F. Holleman, *Inorganic chemistry*, Academic Press ; De Gruyter, San Diego; Berlin; New York, 2001, p.

[27] A. B. P. Lever, *Journal of Chemical Education* 1968, *45*, 711.

[28] K. Wade, *Applied Organometallic Chemistry* 2000, *14*, 449-450.

[29] Z. Zhang, Y. Lu and J. Guo, *Journal of Chemical Crystallography* 2006, *36*, 543-550.

[30] J. Li, Y.-W. Ren, J.-H. Zhang and P. Yang, *Journal of Chemical Crystallography* 2004, *34*, 409-413.

[31] a) J. Barreto, T. Joshi, T. K. Venkatachalam, D. C. Reutens, B. Graham and L. Spiccia, *Journal of Coordination Chemistry* 2015, *68*, 335-349; b) C. V. Esteves, J. Madureira, L. M. P. Lima, P. Mateus, I. Bento and R. Delgado, *Inorganic Chemistry* 2014, *53*, 4371-4386; c) L. M. P. Lima, D. Esteban-Gómez, R. Delgado, C. Platas-Iglesias and R. Tripier, *Inorganic Chemistry* 2012, *51*, 6916-6927; d) L. M. P. Lima, C. V. Esteves, R. Delgado, P. Hermann, J. Kotek, R. Ševčíková and P. Lubal, *European Journal of Inorganic Chemistry* 2012, *2012*, 2533-2547; e) A. Rodriguez-Rodriguez, Z. Garda, E. Ruscsak, D. Esteban-Gomez, A. de Blas, T. Rodriguez-Blas, L. M. P. Lima, M. Beyler, R. Tripier, G. Tircso and C. Platas-Iglesias, *Dalton Transactions* 2015, *44*, 5017-5031.

[32] K. Kumar, M. F. Tweedle, M. F. Malley and J. Z. Gougoutas, *Inorganic Chemistry* 1995, *34*, 6472-6480.

[33] A. Bianchi, L. Calabi, C. Giorgi, P. Losi, P. Mariani, D. Palano, P. Paoli, P. Rossi and B. Valtancoli, *Journal of the Chemical Society, Dalton Transactions* 2001, 917-922.

[34] a) X.-H. Bu, W. Chen, L.-J. Mu, Z.-H. Zhang, R.-H. Zhang and T. Clifford, *Polyhedron* 2000, *19*, 2095-2100; b) S. Wang and T. D. Westmoreland, *Inorganic Chemistry* 2009, *48*, 719-727.

[35] I. S. Lee and J. R. Long, *Dalton Transactions* 2004, 3434-3436.

[36] M. Regueiro-Figueroa, D. Esteban-Gómez, A. de Blas, T. Rodríguez-Blas and C. Platas-Iglesias, *European Journal of Inorganic Chemistry* 2010, *2010*, 3586-3595.

[37] P. Hermann, J. Kotek, V. Kubicek and I. Lukes, *Dalton Transactions* 2008, 3027-3047.

[38] R. Delgado, V. Felix, L. M. P. Lima and D. W. Price, *Dalton Transactions* 2007, 2734-2745.

[39] T. Gunnlaugsson, J. P. Leonard, S. Mulready and M. Nieuwenhuyzen, *Tetrahedron* 2004, *60*, 105-113.

[40] a) A. M. Prokhorov, V. N. Kozhevnikov, D. S. Kopchuk, H. Bernard, N. Le Bris, R. Tripier, H. Handel, B. Koenig and D. N. Kozhevnikov, *Tetrahedron* 2011, *67*, 597-607; b) S. Quici, G. Marzanni, A. Forni, G. Accorsi and F. Barigelletti, *Inorganic Chemistry* 2004, *43*, 1294-1301; c) D. Sannasy, H. M. Marques, M. A. Fernandes and A. S. de Sousa, *Chemical Communications* 2014, *50*, 1582-1584.

[41] a) C. A. Chang, L. C. Francesconi, M. F. Malley, K. Kumar, J. Z. Gougoutas, M. F. Tweedle, D. W. Lee and L. J. Wilson, *Inorganic Chemistry* 1993, *32*, 3501-3508; b) Y. O. Fung, W. Wu, C.-T. Yeung, H.-K. Kong, K. K.-C. Wong, W.-S. Lo, G.-L. Law, K.-L. Wong, C.-K. Lau, C.-S. Lee and W.-T. Wong, *Inorganic Chemistry* 2011, *50*, 5517-5525; c) E. Kriemen, M. Holzapfel, E. Ruf, J. Rehbein and W. Maison, *European Journal of Inorganic Chemistry* 2015, *2015*, 5368-5378; d) N. Raghunand, G. P. Guntle, V. Gokhale, G. S. Nichol, E. A. Mash and B. Jagadish, *Journal of Medicinal Chemistry* 2010, *53*, 6747-6757.

[42] S. Aime, A. Barge, F. Benetollo, G. Bombieri, M. Botta and F. Uggeri, *Inorganic Chemistry* 1997, *36*, 4287-4289.

[43] P. Vojtíšek, J. Rohovec and J. Klimentová, *European Journal of Inorganic Chemistry* 2008, *2008*, 3948-3956.

[44] a) J. Rohovec, P. Vojtisek, P. Hermann, J. Ludvik and I. Lukes, *Journal of the Chemical Society, Dalton Transactions* 2000, 141-148; b) J. J. Wilson, E. R. Birnbaum, E. R. Batista, R. L. Martin and K. D. John, *Inorganic Chemistry* 2015, *54*, 97-109.

[45] a) S. Aime, A. Barge, M. Botta, M. Fasano, J. Danilo Ayala and G. Bombieri, *Inorganica Chimica Acta* 1996, *246*, 423-429; b) P. Vojtíšek, P. Cígler, J. Kotek, J. Rudovský, P. Hermann and I. Lukeš, *Inorganic Chemistry* 2005, *44*, 5591-5599; c) W. Fegler, A. Venugopal, T. P. Spaniol, L. Maron and J. Okuda, *Angewandte Chemie International Edition* 2013, *52*, 7976-7980.

CHAPTER 4

BENZOTHIAZOLE LIGAND SYSTEM

Alzheimer's disease (AD) is the most common form of dementia in elderly people. It is a neurodegenerative disease associated with chronic dementia, memory loss and cognitive impairment, ultimately causing death as the brain effectively shuts down. At present, according to the World Health Organisation (WHO), worldwide 47.5 million people have dementia, with every year 7.7 million new cases projecting the total number of people with dementia to 75.6 million in 2030 and 135.5 million by 2050.

Currently there is no treatment available to cure dementia or to alter its progressive course and also there are no imaging techniques for a definitive diagnosis of Alzheimer's disease. In order to obtain a diagnosis, a system is used whereby the patient is assessed by cognitive tests[1] like Mini-mental state examination[2] evaluating the cognitive functions. Although different laboratory tests are used for a probable AD diagnosis, at this moment a definitive diagnosis can be obtained only post mortem.

Thus the development of an imaging agent is essential to get early and more accurate diagnosis in the first stages of the disease.

The cause for most Alzheimer's cases is still unknown but some hypothesis have been proposed to understand the onset of progressive cognitive decline that characterises the disease. One of the most accepted hypothesis is based on deposition of senile plaques, composed of β-amyloid (Aβ) plaques and neurofibrillary tangles composed of hyperphosphorylated tau proteins, found in high concentration in brain tissue affected by the disease making them neuropathological markers for AD.[3]

At the base of the amyloid hypothesis there is the imbalance between the beta-peptide (Aβ) production and Aβ clearance; the Aβ amyloid is formed by the amyloid precursor protein (APP) where Aβ are a normal product of APP metabolism by the enzymes: the β-secretase and γ-secretase (Figure 4.1).

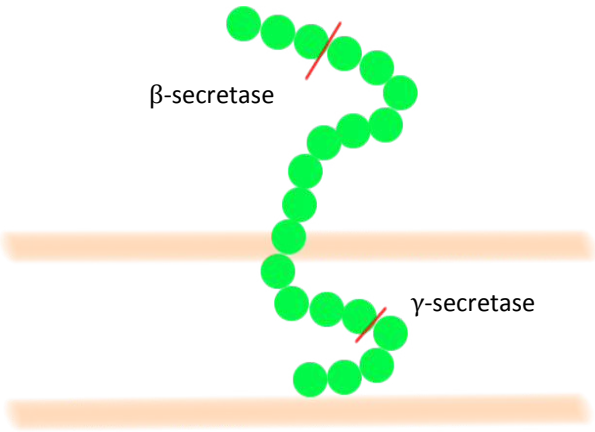

Figure 4.1: The APP membrane is shown in light orange and the peptide, embedded into the membrane, in green. The enzymes cleave Aβ at the two red points indicated (the length shown is not representative of the actual length) (Thomas, Cardiff University, 2013)

Mutations in the APP gene could cause the Aβ deposition, the mutations promote the cleavage of slightly longer Aβ ($Aβ_{1-42}$ as opposed to $Aβ_{1-40}$) that are insoluble and, hence, accumulate together, along with $Aβ_{1-40}$, to form toxic oligomers.[4] While soluble forms of Aβ have been shown to cause synaptic damage[5], the insoluble plaques are thought to be the initiator of AD but not directly cause the physical outcomes of the disease. It is thought that the insoluble Aβ oligomers initiate the hyperphosphorylation of the microtubule stabilising protein tau.[6] Once hyper-phosphorylated, the tau protein can no longer bind to microtubules (Figure 4.2) and so aggregate together forming neurofibrillary tangles. This leaves the microtubule to disintegrate and leads to apoptosis of neurons.[7]

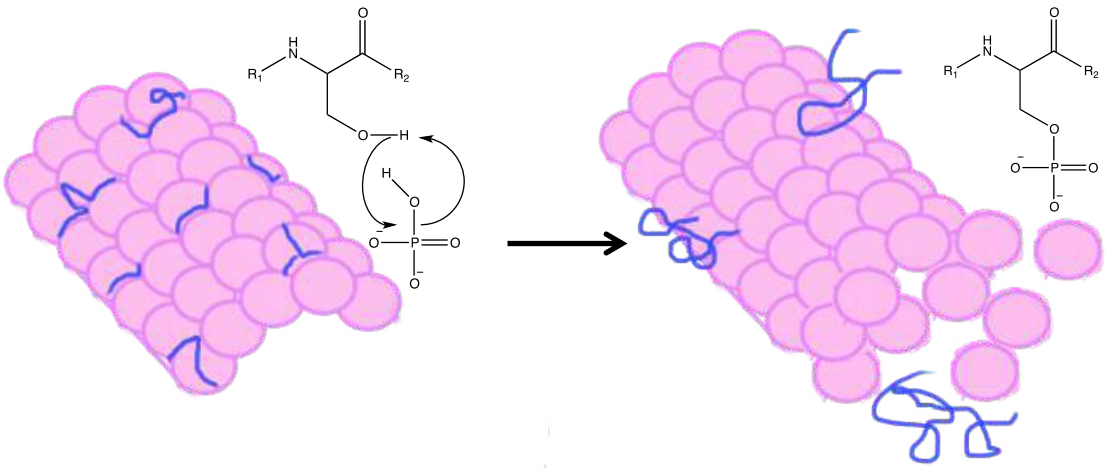

Figure 4.2: Tau protein (blue) shown binding to a microtubule (pink) before being phosphorylated and disassociating after being hyper-phosphorylated[6]

Hence, the development of an imaging agent that could highlight the presence of Aβ *in vivo* rather than via autopsy could give a better understanding of the onset of the disease and improve the possibility for prevention or treatment. Although the structure of Aβ plaques has been difficult to obtain, it is thought that they have a cross-β sheet structure, where the β sheets run in a direction parallel to the fibril axis but the strands run perpendicular to the axis[8] (Figure 4.3). This conformation leaves two different sides of the protein with different features, hydrophobic sections in between the sheets and hydrophilic sections around the sheets.

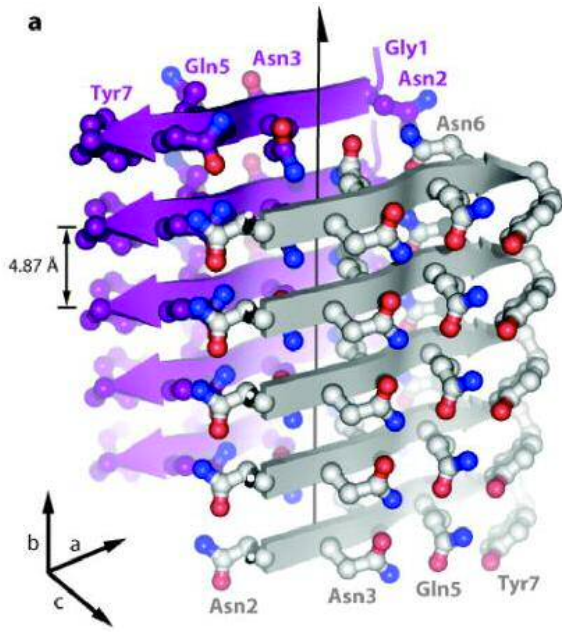

Figure 4.3: Aβ structure[8]

Complexes based on 2-arylbenzothiazole, or similar derivatives, have become of great interest due to their many uses[9]. Benzothiazole derivatives have found applications as anticancer,[10] anti-inflammatory,[11] anti-tuberculosis[12] and anti-microbial agents,[13] and of relevance to this work as Aβ plaque imaging agents.

Currently the only imaging agent approved by the FDA is florobetapir-^{18}F,[14] while compounds based on the benzothiazole core like thioflavin T (ThT) or Pittsburgh compound B (PiB) are in trial phases (Figure 4.4).

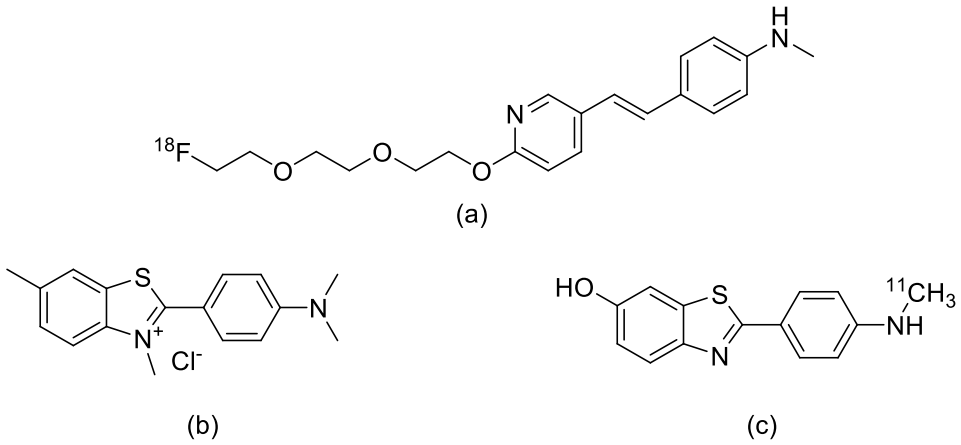

Figure 4.4: (a) florobetapir-^{18}F, (b) ThT, (c) PiB

Thioflavin T is a well-known structure based on 2-arylbenzothiazole used to stain amyloids such as Aβ, but unfortunately ThT is not specific for amyloids of Aβ as it reacts with many types of amyloid fibrils.[15] A study led by LeVine in 1993 showed the interaction between the amyloid plaques and the ThT can be followed by luminescence, the molecule binding to synthesised aggregated Aβ(1-28) and Aβ(1-40) shows a new excitation (absorption) wavelength at 450nm, while the emission wavelength was red-shifted from 445nm to 482nm[16] (Figure 4.5).

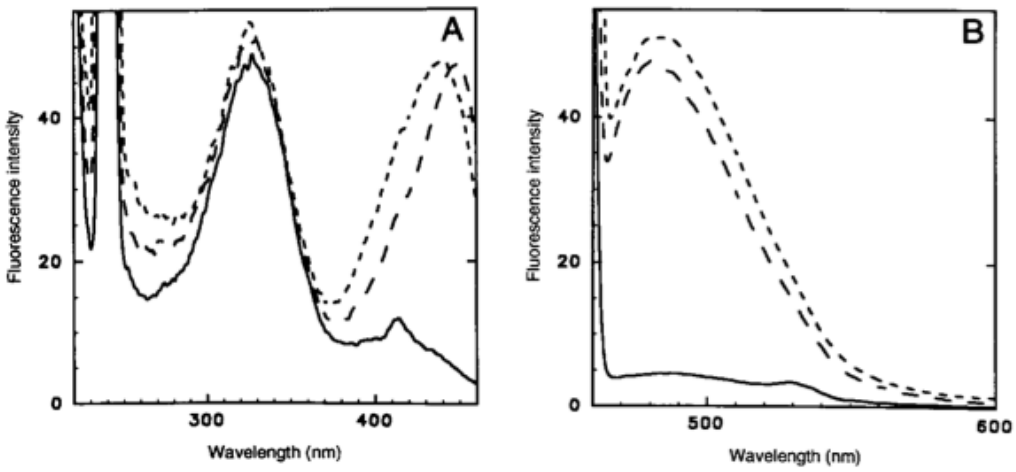

Figure 4.5: ThT absorption spectra (left) and emission spectra (right), in absence of Aβ plaques, with Aβ(1-28) and Aβ(1-40)[16]

The fluorescent changes in the emission spectrum, in fact, occur only when the molecule binds aggregate oligomers of Aβ and not monomeric or dimeric species. This feature makes this compound highly suitable to image *in vitro* the harmful oligomeric plaques.

Unfortunately the study does not provide any explanation about how the molecules are bound to the β-sheets.

Krebs et al[17] investigated the conformation assumed by the ThT as dye when bound to the plaques by confocal microscopy and polarised light. It has been observed that when exciting the dye with polarised light the fluorescence from the molecule formed a consistent pattern rather than an uniform disc. As polarised light was used, this pattern can only occur if the ThT molecules are bound to the amyloid fibrils in a regular, aligned way. Therefore, through knowing which way the amyloid fibrils lay and when the ThT molecules become excited by the polarised light, the study revealed that Thoflavin T must bind perpendicularly to the amyloid fibrils but in the direction of the fibril axis in channels in the β-sheets (Figure 4.6).

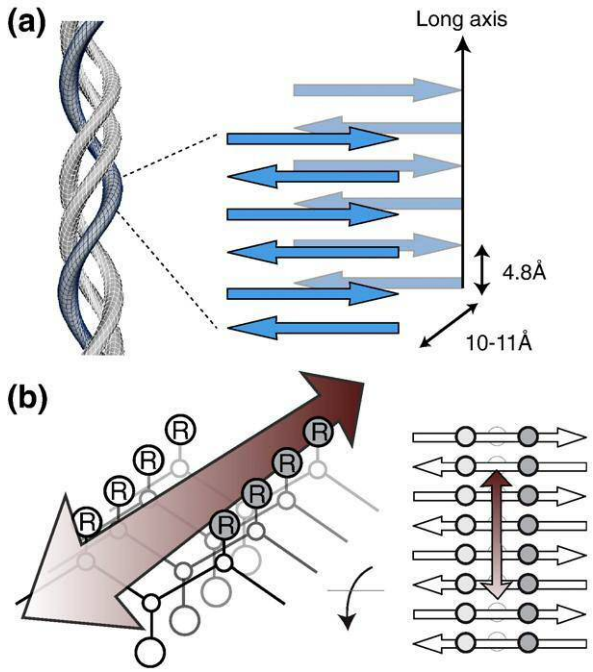

Figure 4.6: β structure of amyloid fibrils (a).“Channel” model of ThT binding to fibril-like β-sheets (b)[18]

In agreement with this there are the studies led by Biancalana,[18] and Wolfe[19] who showed that the ThT behaves like a "molecular rotor". Their analysis demonstrated variation in the photophysical properties during the rotation of the benzothiazole moiety. In fact, in solution the low-energy barrier allows the benzothiazole and benzylamine rings to rotate freely about their carbon-carbon bond and it was believed that the increase in ThT fluorescence results from the selective immobilisation of a subset of Thioflavin

conformers. The results showed how the rotation quenched excited states, causing low fluorescence emission for free ThT.

Opposite to that, the immobilisation of the molecule preserved the excited state, resulting in a high quantum yield of fluorescence. In this way, in conclusion, the Aβ fibrils are likely to provide a binding site that can lock the ThT molecule, increasing the fluorescence emission of the compound.

Since Thioflavin T has revealed itself as such a good imaging agent for Aβ plaques *in vitro*, different attempts to produce a similar structure that could be used for *in vivo* imaging has been undertaken.[20] Different studies led to the conclusion that removing the charge from the 2-arylbenzothiazole derivatives increases the lipophilicity of the compounds, allowing an easier crossing of the blood-brain barrier (BBB) and also showing much higher affinity for Aβ (1-40) fibrils.[20c] Moreover it has been noticed that the removal of the methyl group on the heterocyclic nitrogen of ThT can improve binding affinity to β amyloid plaques as well.[20b] Finally these studies showed how also the presence of only one methyl group on the amine nitrogen in the 4'-position increased the affinity but for unknown reasons. This is an important feature for the synthesis of new derivatives, leaving the amine group free for possible further functionalisation.

For examples of this important characteristic show how, through the use of a linker, it could be possible to bind a macrocycle or a ligand moiety to coordinate an appropriate metal for imaging or with theranostic application.

Recent examples include the synthesis and the develop of MRI agents, bringing a TACN or the DO3A ring as chelator (Figure 4.7) for a gadolinium metal centre and using the chloroacetyl chloride as linker between the coordination site and the benzothiazole moiety.[21]

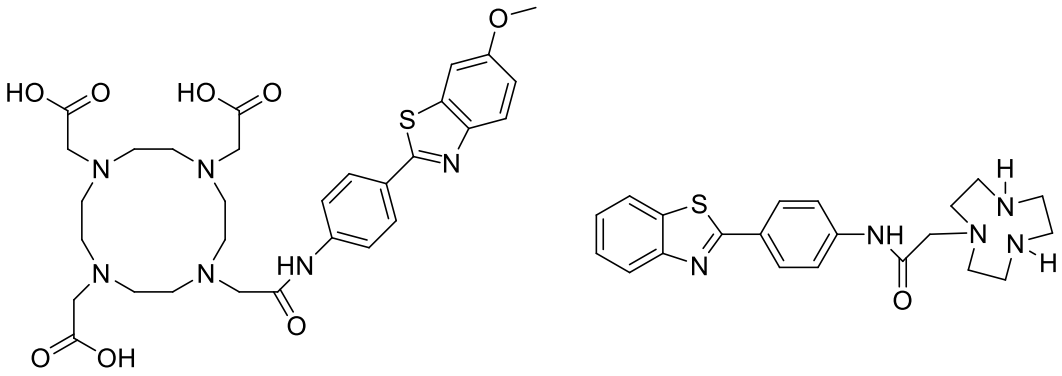

Figure 4.7: examples of DO3A (left)[21d] and TACN ligand (right)[21a] with a benzothiazole moiety

The synthesis of a benzothiazole can follow many different paths, one of the most common approaches is the direct synthesis of a 2-arylbenzothiazole via palladium catalysed C-C bond formation between a benzothiazole and an appropriately substituted aryl.[22]

Another common method is through the condensation of 2-aminothiophenol with different functionalities on an aryl group using polyphosphoric acid as solvent to promote the condensation.[23]

The mechanism of the condensation follow the nucleophilic attack of the amine on the carbonyl to form a Schiff base with elimination of a molecule of water, then the ring closure follows the nucleophilic attack of the sulfur on the double bond formed and finally the oxidation of the secondary amine to a tertiary (Figure 4.8).[24]

This method has been chosen for the synthesis of the precursor derivatives. Heating in polyphosphoric acid as solvent or in ethanol, and neutralisation with a solution of 10% Na_2CO_3 gives the desired compound.[20a, 25]

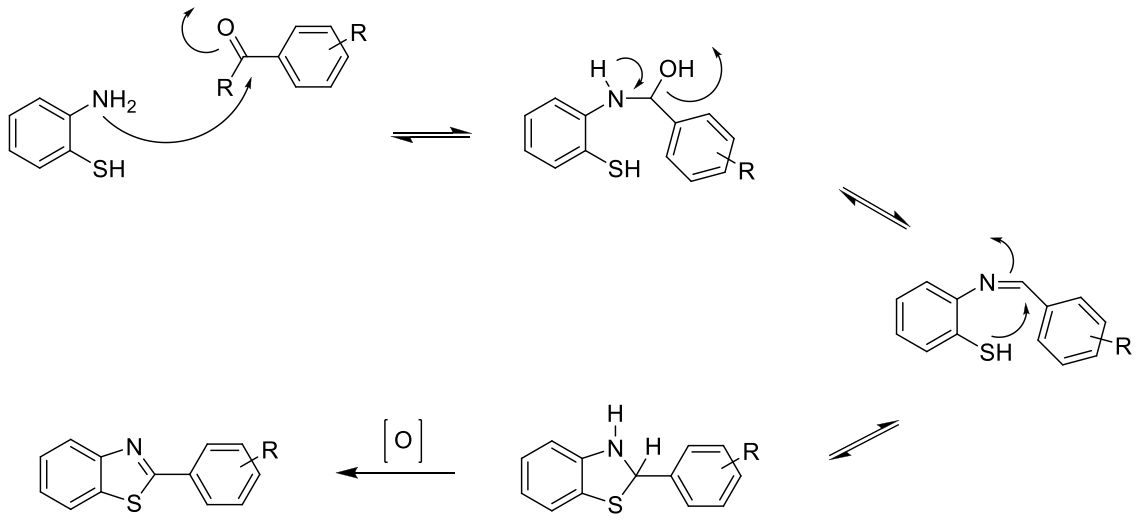

Figure 4.8: condensation mechanism of 2-aminothiophenol with carbonyl derivates

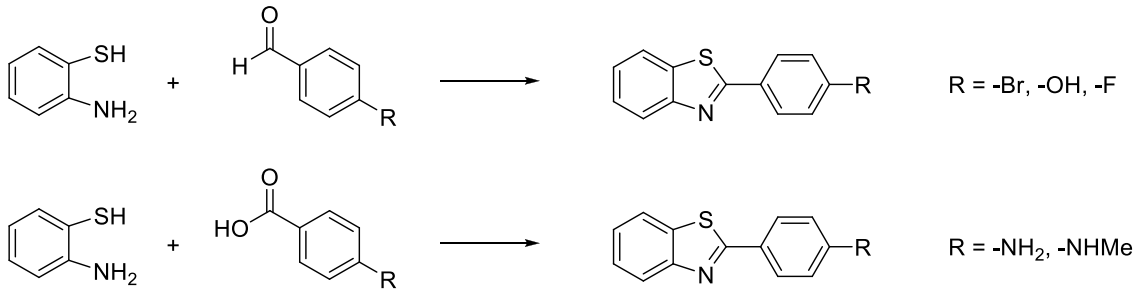

As described above, with the example of chloroacetyl chloride, a linker is necessary between the two moieties of the compound. Several attempts have been made to prepare new ligands. The experimental section includes the attempted failed syntheses of new intermediates. These include the ring opening of succinic or diglycolic anhydrides[26] or the use of Traut's reagent with deferoxamine.[27]

Successful attempts to generate a linker species from reaction of an excess of epichlorohydrin with 4-(benzo[d]thiazol-2-yl)-N-methylaniline. Dissolving the two compounds in ethanol under nitrogen, and refluxing them for three days, then the solvent and the excess of epichlorohydrin have been removed *in vacuo*. The residue was recrystallised in Et_2O and the solid filtered off before to be purified by chromatography column (Figure 4.9).

Figure 4.9: first step of the precursor synthesis

The second step has been the closure of the epoxide ring, stirring the chlorohydrin precursor with a base, under nitrogen in methanol at room temperature, followed by an aqueous work-up to afford the product. (Figure 4.10).

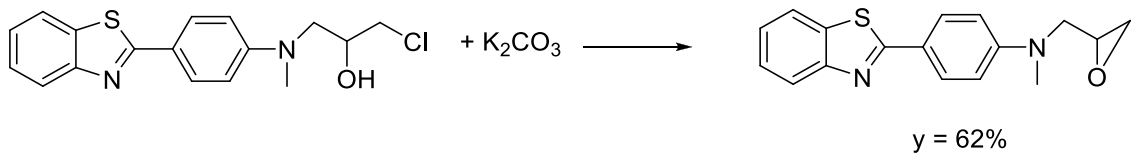

Figure 4.10: second and final step of the precursor synthesis

Using this route a versatile novel precursor (Bz-epox), has been synthesised and fully characterised. Reacting the epoxide function via nucleophilic substitution makes it available to a wide range of new possible chelating agents. This is discussed in the following section.

4.3.1 - DO3A based complexes

As discussed in the previous chapter, DO3A is an azamacrocycle suitable to coordinate a diverse range metals for imaging purposes.[28] Thus DO3A and Bz-epox were combined in ethanol and Et_3N and the solution heated at 50-60° for 24 hours. The second step of the synthesis was the removal of the carboxylate ^{t}Bu protecting groups via treatment with adding trifluoroacetic acid to yield a green oil. Complexes were prepared by the reaction of an aqueous methanol solution of ligand with an aqueous solution of the appropriate metal salt at pH 7 and 50°C. The mixture was purified by flash chromatography on a short column, to afford a clear solution (Figure 4.11).

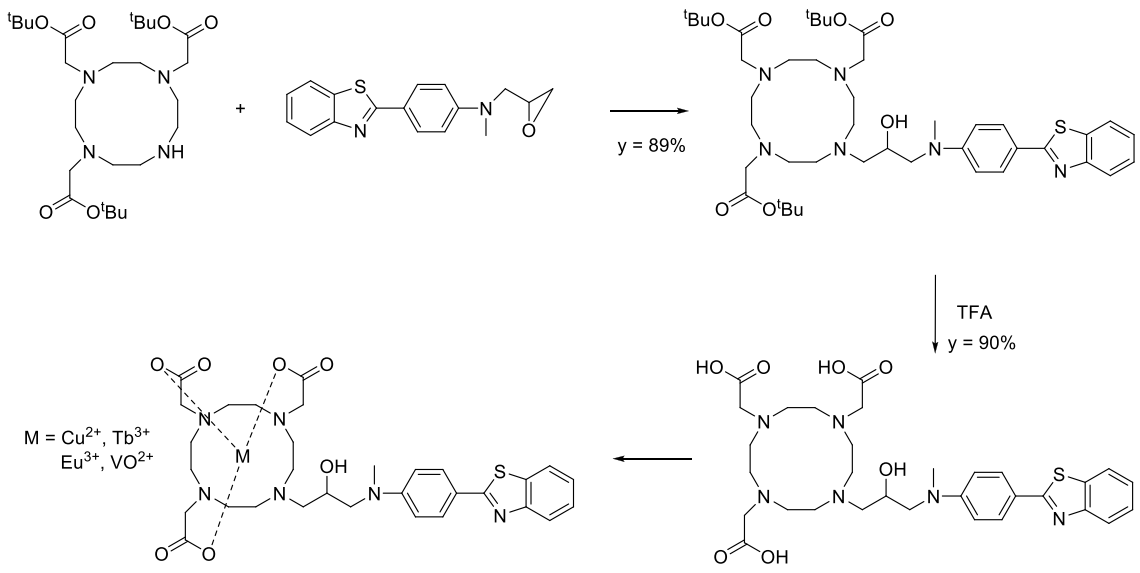

Figure 4.11: synthesis of M-DO3A-Bz-epox complexes, all the characterisation data are reported in the experimental section

4.3.2 - DFO based complexes

The approach to synthesise the complexes containg DFO was different from that used for the previous compounds. Initially DFO is protected by complexation to a metal centre. Followed by the addition of the Bz-epox to the mixture (Figure 4.12).

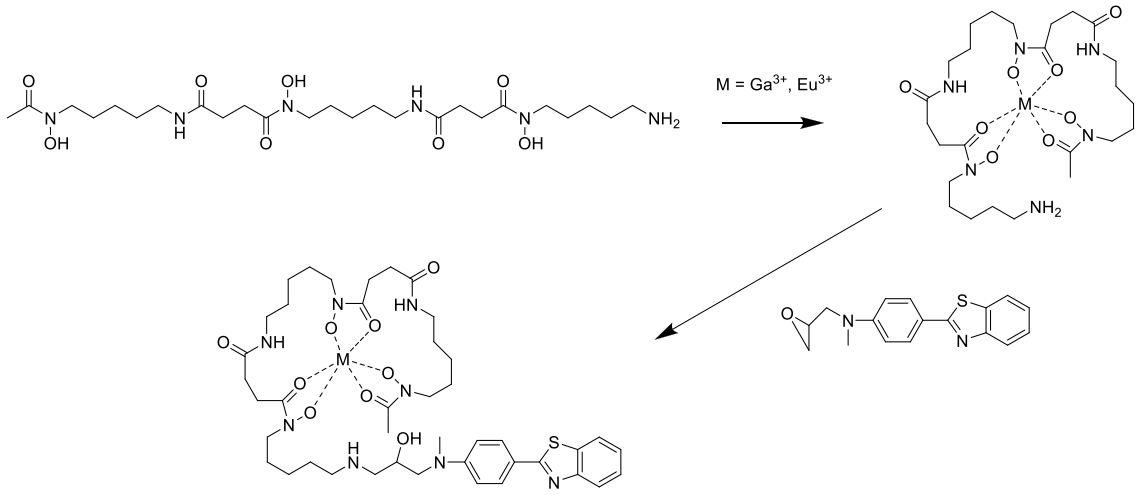

Figure 4.12: synthesis of DFO-Bz-epox complexes

4.3.3 - Cyclen based complex

Cyclen has proved to be an excellent chelator for cold copper,[29] even if the stability of the compound *in vivo* is lower. The study by Jones-Wilson *et al* showed that complexes of cyclen, including cyclam, DO2A, DOTA and TETA form highly stable complexes with Cu(II). Surprisingly, the potential neutral DO2A complex was the least stable of those species (Log K_f (Cu^{II}) = 18.9). This study also showed that the systems examinated were bioavailable, but that neutral and cationics show higher organ absorption.[30]

Working at different pH, it could be possible to deprotonate the hydroxy group presents on the compound, giving a total charge of +1, changing the coordination chemistry of the complex, filling the coordination sphere of the copper,[29, 31] and making the compound more likely to cross the blood-brain barrier.

Thus the azamacrocycle was dissolved in acetonitrile and Bz-epox was added to the solution. The mixture was left under stirring for three days, then the solid filtered off and the solvent removed *in vacuo*, later the residue was dissolved in MeOH; a solution of

$CuSO_4*5H_2O$ was dissolved in MeOH and added to the ligand. The solution was heated to 50°C for five minutes, changing colour in a dark blue solution. The solution was cooled to room temperature and filtered off on a small chromatography column (Figure 4.13).

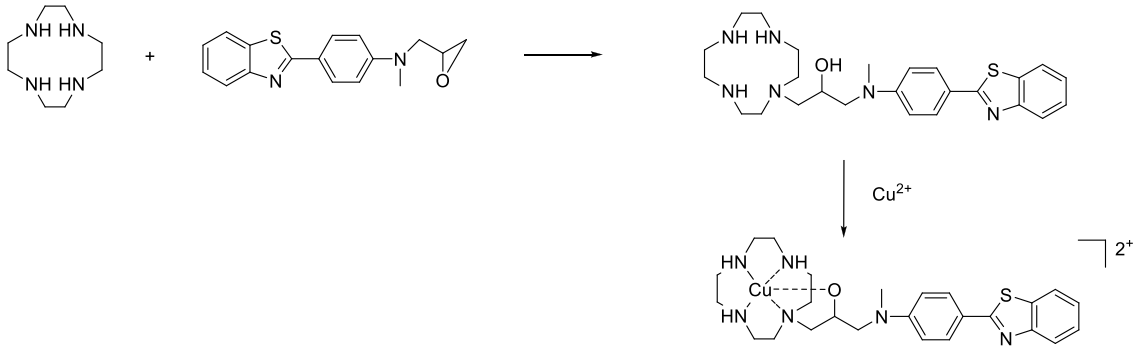

Figure 4.13: synthesis of cyclen-Bz-epox complex

The benzothiazole ligands and complexes showed an interesting activity as luminescence probes that has led to their investigation in more detail. All the ligands and complexes synthesised and described in the previous paragraph have been measured by Dr. Simon Pope's research group (Cardiff University), unfortunately due to the different solubility of the compounds it was not possible to use the same solvent system, thus the results will be discussed dividing the compounds into discreet groups.

Initially for all the compounds 10^{-5} M solutions (except for the ligand DO3A-Bz-epox that was 10^{-6} M) were used for measuring the UV spectra and then the same solution used for the luminescence spectra at room temperature and the results obtained in terms of λ_{abs}, λ_{em} and τ are reported in the underlying table.

Compound	λ_{abs} (nm)[d]	λ_{em} (nm)	τ (ns)[e]
Bz[a]	353.5 (22000), 313.5 (16800), 229.5 (51000)	410	1.54
Bz-epox[a]	353 (40800), 302 (17600), 229 (113900)	407	1.53
DO3A-Bz-epox[c]	368 (1287000)	434	1.83
Cu-DO3A-Bz-epox[c]	364.5 (5200)	432	1.83
Eu-DO3A-Bz-epox[c]	364 (8300)	433	1.82
Tb-DO3A-Bz-epox[c]	364.5 (5000)	431	1.74
VO-DO3A-Bz-epox[c]	364.5 (6300)	433	1.82
Ga-DFO-Bz-epox[b]	358 (27900), 225.5 (53800)	427	1.85
Eu-DFO-Bz-epox[b]	358 (22900), 319 (16300), 228 (40500)	428	1.81
Cu-cyclen-Bz-epox[c]	361 (2300)	431	1.82

[a] DCM; [b] 1:1 EtOH:H_2O; [c] 1:1 H_2O:DMSO; [d] λ_{ex} lowest energy from corresponding UV; [e] λ_{ex} = 372 nm

Analysing the data (Figure 4.14 and 4.15) is possible to see from the spectra that there are no peaks characteristic of lanthanide emission, under the conditions used to excite the compounds.

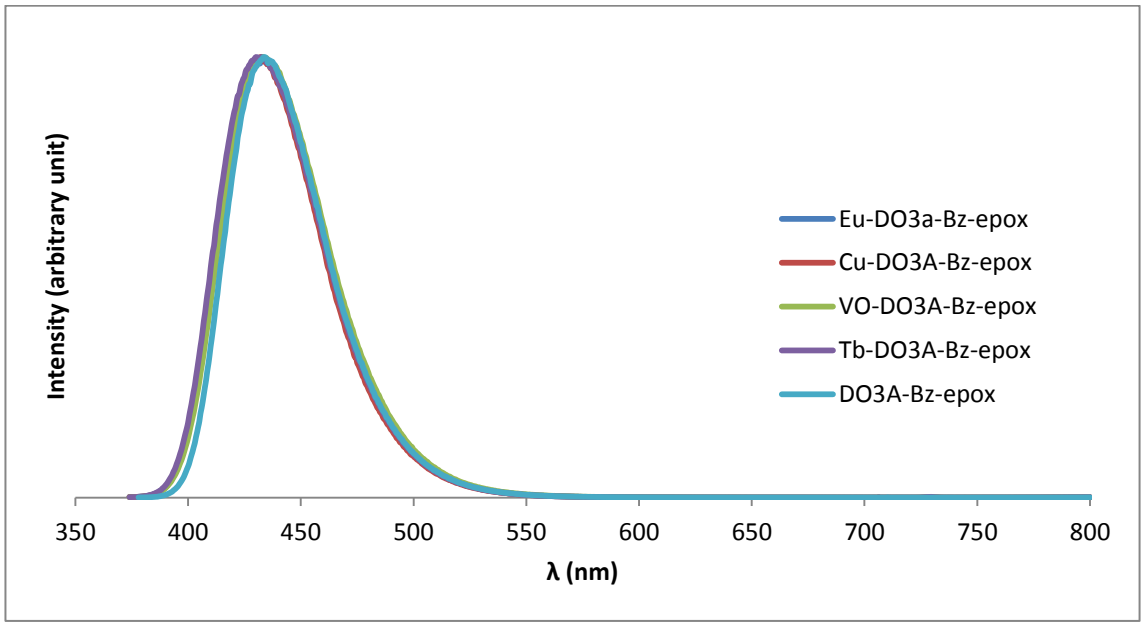

Figure 4.14: emission spectra of DO3A-Bz-epox and related complexes

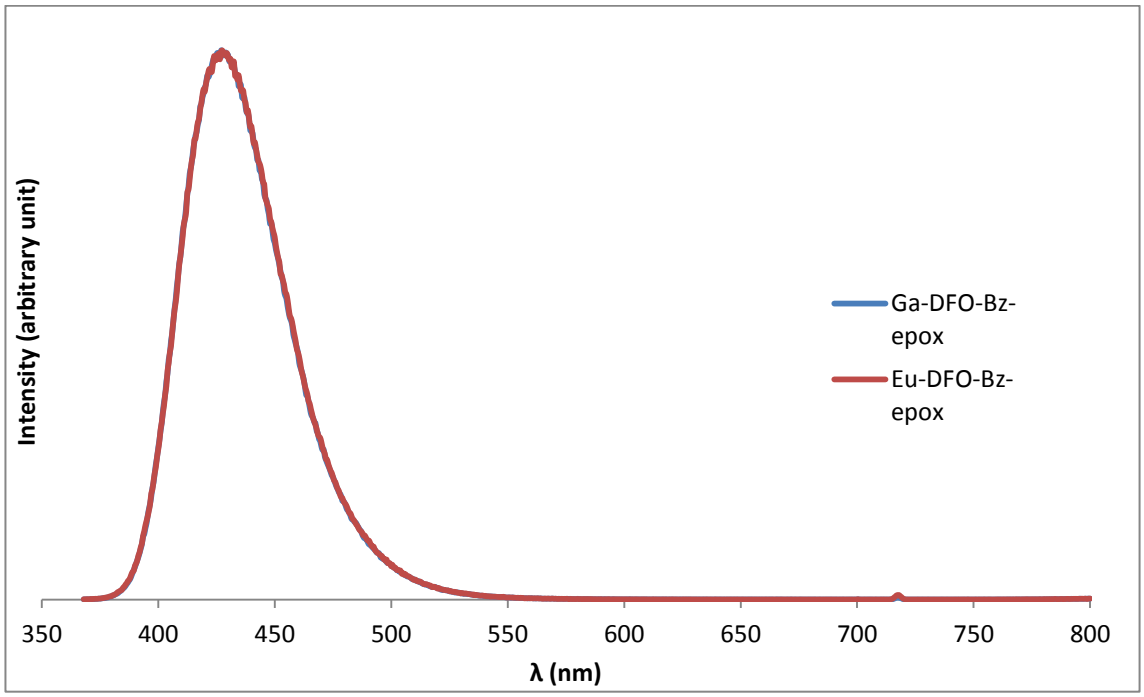

Figure 4.15: emission spectra of DFO-Bz-epox complexes

Thus, it is obvious that the spectrum of all these species are essentially identical, being dominated by ligand centred emission. It is also possible to conclude that there is no significant energy transfer to the metal centres.

One of the possible cause why there is not energy transfer could the distance between the antenna and the lanthanide metal centre. According to Förster's theory of resonance energy transfer (FRET), the distance between the donor species (the organic fluorophore as antenna) and the acceptor (the metal centre) is in the range of 8-10 Ă.[32] The complex of Tb(III) and Eu(III) DO3A-Bz-epox show a distance of 8.65 Ă. The lack of electronic communication between the fluorophore and the metal suggest that the distance (8.65 Ă in this case) is too great for any significant energy transfer and/or the relative orientation of the fluorophore and the metal is unsuitable for energy transfer.

More likely the absence of the lanthanide peaks could be the consequence of a poor overlap of the energies states between the metal centre and the excited states of the ligand. Unfortunately studies about the energy states has not been done as part of this work; possible future studies will be useful to explain and understand the energy levels of the compounds and if the absence of an efficient overlap of the electronic states is the main reason of the lack of the energy transfer to the lanthanide centres.

This chapter has described the synthesis of several benzothiazioles (and their precursors), and the formation and characterisation of three new kind of ligands based on an appropriate benzothiazole moiety (Bz-epox). These benzathiazole derivatives have been further coupled to several coordinating molecules to obtain a new versatile group of ligand, able to bind several different metals.

These ligands have been used to form a number of species; DO3A-Bz-epox complexes have been formed containing Cu(II), Tb(III), Eu(III) and VO(II), while DFO-Bz-epox has been reacted with Eu(III) and Ga(III) to form novel complexes. Furthermore, cyclen-Bz-epox was used to successfully form a novel Cu(II) complex. All complexes were synthesised using a 1:1 metal:ligand ratio and characterised by EMI-MS to confirm binding of the metal in solution.

Finally a spectroscopic study of the ligands and the complexes has been described. The data shows that under excitation, there are no peaks characteristic of lanthanide emission, leaving the luminescence properties dominated by ligand centred emission and suggesting that there is not significant energy transfer to the metal centres.

The reasons behind this result have been discussed. It has been hypothesised that the reasons for this observed lack of energy transfer is due to the orientation of the fluorophore and the metal, and that the distance between the antenna and the lanthanide metal centre (8.65 Å for the complexes) is too great for any significant energy transfer. Alternatively, it may be that poor overlap of excited energy levels between the metal centre and the ligand prevents fluorescence. Future studies could examine this in more detail to determine the main reason for the observed lack of energy transfer to the lanthanide centres.

[1] G. McKhann, D. Drachman, M. Folstein, R. Katzman, D. Price and E. M. Stadlan, *Neurology* 1984, *34*, 939-939.

[2] M. F. Folstein, S. E. Folstein and P. R. McHugh, *Journal of Psychiatric Research* 1975, *12*, 189-198.

[3] J. Hardy and D. J. Selkoe, *Science* 2002, *297*, 353-356.

[4] N. Suzuki, T. T. Cheung, X. D. Cai, A. Odaka, L. Otvos, C. Eckman, T. E. Golde and S. G. Younkin, *Science* 1994, *264*, 1336-1340.

[5] P. N. Lacor, M. C. Buniel, P. W. Furlow, A. Sanz Clemente, P. T. Velasco, M. Wood, K. L. Viola and W. L. Klein, *The Journal of Neuroscience* 2007, *27*, 796-807.

[6] H. C. Huang and Z. F. Jiang, *J Alzheimers Dis* 2009, *16*, 15-27.

[7] K. Iqbal and I. Grundke-Iqbal, *Acta Neuropathologica* 2005, *109*, 25-31.

[8] R. Nelson, M. R. Sawaya, M. Balbirnie, A. O. Madsen, C. Riekel, R. Grothe and D. Eisenberg, *Nature* 2005, *435*, 773-778.

[9] S. Sonakshi, *Anti-Inflammatory & Anti-Allergy Agents in Medicinal Chemistry* 2015, *14*, 98-112.

[10] a) R. M. Kumbhare, T. Dadmal, U. Kosurkar, V. Sridhar and J. V. Rao, *Bioorganic & Medicinal Chemistry Letters* 2012, *22*, 453-455; b) M. F. G. Stevens, C. J. McCall, P. Lelievald, P. Alexander, A. Richter and D. E. Davies, *Journal of Medicinal Chemistry* 1994, *37*, 1689-1695.

[11] a) J. Das, R. V. Moquin, J. Lin, C. Liu, A. M. Doweyko, H. F. DeFex, Q. Fang, S. Pang, S. Pitt, D. R. Shen, G. L. Schieven, J. C. Barrish and J. Wityak, *Bioorganic & Medicinal Chemistry Letters* 2003, *13*, 2587-2590; b) J. Wada, T. Suzuki, M. Iwasaki, H. Miyamatsu, S. Ueno and M. Shimizu, *Journal of Medicinal Chemistry* 1973, *16*, 930-934.

[12] W. Huang and G.-F. Yang, *Bioorganic & Medicinal Chemistry* 2006, *14*, 8280-8285.

[13] S. T. Asundaria and K. C. Patel, *Pharmaceutical Chemistry Journal* 2012, *45*, 725-731.

[14] D. F. Wong, P. B. Rosenberg, Y. Zhou, A. Kumar, V. Raymont, H. T. Ravert, R. F. Dannals, A. Nandi, J. R. Brašić, W. Ye, J. Hilton, C. Lyketsos, H. F. Kung, A. D. Joshi, D. M. Skovronsky and M. J. Pontecorvo, *Journal of Nuclear Medicine* 2010, *51*, 913-920.

[15] Y. Yang and M. Cui, *European Journal of Medicinal Chemistry* 2014, *87*, 703-721.

[16] H. Levine, *Protein Science* 1993, *2*, 404-410.

[17] M. R. H. Krebs, E. H. C. Bromley and A. M. Donald, *Journal of Structural Biology* 2005, *149*, 30-37.

[18] M. Biancalana and S. Koide, *Biochimica et Biophysica Acta (BBA) - Proteins and Proteomics* 2010, *1804*, 1405-1412.

[19] L. S. Wolfe, M. F. Calabrese, A. Nath, D. V. Blaho, A. D. Miranker and Y. Xiong, *Proceedings of the National Academy of Sciences* 2010, *107*, 16863-16868.

[20] a) C. A. Mathis, B. J. Bacskai, S. T. Kajdasz, M. E. McLellan, M. P. Frosch, B. T. Hyman, D. P. Holt, Y. Wang, G.-F. Huang, M. L. Debnath and W. E. Klunk, *Bioorganic & Medicinal Chemistry Letters* 2002, *12*, 295-298; b) M.-Q. Zheng, D.-Z. Yin, J.-P. Qiao, L. Zhang and Y.-X. Wang, *Journal of Fluorine Chemistry* 2008, *129*, 210-216; c) R. Leuma Yona, S. Mazères, P. Faller and E. Gras, *ChemMedChem* 2008, *3*, 63-66.

[21] a) J. Barreto, T. K. Venkatachalam, T. Joshi, U. Kreher, C. M. Forsyth, D. Reutens and L. Spiccia, *Polyhedron* 2013, *52*, 128-138; b) H.-K. Kim, M.-K. Kang, K.-H. Jung, S.-H. Kang, Y.-H. Kim, J.-C. Jung, G. H. Lee, Y. Chang and T.-J. Kim, *Journal of Medicinal Chemistry* 2013, *56*, 8104-8111; c) G.-W. Lin, Y. Wang, Q.-M. Jin, T.-T. Yang, J.-M. Song, Y. Lu, Q.-J. Huang, K. Song, J. Zhou and T. Lu, *Inorganica Chimica Acta* 2012, *382*, 35-42; d) A. F. Martins, J.-F. Morfin, C. F. G. C. Geraldes and É. Tóth, *JBIC Journal of Biological Inorganic Chemistry* 2014, *19*, 281-295; e) A. F. Martins, J.-F. Morfin, A. Kubíčková, V. Kubíček, F. Buron, F. Suzenet, M. Salerno, A. N. Lazar, C. Duyckaerts, N. Arlicot, D. Guilloteau, C. F. G. C. Geraldes and É. Tóth, *ACS Medicinal Chemistry Letters* 2013, *4*, 436-440; f) N. Saini, R. Varshney, A. K. Tiwari, A. Kaul, M. Allard, M. P. S. Ishar and A. K. Mishra, *Dalton Transactions* 2013, *42*, 4994-5003.

[22] a) V. J. Majo, J. Prabhakaran, J. J. Mann and J. S. Dileep Kumar, *Tetrahedron Letters* 2003, *44*, 8535-8537; b) S. Ranjit and X. Liu, *Chemistry – A European Journal* 2011, *17*, 1105-1108.

[23] D. W. Hein, R. J. Alheim and J. J. Leavitt, *Journal of the American Chemical Society* 1957, *79*, 427-429.

[24] a) K. Bahrami, M. M. Khodaei and F. Naali, *The Journal of Organic Chemistry* 2008, *73*, 6835-6837; b) F. M. Moghaddam, H. Ismaili and G. R. Bardajee, *Heteroatom Chemistry* 2006, *17*, 136-141.

[25] X.-Q. Zhu, M.-T. Zhang, A. Yu, C.-H. Wang and J.-P. Cheng, *Journal of the American Chemical Society* 2008, *130*, 2501-2516.

[26] a) K. Cui, X. Lu, W. Cui, J. Wu, X. Chen and Q. Lu, *Chemical Communications* 2011, *47*, 920-922; b) M. Schlitzer, L. Rodriguez and P. F. Kador, *Journal of Pharmacy and Pharmacology* 2001, *53*, 831-839.

[27] P. Galinetto, A. Taglietti, L. Pasotti, P. Pallavicini, G. Dacarro, E. Giulotto and M. S. Grandi, *Journal of Applied Spectroscopy* 2016, *82*, 1052-1059.

[28] R. E. Mewis and S. J. Archibald, *Coordination Chemistry Reviews* 2010, *254*, 1686-1712.

[29] P. C. Griffiths, I. A. Fallis, D. J. Willock, A. Paul, C. L. Barrie, P. M. Griffiths, G. M. Williams, S. M. King, R. K. Heenan and R. Görgl, *Chemistry – A European Journal* 2004, *10*, 2022-2028.

[30] T. M. Jones-Wilson, K. A. Deal, C. J. Anderson, D. W. McCarthy, Z. Kovacs, R. J. Motekaitis, A. D. Sherry, A. E. Martell and M. J. Welch, *Nuclear Medicine and Biology* 1998, *25*, 523-530.

[31] R. Gilson and M. C. Durrant, *Dalton Transactions* 2009, 10223-10230.

[32] S. V. Eliseeva and J.-C. G. Bunzli, *Chemical Society Reviews* 2010, *39*, 189-227.

CHAPTER 5

^{48}VANADIUM PET DATA

The interest in new accessible radioisotopes for PET has lead the research to be more focused on metals in the recent years. ^{48}V, with its 16 days of half-life value would be generally useful for process with slow pharmacokinetics.

As introduced in the Chapter 1 the metal radioisotopes present some advantages compared to the organic molecules. As example it is possible to make a comparison between the most used isotopes ^{18}F and ^{48}V, the metal used to test the ligand Bz-epox-DO3A for PET studies.

Both of the isotopes decay mainly emitting β^+, but more interesting with similar energy, 633 keV for the ^{18}F and 694 keV for the metal. Considering these levels of energy the positrons do not travel far before to be annihilated by electrons (the mean free path); allowing a better localization of the targeting compound.

The main advantage of radiometals, is the longer half life, if the ^{18}F has a half life of 110 mins, while ^{48}V is 16 days; pragmatically this feature allows scans over an imaging timescale that is impossible for main group radiotracers.

Finally, we should note that, ^{48}V is not a pure β^+ emitter, but it is also an γ-emitter. These high energy γ-emissions at 944, 983 and 1312 keV are easily filtered in PET detection. These are the electrons downscattered by in the environment, to lower energies, interfering with the photons that can be visualised by the detector.[1]

All the features have lead to use the ^{48}V as possible radiotracer for PET studies and the develop of new or modified ligands capable to coordinate the metal. The compound V-Bz-epox-DO3A, reported in the Chapter 3, has showed suitable features to be considered suitable for further studies *in vivo*.

5.1.1 - Production and purification of ^{48}V

The ^{48}V has been produced and purified by Dr Stephen Paisey at PETIC (Cardiff University), adapting the procedure developed by Mainardi's group.[2] Production used a cyclotron with a target process of ^{48}Ti(p, n) ^{48}V. The purification was achieved by

digestion of target (H_2SO_4 - HF) and then an alkaline aqueous work-up and purification on a resin column. The supernatant has been corrected to pH 3-4 by addition of diluted HCl and the solution was passed through a resin column. The ^{48}V is retained in the column as cationic species and then eluted with a solution of 20% ammonia; the solution was neutralised with diluted HCl and once dry dissolved in the desired media.

5.1.2 - Radiolabelling and results

The studies with ^{48}V have been carried at PETIC (Cardiff University) by Dr. Stephen Paisey, with mice provided by Professor Paul Morgan and Dr. Timothy Hughes's research group, Cardiff University. ^{48}V was supplied by PETIC as an oxalate solution (0.01 M) in aqueous solution at pH 7. At this stage the exact speciation of this complex is unknown.

The ^{48}V was supplied with an activity of 1 MBq, while the radiolabeling efficiency was determined through the use of paper ITLC strips; initially we used the method adopted for "cold" metal complex preparation in the Chapter 4, using a silica TLC eluent of 1:1 H_2O : MeCN. Under these conditions V-Bz-epox-DO3A showed on a silica TLC a value of $R_f = 0.7$.

In a different way the "hot" complex did not show the same behaviour at these conditions, remaining on the baseline; thus the choice has been moved to utilise as eluent the standard method applied for the ^{89}Zr.[3]

As reference compound, we employed neutralised ^{48}V in 0.1mM oxalic acid with 50mM DTPA as eluent. For V-Bz-epox-DO3A to a solution in water of the ligand has been added free ^{48}V oxalate and the pH of the solution corrected to 7 by addition of 0.1M NaOH.Radio-TLC was run with 50mM DTPA as eluent system, showing that the coordinated compound remains on the baseline. The two overlaid radio-TLCs traces are shown in figure 5.1.

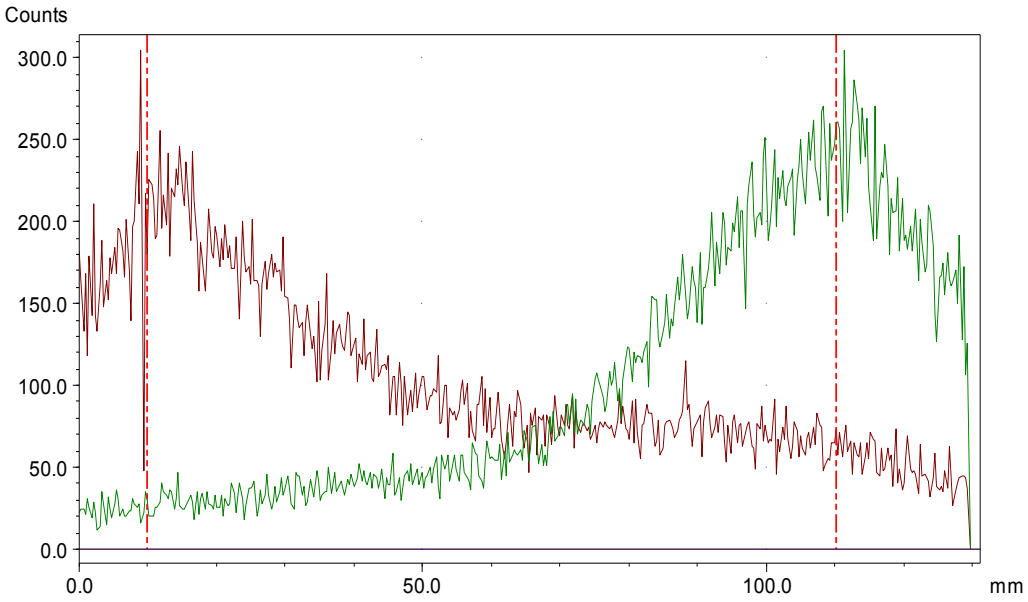

Figure 5.1: overlaid radio-TLCs of coordinated compound (red) and ^{48}V oxalate (green)

This effective complexation obtained has led to further studies and allowed a study *in vivo* PET-CT on a murine (mouse) model of Alzheimer's disease. Figure 5.2 illustrates the PET-CT scan obtained 43 hours after injection.

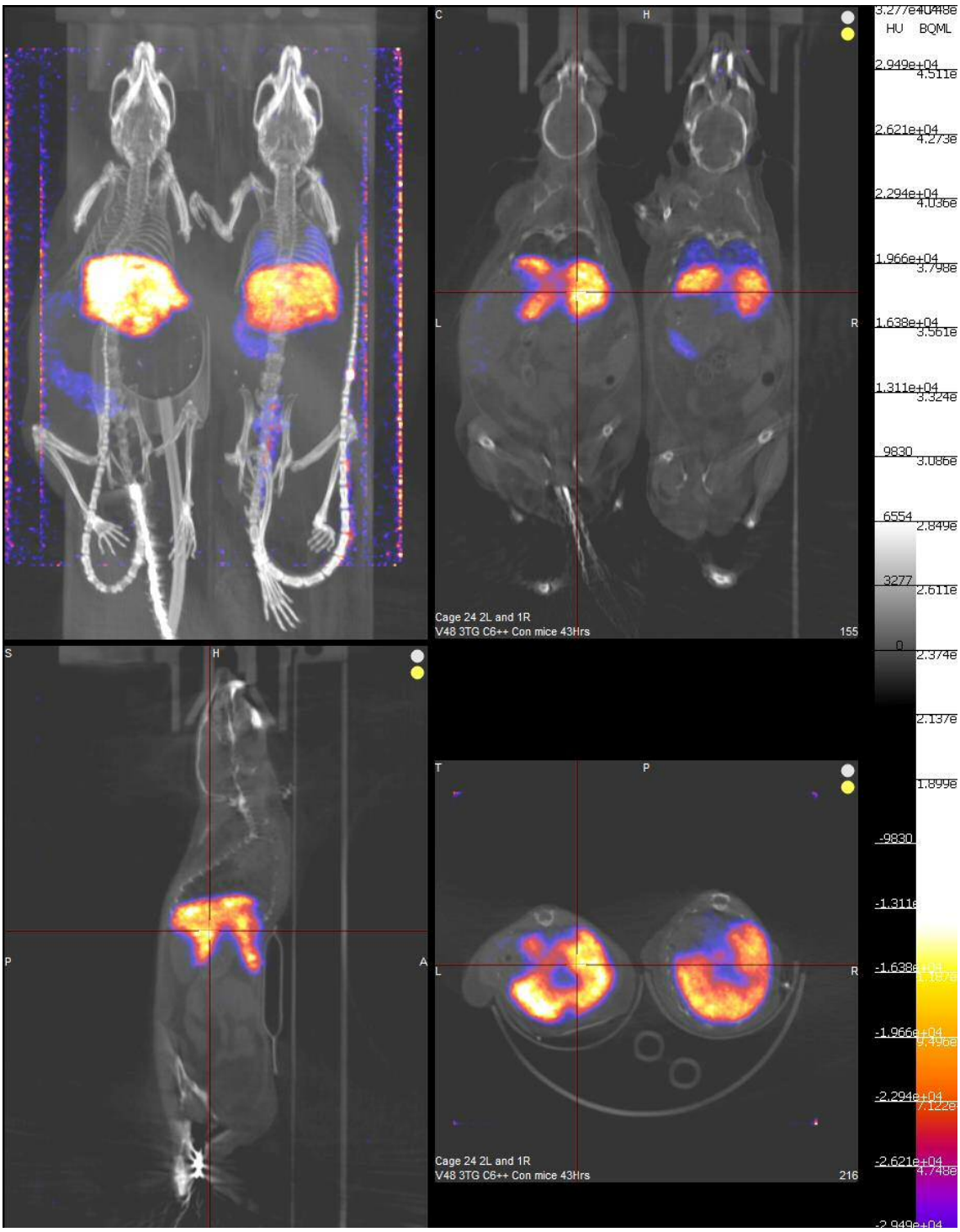

Figure 5.2: *In vivo* PET-CT images of 3TG C6 con +/+ Alzheimer's' disease mice 43 hours after injection.
LHS = ^{48}V complex uptake in liver and spleen,
RHS = ^{48}V oxalate uptake in liver spleen lungs and bone/joints

The maximum intensity projection (MIP, top left image) shows the distribution of the two compounds in the mices. The left mice has been exposed to the new synthesised "hot" complex and it is possible to see how the ^{48}V has been detected only in liver and spleen, not surprising, considering that are organs normally involved in the excretion of

molecules from the body. This suggests the compound unfortunately is not able to cross the blood-brain barrier (BBB), indeed there is not sign of any uptake of activity in the brain where the β-amyloid plaques are located.

The animals on the right of the image were injected with the free ^{48}V oxalate solution, and from the data apparent that there is an accumulation of radiation in liver, spleen, lungs and bone/joints. Again this implies that free ^{48}V beyond to be found in the organs designed to the excretion of molecules is not uptake clearly in the brain, being not able to cross the BBB, but instead can be accumulated in other region and/or organs of the body.

This results shows how, even if the new compound is not able to cross the BBB, that the complex has good stability *in vivo* and the animals injected with the ^{48}V-Bz-epox-DO3A does not show any presence of hot metal in another area or organs except liver and spleen, similar to the "free" ^{48}V.

This study may be regarded as a toxicology experiment in which the subject tolerated both the "free" ^{48}V oxalate and the ^{48}V-Bz-epox-DO3A complex used. Work in the group continues to develop more effective elucidator for this exacting new tracer.

This chapter has described the production and purification of the ^{48}V isotope that has been used as radiometal with the ligand Bz-epox-DO3A. It has been shown that successful complexation of 48Vn by the ligand generated ^{48}V-Bz-epox-DO3A; the radiometal with an activity of 1 MBq, and binding efficiency tested using paper ITLC strips using the standard method applied to ^{89}Zr shown previously. This showed that the ligand fully complexed the radiometal.

Finally the ^{48}V-Bz-epox-DO3A has been tested *in vivo* on a murine (mouse) model of Alzheimer's disease. Combined PET/CT imaging indicates that the complexed radiometal is not able to cross the blood-brain barrier, but shows a good stability *in vivo*, with accumulation of the radiotracer only in the liver and spleen and overall with good tolerance of the test subject to both the "free" ^{48}V oxalate and the ^{48}V-Bz-epox-DO3A complex.

[1] L. Jødal, P. Afzelius and S. B. Jensen, *Journal of Nuclear Medicine Technology* 2014, *42*, 42-50.

[2] M. L. Bonardi, E. Rizzio, M. Gallorini, F. Groppi and H. S. Mainardi, *Journal of Radioanalytical and Nuclear Chemistry* 2005, *263*, 23-28.

[3] J. C. Knight, S. J. Paisey, A. M. Dabkowski, C. Marculescu, A. S. Williams, C. Marshall and B. Cornelissen, *Dalton Transactions* 2016, *45*, 6343-6347.